MASSACHUSETTS INSTITUTE OF TECHNOLOGY

DEPARTMENT OF NUCLEAR ENGINEERING

Cambridge, Massachusetts 02139

COO-2250-28 MITNE-211

ERDA Research and Development Contract

UC-79P LMFBR-Physics

LMFBR BLANKET PHYSICS PROJECT PROGRESS REPORT NO. 7

September 30, 1976

Contract E(11-1)2250

U.S. Energy Research and Development Administration

Editor:

M.J. Driscoll

Contributors:

D.C. Aldrich
M.J. Driscoll
O.K. Kadiroglu
S. Keyvan
H.U.R. Khan
D.D. Lanning
R. Morton
J. Pasztor
T.J. Reckart
A.A. Salehi
J.I. Shin
A.T. Supple
D.J. Wargo
S.S. Wu

DISCLAIMER

DISTRIBUTION

COO-2250-28 MITNE-211

ERDA Research and Development Contracts

E(11-1)-2250

UC-79P LMFBR - Physics

Copies

1-3 U.S. Energy Research and Development Administration
Division of Reactor Development and Technology
Reactor Physics Branch
Washington, D.C. 20545

4-9 U.S. Energy Research and Development Administration
Chicago Operations Office
9800 South Cass Avenue
Argonne, Illinios 60439
(for distribution in accordance with Category UC-79P)

10 Director, Nuclear Power
Electric Power Research Institute
Post Office Box 10412
Palo Alto, California 94303

ABSTRACT

This is the seventh annual report of an experimental and analytical program for investigation of the neutronics of benchmark mockups of LMFBR blankets.

During the period covered by the report, July 1, 1975 through September 30, 1976 work was devoted primarily to a range of analytical/numerical investigations, including evaluation of means to improve external blanket designs, beneficial attributes of the use of internal blankets, improved methods for the calculation of heterogeneous self shielding and parametric studies of calculated spectral indices.

Experimental work included measurements of the ratio of U-238 captures to U-235 fissions in a standard blanket mockup, and completion of development work on the radio-photoluminescent readout of LiF thermoluminescent detectors.

The most significant findings were that there is very little prospect for substantial improvement in the breeding performance of external blankets, but internal blankets continue to show promise, particularly if they are used in such a way as to increase the volume fraction of fuel inside the core envelope. An improved equivalence theorem was developed which may allow use of fast reactor methods to calculate heterogeneously self-shielded cross sections in both fast and thermal reactors.

TABLE OF CONTENTS

CHAPTER 6. (Continued)

CHAPTER 6. (Continued)

LIST OF TABLES

List of Tables (Continued)

LIST OF FIGURES

List of Figures (Continued)

CHAPTER 1

INTRODUCTION

1.1 Foreword

This is the seventh annual report of the LMFBR Blanket Physics Project. This report covers work done since the last progress report, Ref. (1), during the period from July 1, 1975 through September 30, 1976: i.e., including the transition quarter (Summer 1976) required to accommodate the changeover to the new federal fiscal year.

The subject project is part of the ERDA LMFBR development program, having as its primary objective the experimental investigation of clean, but realistic, benchmark mockups of the blanket-reflector region of large LMFBR reactors. The key experimental tool used in this research is the Blanket Test Facility at the MIT Research Reactor. The BTF contains a fission-converter plate tailored to deliver a neutron spectrum simulating LMFBR core leakage, which can be used to drive fact reactor blanket-reflector mockups. Blanket subassemblies are constructed of uranium metal fuel rods, clad in carbon steel, surrounded by anhydrous sodium chromate. The homogenized mixture closely simulates UO_2 fuel, stainless steel clad and sodium metal coolant.

1.2 Active Research Areas

The MIT Research Reactor, which was shut down for renovation in May 1974, resumed routine operations at 50% power in late Spring 1976. Thus non-experimental activities constituted a large part of project efforts during the report period. However, as discussed in Chapter 2 of this report, breeding performance related measurements were made during Summer 1976: also discussed are related interpretative calculations by Wu (2).

In Chapter 3 a brief summary is presented of work on development of methods for gamma heating measurements completed since Morneau's efforts (3), which were discussed in Ref. (1).

Chapter 4 presents an update on all MIT work carried out to date on LMFBR cores with internal blankets.

In Chapter 5 a topical report now under preparation on unit cell heterogeneity is summarized. This will incorporate, generalize upon, and hence supercede a prior topical report, also issued during the report period (4).

Studies of the potential for improving external blanket breeding performance are reported in Chapter 6, which summarizes a forthcoming topical report in this area. This work also completes a series of economic analyses begun during the previous fiscal year (5)(6).

The final Chapter, 7, summarizes the past year's efforts, draws conclusions regarding their significance, and discusses future work plans.

Appendix A lists all publications to date under the subject research project.

1.3 Staff

The project staff, including thesis students, during the report period was as follows:

M.J. Driscoll, Associate Professor of Nuclear Engineering

D.D. Lanning, Professor of Nuclear Engineering

A.T. Supple, Engineering Assistant (part-time)

R. Morton, Computer Operations Assistant (part-time)

J.I. Shin, ScD Student, Research Assistant

A.A. Salehi, ScD Student, Research Assistant

O.K. Kadiroglu, ScD Student, Research Assistant

S.S. Wu, Nuclear Engineer's Degree Student

D.C. Aldrich, SM Student

S. Keyvan, Half-time Research Assistant, Summer 1976

J. Pasztor, Part-time Undergraduate Lab Assistant

D.J. Wargo, Part-time Graduate Lab Assistant, Summer 1976

T.J. Reckart, Undergraduate Research Opportunities Program

H.U.R. Khan, Part-time Computer Assistant, Since 6/1/76

1.4 References

(1) LMFBR Blanket Physics Project Progress Report No. 6, COO-2250-21, MITNE-185, June 30, 1975.

(2) S.S. Wu, "Experimental Verification of Breeding Performance in Fast Reactor Blankets," Nucl. Eng. Thesis, MIT Nuclear Engineering Department, June 1976.

(3) R.A. Morneau, "Improved Radiophotoluminescence Techniques for Gamma Heating Dosimetry," SM Thesis, MIT Nuclear Engineering Department, September 1975.

(4) O.K. Kadiroglu, M.J. Driscoll, I. Kaplan, "Uranium Self-Shielding in Fast Reactor Blankets," COO-2250-17, MITNE-178, March 1976.

(5) M. Ketabi, "The Breeding-Economic Performance of Fast Reactor Blankets," SM Thesis, MIT Nuclear Engineering Department, May 1975.

(6) D. Bruyer, "Breeding-Economics of FBR Blankets Having Non-Linear Fissile Buildup Histories," SM Thesis, MIT Nuclear Engineering Department, August 1975.

CHAPTER 2

BLANKET EXPERIMENTS AND THEIR ANALYSIS

2.1 Introduction

Shutdown of the MIT Reactor for renovation has precluded blanket experiments through late Spring of 1976. Furthermore, operation at 50% power is scheduled for the remainder of calendar year 1976. Finally, startup testing has shown that the thermal neutron flux in the MITR hohlraum, which powers the Blanket Test Facility's converter assembly, has been reduced by a factor of three by the renovation. Thus, the experimental program had to be planned within these constraints. A two-phase schedule resulted : during Summer 1976, Blanket Mockup 5A would be used to obtain more accurate measurements on standard blanket performance, then, during Fall 1976 a changeover to Mockup 5B would be effected. Mockup 5B would employ only one blanket row and a thick steel reflector region, and would be used to study fast neutron penetration in the reflector region during calendar 1977.

In this chapter, Mockups No. 5A and 5B will be described, followed by a discussion of the measurements carried out on Mockup No. 5A, and related parametric studies.

2.2 Blanket Mockups 5A and 5B

Blanket Mockup 5A is almost identical to previous mockups No. 2 and 4: the same blanket assemblies are used; unlike 2, but like 4, the harder-spectrum version of the converter assembly

is used to drive the mockup; and, unlike either, new steel reflector assemblies rather than steel sheets are used for the reflector region.

Figure 2.1 shows the layout of Mockup No. 5A, and Figs. 2.2 and 2.3 show details of the new reflector assemblies. The reflector assemblies are constructed of carbon steel, for which a representative composition is listed in Table 2.1.

Square cross section steel rods (7/16" x 7/16") have been fabricated for insertion into the vertical square channels (1/2" x 1/2") of the traversing assemblies. Circular spots have been milled into the surface of these rods to accommodate the various foils which will be irradiated in the reflector region. By rotating the holder 90°, the foils can be irradiated either perpendicular to, or parallel to, the "radial" axis of the blanket/reflector assembly. Vertical slots are also milled into the traversing rods to accommodate the standard TLD holders used for gamma heating measurements (1). Blanket Mockup No. 5A has been used for the experiments discussed in section 2.3.

It was originally planned that Mockup 5A (previously designated 5, without letter designation) would be used for both blanket and reflector studies. However, the lower converter assembly fast neutron source strength available with the redesigned MITR would make the achievement of acceptable precision deep in the reflector difficult. Hence it was decided that a revised version, Mockup 5B, would be constructed, consisting of only one blanket row, followed by the three available rows of steel reflector assemblies, then by one foot of the older steel

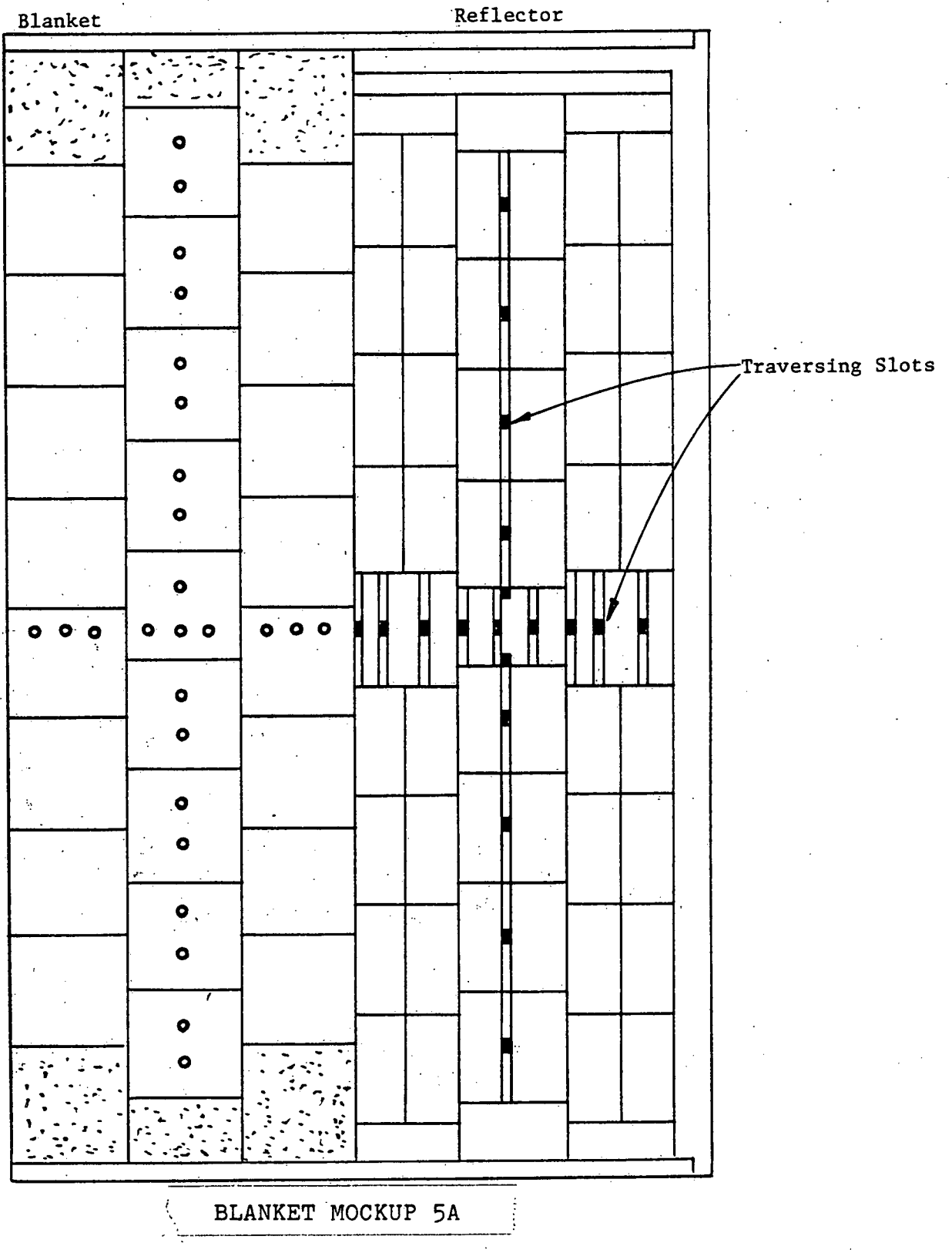

Fig. 2.1 Blanket Mockup 5A

Key

1	2½ x 6 x 48 4 x 6 x 48
2	3 x 6 x 48
3	1½ x 6 x 48
4	1½ x 4 x 48
5	1½ x 3 x 48
6	½ x $2^{3}/_{4}$ x 48
7	½ x $1^{3}/_{4}$ x 48
8	½ x 1 x 48

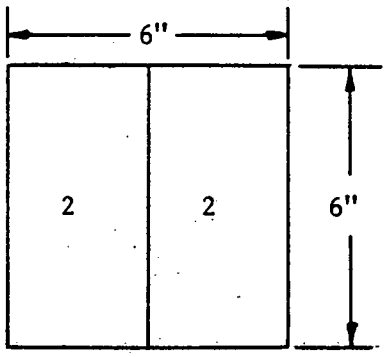

Standard Assemblies (16)

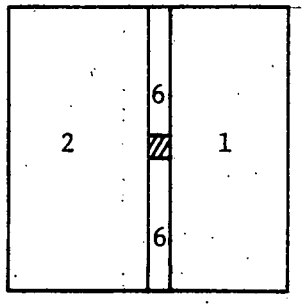

Transverse Traversing Assemblies (8)

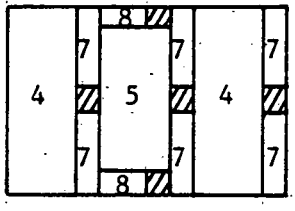

Central-Interior Traversing Assembly (1)

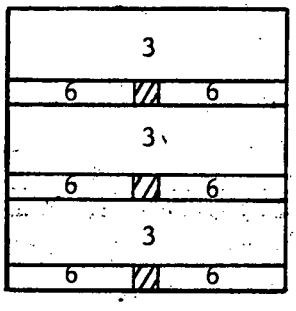

Central-Peripheral Traversing Assemblies (2)

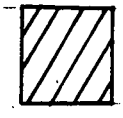

½" x ½" Traversing Slots

Fig. 2.2 Horizontal Cross Section Through Reflector Assemblies

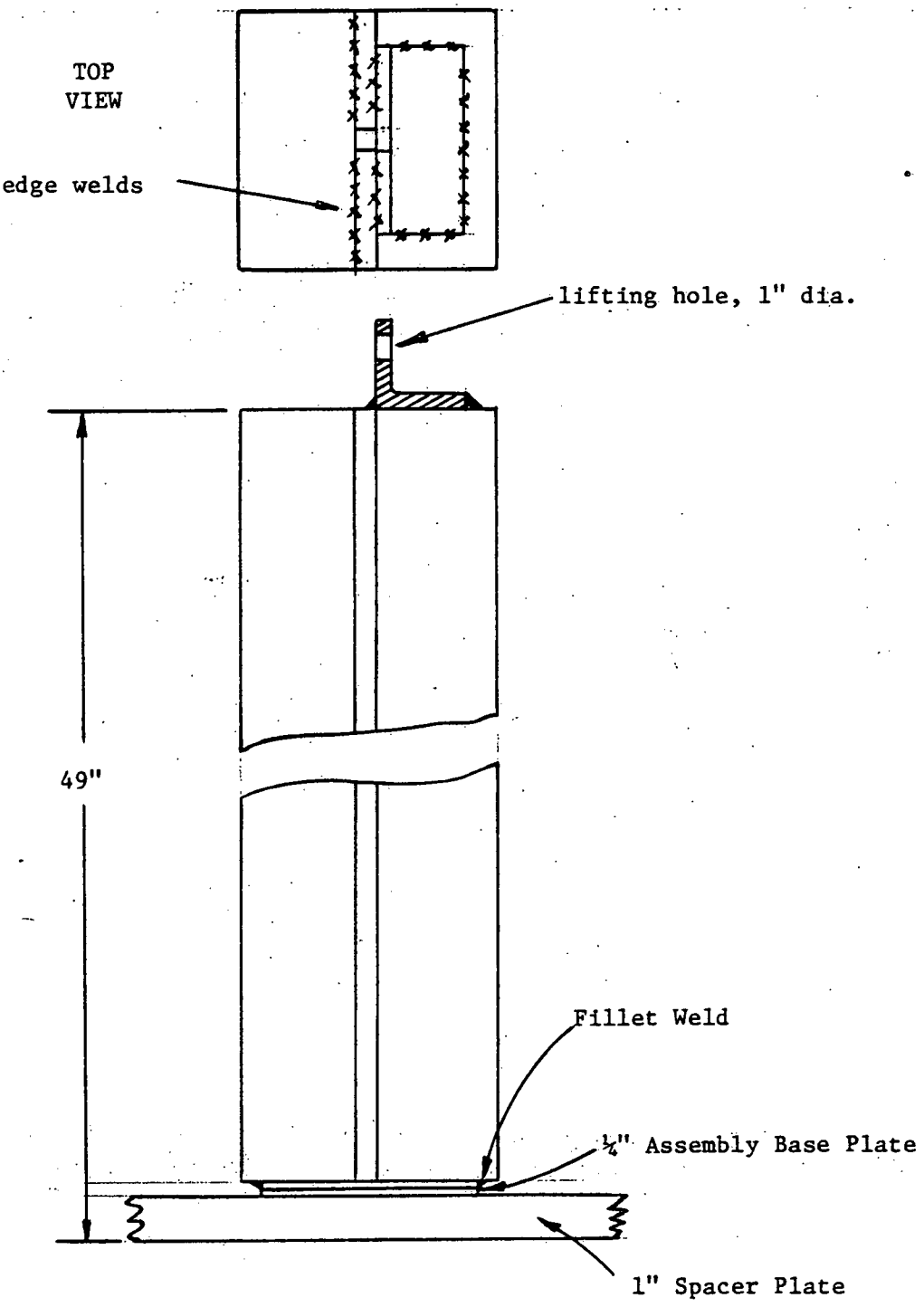

Fig. 2.3 Vertical Section of Typical Traversing Assembly (Sideview)

Table 2.1. New Reflector Composition

MATERIAL: Type C-1018 Steel, Cold Rolled

CHEMICAL COMPOSITION:

CONSTITUENT	LOWER/UPPER, WT.%
Carbon	0.15/0.20
Manganese	0.60/0.90
Phosphorous	0.04 max.
Sulphur	0.05 max.
Iron (remainder)	98.81/99.25

DENSITY: 490.58 lbs/ft^3 = 7.86 gms/cc

IN SUBSEQUENT CALCULATIONS THE REFLECTOR WILL BE TREATED AS PURE Fe WITH:

N = 0.08476 nuclei/barn cm

sheet reflector. This would increase the fast flux in the reflector by a factor of approximately ten compared to Mockup 5B (and the total flux by a factor of around three) and thereby permit us to carry out the reflector-oriented research originally planned for Mockup 5(≡5A).

Figures 2.4 and 2.5 show Mockup 5B in some detail. Since Mockup 5B is constructed entirely of components from previous mockups (the blanket row is the center row of Mockups 2 and 4; the inner reflector is from Mockup 5A; the outer reflector is from Mockup 4) no further description is required here.

Mockup 5B will be used for experiments planned for calendar 1977, to be described in next years annual report.

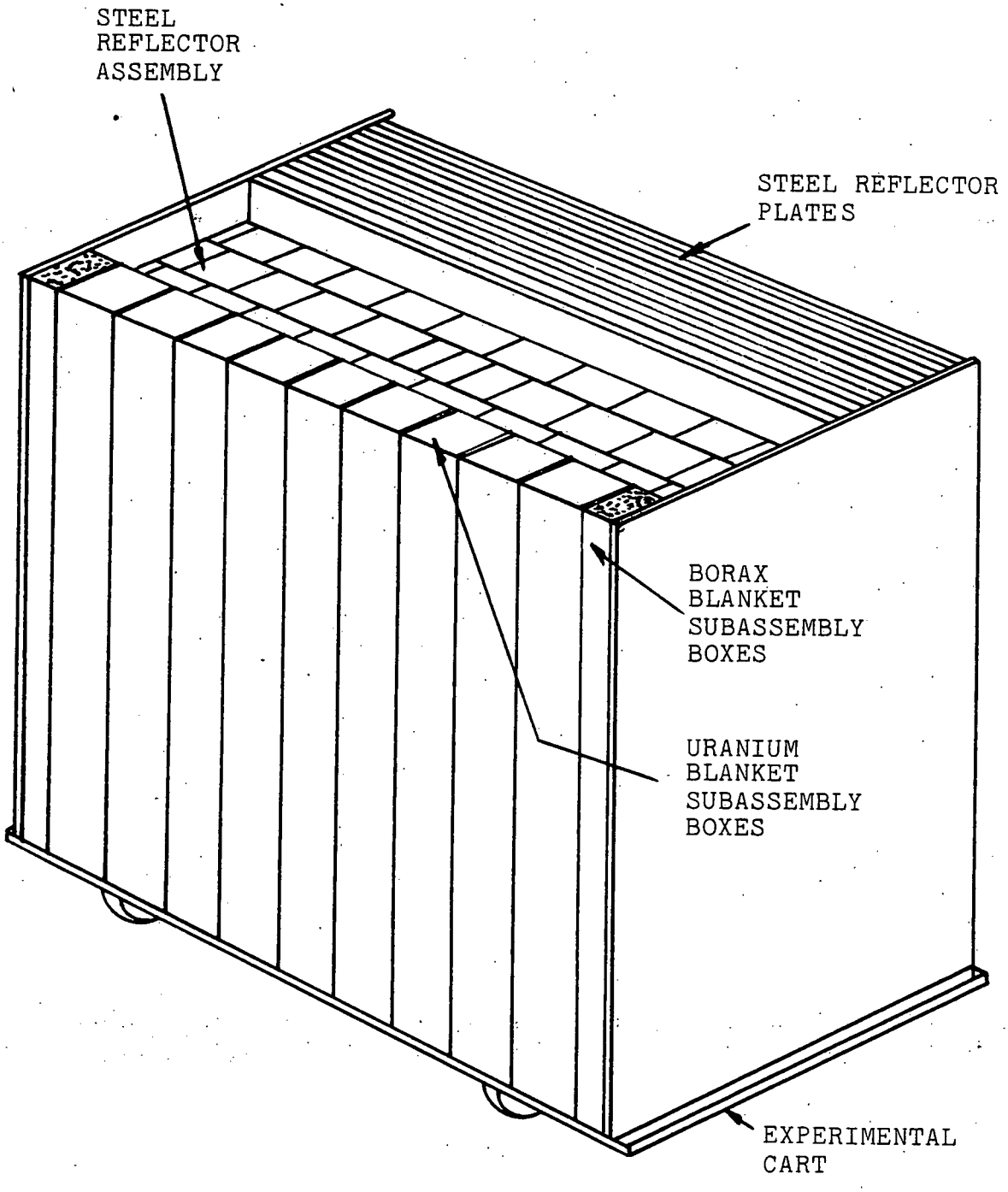

Figure 2.4 ISOMETRIC VIEW OF BLANKET/REFLECTOR MOCKUP 5B

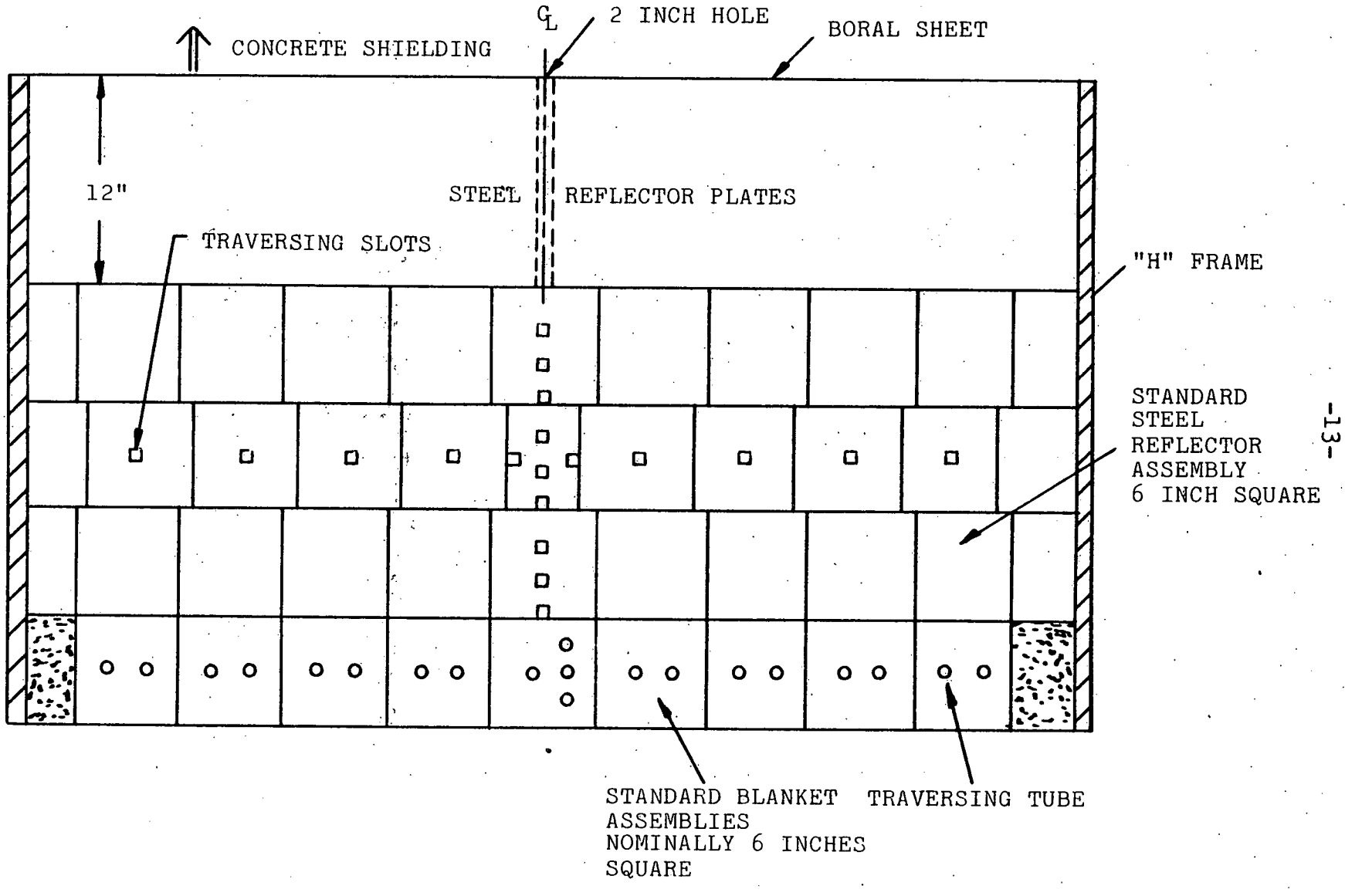

Figure 2.5 TOP VIEW OF BLANKET/REFLECTOR MOCKUP 5B

2.3 Blanket Experiments

The external (blanket) breeding ratio, b, can be expressed in terms of measurable quantities:

$$b = \left(\frac{1}{1+\alpha^{49}}\right)_c F_{49c}^{25b} \cdot \left(\frac{N_{28}}{N_{25}}\right)_b \left(\frac{\bar{\sigma}_c^{28}}{\bar{\sigma}_f^{25}}\right)_b \qquad (2.1)$$

where

α^{49} = capture to fission ratio of fissile plutonium in the core region (core term)

F_{49c}^{25b} = ratio of U-235 fission rate in the blanket to the fissile fission rate in the core (coupling term)

$\left(\frac{N_{28}}{N_{25}}\right)_b$ = ratio of U-238 to U-235 nuclei in the blanket

$\left(\frac{\bar{\sigma}_c^{28}}{\bar{\sigma}_f^{25}}\right)$ = ratio of blanket-averaged capture cross section of U-238 to fission cross section of U-235 (blanket term)

Thus the spectral index $\bar{\sigma}_c^{28}/\bar{\sigma}_f^{25}$ is a particularly meaningful one for characterizing fast reactor blanket performance.

In view of this significance, a careful set of measurements of this parameter were made in Blanket Mockup No. 5A.

The result was as follows:

$$\frac{\bar{\sigma}_c^{28}}{\bar{\sigma}_f^{25}} = 0.114 \pm 3.5\%$$

The result quoted above is the mean of ten independent determinations. U-238 capture was measured using both singles and coincidence counting techniques -- no significant difference was evident. Eight measurements were made in the

UO_2-fueled, stainless-steel-clad, sodium cooled assembly; two measurements were made in a U metal-fueled, carbon-steel-clad, sodium-chromate-moderated assembly: no difference was evident between the two groups of data. Likewise no difference was observed when moderately depleted U-238 foils (170 ppm U-235) were substitute for the usual highly depleted foils (18 ppm U-235); 93% U-235 in aluminum was used throughout the fission rate measurements (gross fission products counted $\geq$ 0.72 Mev). The absolute ratio was obtained by thermal-spectrum normalization, using simultaneous cadmium-ratio-corrected foil irradiations in the hohlraum which drives the blanket facility's converter. The quoted results are corrected for the difference between fast and thermal U-235 fission product yields (multiplicative factor of 1.033), and the results, which were measured inside blanket fuel pins at the center of the blanket, are also "corrected" to the whole-blanket average using the factor determine by Wu (1) (multiplicative factor of 1.00).

Supplementary measurements made during these studies included cadmium ratio measurements for U-238 and U-235 in both the blanket and the thermal neutron hohlraum, with results as follows:

		Cd Ratio
U-238:	blanket	0.99 ± 0.05
	hohlraum	7.4 ± 1
U-235:	blanket	1.00 ± 0.05
	hohlraum	261 ± 17

Based on these results there is no reason to suspect thermal neutron contamination in the blanket, or fast neutron contamination in the hohlraum.

These results are in good agreement with those measured by Leung and Wu, on Blanket Mockups No. 2 and 4: 0.112 ± 6% and 0.105 ± 5% respectively (their values as corrected here for U-235 fission yield).

2.4 Parametric Studies

Studies reported in Ref. (1), and work done subsequently, have been concerned with parametric and sensitivity studies to examine the suitability of state-of-the-art methods and cross section sets for calculation of the spectral index $\bar{\sigma}_c^{28}/\bar{\sigma}_f^{25}$. Most of this work has dealt with measurements on Mockup No. 4, and calculations using the ABBN (Russian) 26-group cross section set. During the coming year the newer measurements reported in section 2.3 of this chapter will be analyzed using newer cross sections derived from ENDF/B-IV.

Table 2.2 summarizes Wu's analysis of Mockup No. 4 data. Of concern here is the overestimation of $\bar{\sigma}_c^{28}/\bar{\sigma}_f^{25}$. Table 2.3 summarizes the results of a parametric study carried out to seek possible explanations for this discrepancy. One plausible explanation is use of too high a value for the capture cross section of U-238. Other causes involve factors influencing the shape of the energy spectrum of the neutron flux. Figure 2.6 shows a group-by-group plot of the ratios

Table 2.2 Comparison of Final Measured and Calculated Parameters for MIT Blanket Mockup No. 4

Parameters**	Measured	Calculated	C/E
$\sigma_c^{28}/\sigma_f^{28}$	14.60±0.18	16.10	1.10
$\sigma_f^{25}/\sigma_f^{28}$	142.9±7.3	146.37	1.02
$\sigma_c^{28}/\sigma_f^{25}$	0.102±0.005	0.110	1.08

** All values are the ratio of reaction rates averaged over the entire blanket volume.

Table 2.3 Sensitivity Study for $\bar{\sigma}_c^{28}/\bar{\sigma}_f^{25}$

Parameter Varied in Blanket	% Change* in $\bar{\sigma}_c^{25}/\bar{\sigma}_f^{28}$
1. Remove 10% of U-238	-2
2. Remove 10% of Na	+1
3. Remove 10% of Fe	0
4. Remove 10% of O_2	+1
5. Decrease $\sigma_c^{28}(E)$ by 10%	-12
6. Increase inelastic $\sigma^{28}(E)$ by 20%	0
7. Increase inelastic downscatter $\sigma_{i\to j}^{28}$ by 20%	-1
8. Drive Blanket with much softer converter spectrum (Mockup No. 2 vs. Mockup No. 4)	-4
9. Increase background scattering cross section per U-238 nucleus, σ_o, by 10%	+1
10. Decrease σ_o to 0 in core (or BTF converter	-1
11. Replace UO_2 fuel by UC	+4
12. Replace UO_2 fuel by U_2Ti metal alloy fuel	+11
13. Typical axial vs. typical radial blanket	+4
14. Demo vs. commercial size core driving blanket	0
15. 2 row vs. 3 row blanket	+1
16. Natural vs. Depleted U @ BOL	+1
17. EOL batch blanket vs. BOL	+5

*All results: 26 group S_8 ANISN and/or 4 group 2DB; Radial Blanket (unless otherwise indicated)

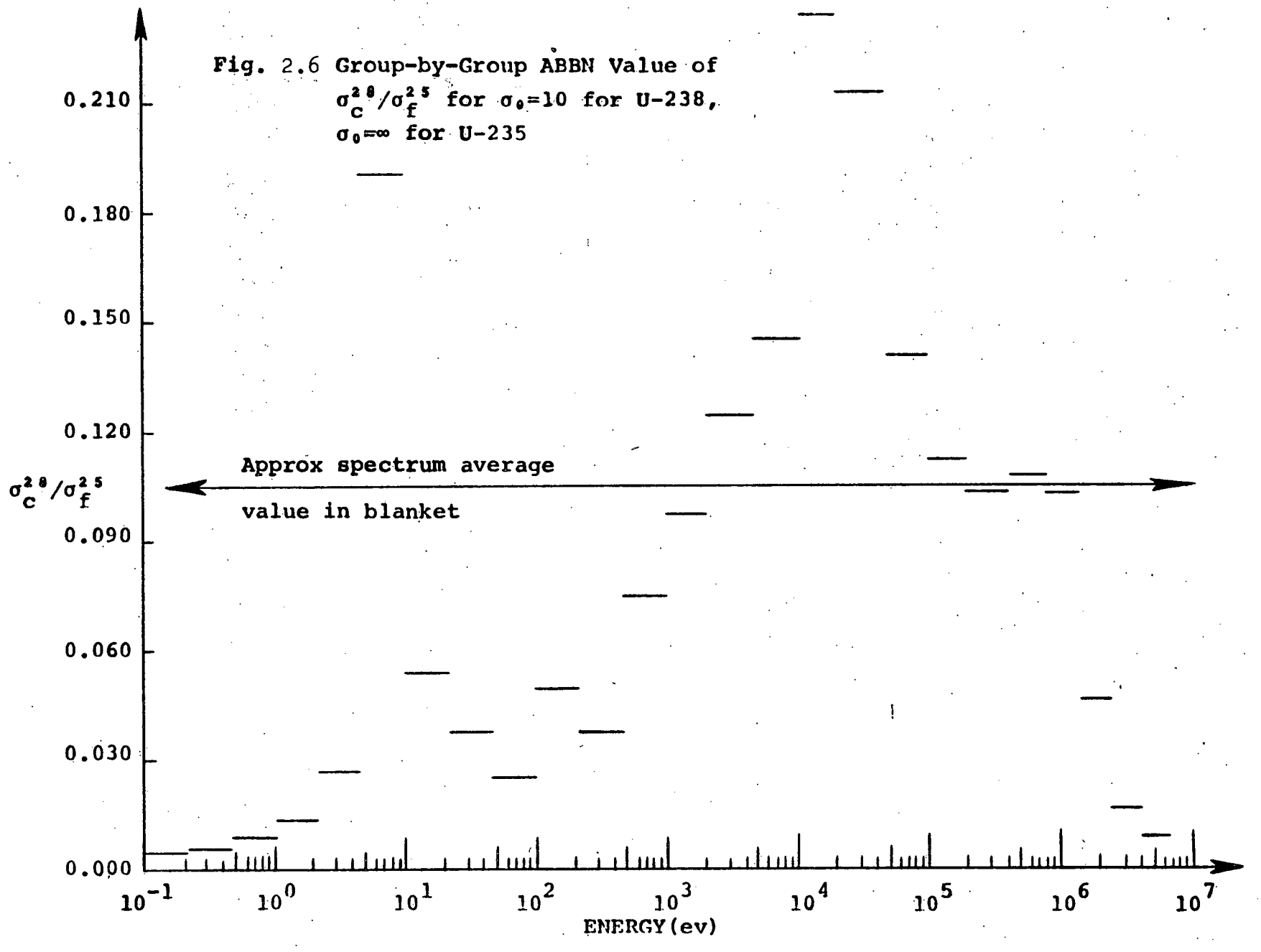

Fig. 2.6 Group-by-Group ABBN Value of $\sigma_c^{28}/\sigma_f^{25}$ for σ_0=10 for U-238, σ_0=∞ for U-235

of $(\sigma_c^{28}/\sigma_f^{25})$. As can be seen a high value of σ_c^{28} or calculated $\phi(E)$ in the energy range between 1 and 100 Kev could account for the observed overestimate of the spectral index; as could too low a value of σ_f^{25} or calculated $\phi(E)$ below 1 Kev.

As part of this study a survey of results calculated by other laboratories/contractors involved in the U.S. LMFBR program was made. The results are shown in Table 2.4. As can be seen the calculated values average slightly higher than our measured results. However our blanket composition is closer to an axial blanket than a radial blanket, and our driving spectrum may be softer than some of the cores involved in the survey: both effects would reduce the discrepancy. Finally, ANL experience appears to be that they also measure values of $\sigma_c^{28}/\sigma_f^{25}$ lower than they calculate.

This discrepancy will be examine further during the coming year. It should be noted that the fact that the calculated value of $\bar{\sigma}_c^{28}/\bar{\sigma}_f^{25}$ exceeds the experimental value does <u>not</u> necessarily mean that the breeding ratio is being overestimated. Most (over ~85%) of the neutrons leaking into, or produced in, the blanket are captured by U-238, almost independent of changes in the composition and cross sections of blanket materials (see Chapter 6 of this report). However analysis can lead to identification of deficiencies which may be of greater importance elsewhere.

Table 2.4 Comparison of the Spectral Index $\bar{\sigma}_c^{28}/\bar{\sigma}_f^{25}$ Calculated for LMFBR Blankets

REPORTING ORGANIZATION	ASSEMBLY	DATA BASE	METHOD	BLANKET AVERAGE $\bar{\sigma}_c^{28}/\bar{\sigma}_f^{25}$
WARD	ZPPR - 4/1	ENDF/B-III	9 Group	
	Radial Bkt.	"	2 DB	0.1277
	Axial Bkt.	"	"	0.1222
	ZPPR - 4/4			
	Radial Bkt.	"	"	0.1333
	Axial Bkt.	"	"	0.1223
WARD	CRBR			
	BOC-1			
	Radial Bkt.	"	"	0.1379
	Axial Bkt.	"	"	0.1423 Upper 0.1364 Lower
	EOC-6			
	Radial Bkt.	"	"	0.1417
ANL	ZPPR - 4/1	"	28 Group	
	Radial Bkt.		VENTURE 3D	0.1218
	Axial Bkt.	"	"	0.1165
GE	GE 1200 MWe	ENDF/B -	16&6 GROUP	
	Radial Bkt.	II,III,IV	SYN, SN2D	0.145

2.5 References

(1) S.S. Wu, "Experimental Verification of Breeding Peroformance of Fast Reactor Blankets," Nucl. Eng. Thesis, MIT Nucl. Eng. Dept., June 1976.

CHAPTER 3

GAMMA HEATING MEASUREMENTS

3.1 Introduction

The prolonged MITR shutdown obviated the need for extensive work in this area. However, work was carried out to complete development of a radiophotoluminescence (RPL) readout device for use with standard LiF thermoluminescent dosimeters (TLD). Earlier versions of this apparatus have been described in references (1) and (2), thus in this chapter we will only report on improvements made since the earlier documentation, and describe the final version of the device, its performance characteristics and limitations

3.2 Experimental Apparatus

The principle of operation of the RPL reader is simple: a beam of blue light is allowed to strike an irradiated TLD and the re-emitted red light photons are counted. The response is linearly proportional to the gamma dose deposited in the TLD.

Figure 3.1 is a schematic diagram, illustrating the following important features of the reader:

1. An intense source of white light (1)*: a GE Type 4537-2 13 volt, 100 watt spotlight, with built in parabolic reflector. This, together with a pair of 12 cm dia. condenser lenses (2) provides a 1 cm dia. spot of focused light on the inlet assembly.

*Circled numbers correspond to numbered features shown in Fig. 3.1.

Fig. 3.1. Schematic of RPL Readout for TLDs

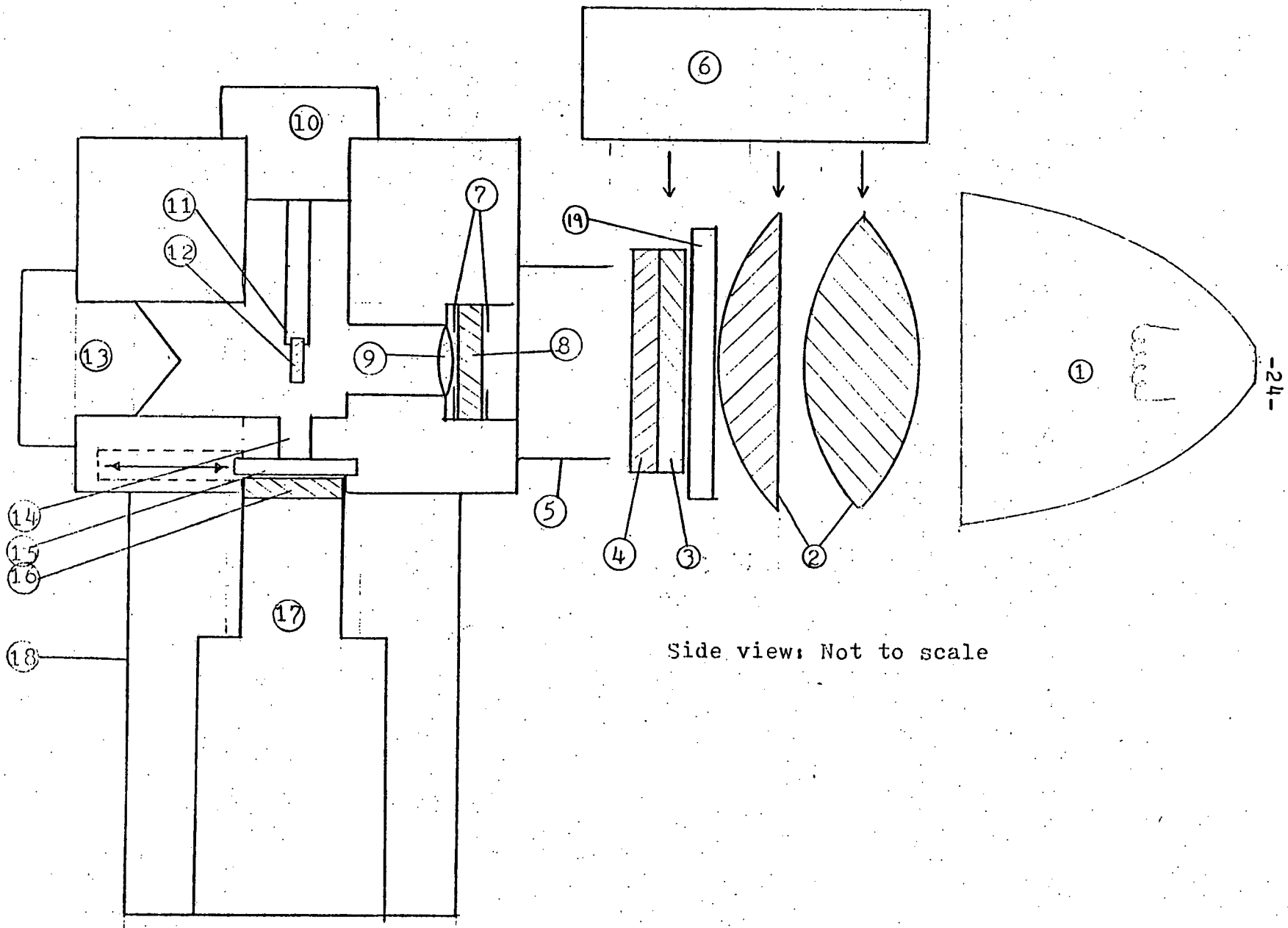

Side view: Not to scale

2. The inlet assembly consist of the following parts, in order from right to left:

   - 6 mm thick sheet of heat absorbing glass (19)* (optional)
   - Blue dichroic filter (3) /Edmund Scientific No. 30635
   - Blue glass filter (4) /Schott BG-12
   - Black shade (5)
   - Aluminum collimator mask (7)
   - Blue dielectric interference filter 447.5 nm 8 wide pass/Thin Film Products; approx.100 nm bandwidth
   - Aluminum collimator mask (7)
   - Short focal length lens to focus transmitted light onto the TLD (9)

3. The TLD holder (10) is a spring-loaded split-collet chuck (11) (adapted from a drawing pencil) which holds the cylindrical TLD by its end, with its axis perpendicular to the incident beam and centered on the vertical axis of the photomultiplier tube. The clamp is covered with optical blank paint.

4. The outlet assembly consists of the following parts, in order from top to bottom:

   - An outlet collimator (14) : a 3/8 inch dia. hole drilled into the bottom of the aluminum housing
   - A sliding valve to close off the PM tube from the beam during loading (15)

---

* Circled numbers correspond to numbered features shown in Fig. 3.1.

- A red dielectric interference filter, 650 nm (16) wide pass./ORIEL Co. of America No. 5761; approx. 100 nm bandwidth

- The detector, an ITT FW-130-1 Type photomultiplier tube (17) designed for single photon counting. It is housed in an optically sealed tube (18) painted black on the inside.

5. Associated electronics: See Figs. 3.2 and 3.3

   - A FLUKE Model 402 M high voltage power supply, to provide the PM tube with 1630 volts.

   - MECH TRONICS Model 511 photon discriminator, to amplify and pulse-shape the signal from the PM tube

   - Hewlett Packard 5381 A 80 MHz frequency counter, to display the output

   - Power Mate Corp. regulated power supply, to supply the lamp with 12 volts ± 0.02 volts

   - Analog Devices, AD 2006 digital voltmeter, to check the voltage across the lamp

   - Two SPRITE Model SP2A2, 120 volt cooling fans to cool the inlet assembly and the 12 volt power supply.

Adherence to good practice was found to be quite beneficial: performance was considerably enhanced by careful alignment and collimation of the optical path, by coating all interior surfaces with optical grade black paint, by rigid mounting of all components in the light path and by assiduous ellimination of all light leakage. A sliding gate valve was incorporated to close off the PM tube from the signal during loading of the reader. Care was taken that the TLD was held by the clamp properly and the same way after each reloading: small fans were used to dissipate heat from the inlet assembly and the low voltage power supply. Care was taken in the selection of the cables to minimize pickup of electronic noise. Great care was

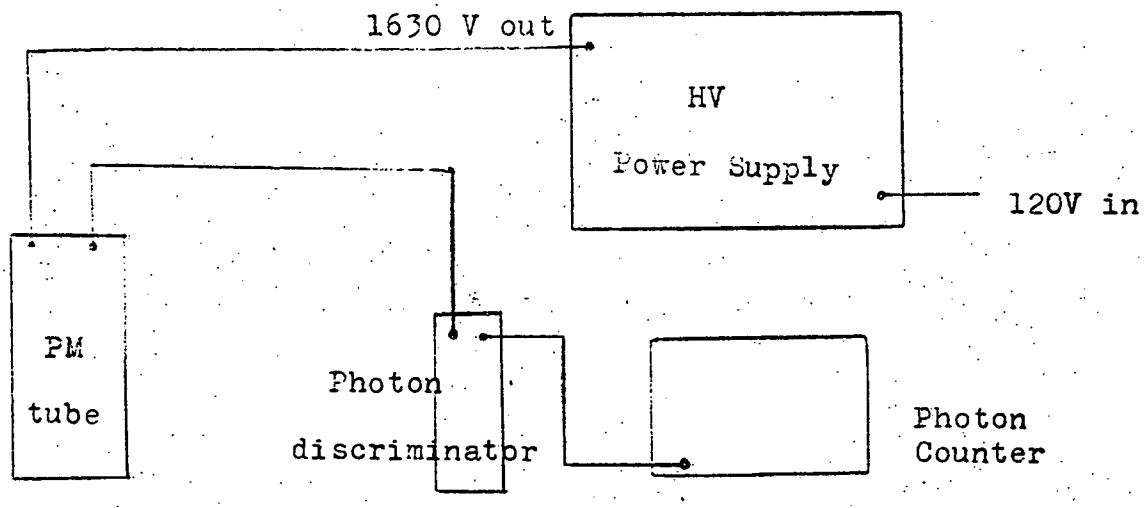

Fig. 3.2. Schematic of the Counting Electronics

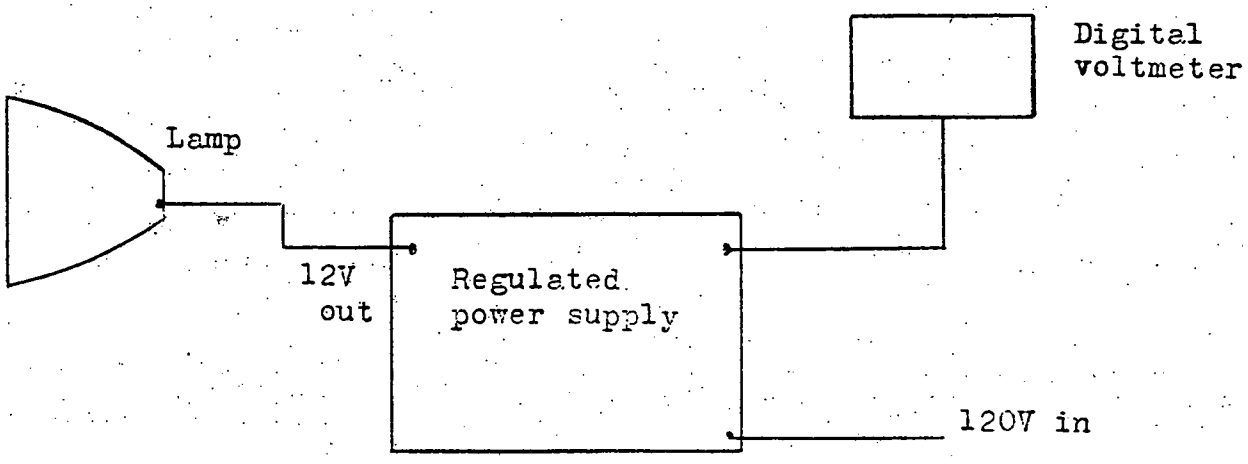

Fig. 3.3. Schematic of the Lamp Power Supply

taken in the handling of the TLDs, since both dirt and scratches on the surface of the TLD can give substantial deviations from the expected response.

3.3 Performance Evaluation

Harshaw Lithium Fluoride, LiF, TLD-100s were irradiated in a Co-60 calibration facility, and used to evaluate the performance of the reader, with the following results:

(a) Excellent linearity was observed between response and exposure dose in the range examined, i.e., 0-10,000 rads, consistent with the observation that RPL response does not exhibit the supralinearity observed in TLD methods.

(b) An acceptably low background was achieved for our purposes. Unirradiated, annealed TLDs emitted a signal which was approximately equivalent to 80 rads of exposure. Under the same conditions the dark signal was equivalent to about 8 rads. Background was the same for all TLDs within the reproducibility of the measurement technique.

(c) Reproducibility was also acceptable:

- repetitive readings on the same TLD during the same loading confirmed the applicability of Poisson statistics
- repetitive reloads of a single TLD gave readings reproducible within 2.5%
- different TLDs irradiated to the same dose gave readings within 5% of the mean value.

(d) Insignificant fading or drift was observed over a several day period, however normalization of all runs

to a standard is commonly employed in observation of general good practice.

(e) RPL readout was shown not to effect subsequent normal TLD readout of the same detectors.

(f) Irradiated TLDs, having a reduced length or diameter were used to confirm that normalization of the observed count rate by weight improved precision.

(g) In our prototype reader, a 1 mm dia., 6 mm long TLD, exposed to 5700 rads will give rise to a signal of approximately 300,000 Cts/10 sec.

3.4 Discussion

The final version of the readout device, described above, evolved via a sequence of analytic and trial-and-error improvements implemented by a series of investigators over an 18-month period. A variety of optical filters were tried both on the inlet and the outlet. Conventional glass filters were found to be unacceptable inside the reader, because of weak fluorescence by even selected varieties. A sequence of a dozen dielectric filters were tested on the output signal to vary the selected wavelength between 500 and 800 nm. The 650 nm filter gave the best signal to background ratio, although the signal was maximum near 520 nm, as expected from the prior work, discussed in ref. (2); the inlet wavelength was also varied and 450 nm light shown to be optimum, again in agreement with the literature.

The filter combinations chosen represent a compromise between maximizing the signal and maximizing the signal-to-

background ratio. For example, using 450 and 650 nm dielectric filters having one-tenth the bandwidth of those specified above can double the signal-to-background ratio at the expense of a factor of 50 reduction in signal. For our probable range of operation, the higher signal was better, resulting in a smaller fractional error in results. The sensitivity of 5 cps/rad achieved here is much higher than the value of 0.1 cps/rad obtained with the earlier versions of this device (1).

In general, we conclude that RPL readout of TLD detectors is a useful experimental technique. Precision equal to or better than that of TLD readout can be attained. The major shortcoming is the background inherent to the TLDs themselves, which makes measurement of doses less than about 5 rad impractical. We have not investigated the use of special annealing procedures, or use of TLDs having different properties, to reduce background.

3.5 Gamma Heating Measurements

In a related effort, using standard TLD readout methods, MIT participated in an interlaboratory comparison of measurements in a shield mockup at ORNL. The results have been documented and reported by ORNL (3)(4), and will not be reproduced here. One discrepancy requiring follow-up by MIT is the difference in TLD response measured at MIT for MIT's TLDs irradiated in MIT vs. ORNL capsules.

3.6 References

(1) LMFBR Blanket Physics Project Progress Report No. 6, COO-2250-21, MITNE-185, June 30, 1975; esp. Chapter 2, Section 2.3.

(2) R.A. Morneau, "Improved Radiophotoluminescence Techniques for Gamma Heating Dosimetry," SM Thesis, MIT Nuclear Engineering Department, September 1975

(3) C.E. Clifford, et al., "Experimental Studies of Radiation Heating in Iron and Stainless Steel Shields for the CRBR Project," ORNL-TM-4998, 1975.

(4) C.E. Clifford, et al., "Radiation Heating Studies in Iron and Stainless Steel CRBR Shields," Trans. Am. Nucl. Soc., Vol. 21, June 1975.

CHAPTER 4

INTERNALLY-BLANKETED CORES

4.0 Foreword

A verbatim transcript follows of the paper:

M.J. Driscoll, G.A. Ducat, R.A. Pinnock, and D.C. Aldrich
"Safety and Breeding-Related Aspects of
Fast Reactor Cores Having Internal Blankets"

This paper was drafted for presentation at the ANS/ENS International Meeting on Fast Reactor Safety and Related Physics, held in Chicago, Ill., October 1976. It will be published in the proceedings of that meeting.

The paper summarizes work to date at MIT on internal blankets in LMFBR cores. Work has almost exclusively been limited to the so-called "parfait" configuration, in which an internal axial blanket is employed at the center of the inner core zone: in contrast to other heterogeneous designs in which only radial blankets are used, or in which both radial and axial blanket inserts are employed.

SAFETY AND BREEDING - RELATED ASPECTS OF FAST REACTOR CORES HAVING INTERNAL BLANKETS

M.J. Driscoll, G.A. Ducat*
R.A. Pinnock**, D.C. Aldrich

Massachusetts Institute of Technology
Department of Nuclear Engineering
Cambridge, Massachusetts 02139

ABSTRACT

The safety characteristics and breeding performance of fast reactor cores having internal axial blankets are examined. Worthwhile improvements and tolerable penalties are identified in both areas based on comparisons with conventional core designs having identical external and fuel assembly dimensions. Internally-blanketed cores have smaller sodium void reactivity contributions and, if properly designed, higher breeding gains and shorter fissile inventory doubling times than conventional cores. The potential for additional improvements in breeding gain is also identified for internally-blanketed cores which are optimized to exploit the inherently lower neutron fluence and fluence/power/temperature gradients characteristic of these cores.

I. INTRODUCTION

Fast reactor cores having internal blankets limited in both radial and axial extent have many advantages over more conventional designs (1,2,3,). One particular version of this generic class of core designs has been studied at MIT since 1972 (4). Figure 1 illustrates the configuration, designated "parfait" because of the layered arrangement of materials in the inner core zone. The internal blanket is made up of axial blanket pellets loaded in place of the fissile-fueled pellets which would otherwise occupy this zone in the fuel pins of a conventional fuel assembly; otherwise the fuel pins and assemblies are identical.

Table I compares representative parfait and conventional 1000 MWe designs having the same external core dimensions and volumetric compositions. Of particular note in this table are the reduced sodium void coefficient and the reduced neutron fluence — unlike many of the other quantities listed, which can be readily modified by various design tradeoffs, these differences appear to be persistent. Dimensional and other constraints imposed on the parfait

*Present Address: Department of Nuclear Engineering, Texas A&M University, College Station, Texas 77843

**Present Address: Commonwealth Edison Co., Chicago, Illinois 60690

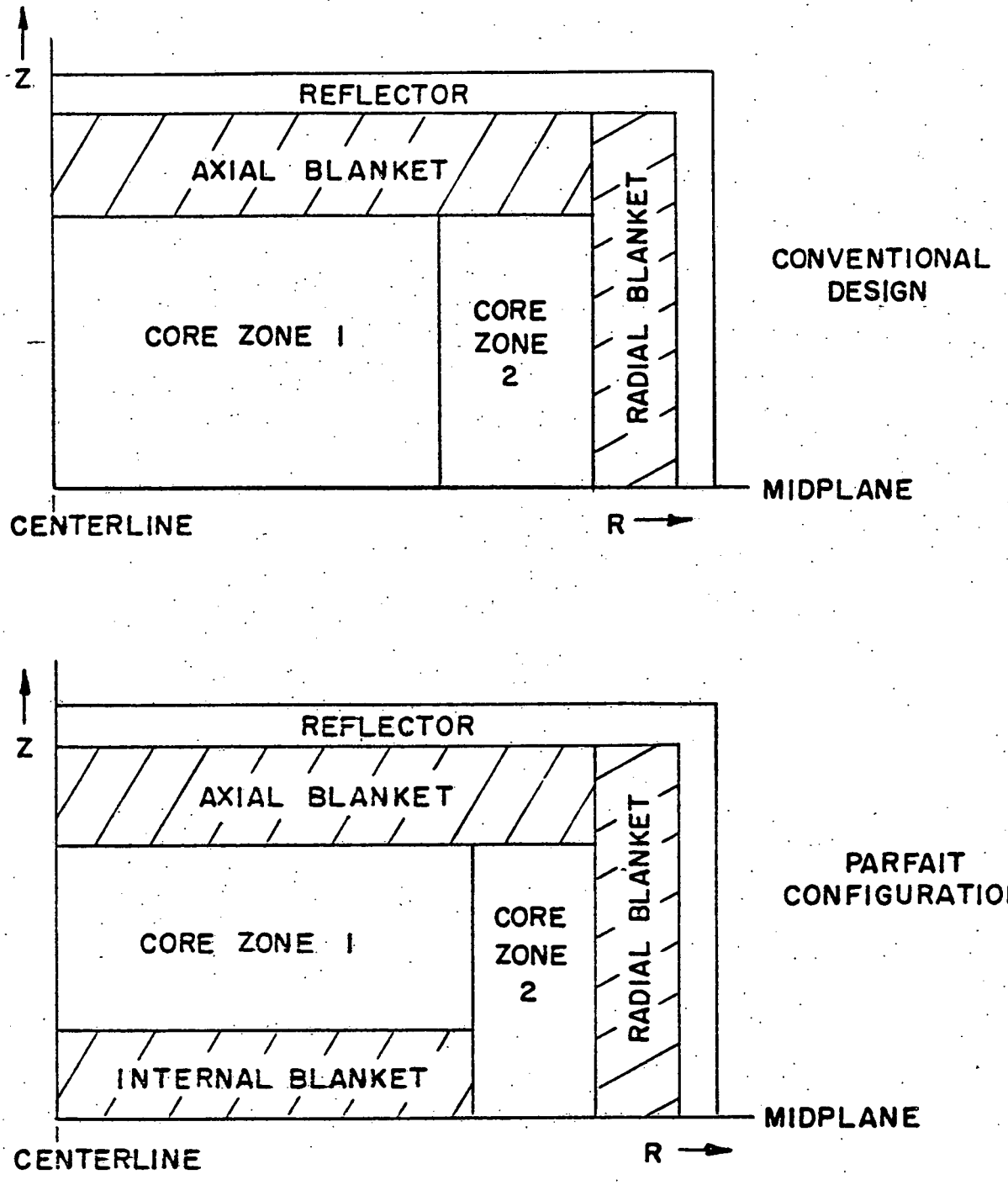

FIG. 1 CONVENTIONAL AND PARFAIT CORE CONFIGURATIONS

TABLE I

Comparisons Between a Representative Pair of Parfait and Conventional Core Designs[a]

Advantageous Changes

Decreased Sodium Void Coefficient (25 - 50%)
Decreased Sodium Temperature Coefficient (40%)
Decreased Peak Power Density (5%)
Increased Overpower Operating Margin[b] (7%)
Decreased power production by the fissile-fueled zones (9% at mid-cycle) due to increased blanket power production (including the internal blanket)
Decreased Peak Fuel Burnup (8%)
Decreased average fissile-fueled zone burnup (5%)
Decreased Burnup Reactivity Swing (25%)
Decreased Peak Fast Flux (25%)
Decreased average fissile-fueled zone flux (15%)
Decreased Wrapper Tube Elongation in Inner Core Zone (29%)
Decreased Wrapper Tube Dilation in Inner Core Zone (38%)
Decreased Radial Flux Gradient in Inner Core Zone (50%)
Decreased Fluence-Induced Bowing in Inner Core Zone (90%)
Increased Breeding Ratio (2%)
Decreased Doubling Time (6%)

Disadvantageous Aspects

Increased Core Fissile Inventory (4%)
Reduced Doppler Power Coefficient (8%)
Increased Isothermal Doppler Coefficient (7%)
Higher Peak Clad Temperature (17°F)
Increased average fissile-fueled zone power density (15%)
Reduced prompt neutron lifetime (3%)
Reduced delayed neutron fraction (1%)
Magnitude and Gradients of fluence/power/temperature are not improved in the outer core zone or radial blanket
Increased Coherence: above 32% overpower more fuel is molten - at 50% overpower 23% of the parfait fuel reaches Q_L melting vs. 18% of the conventional core; more of the parfait core goes into boiling at higher power/flow ratios
Increased leakage to reflector (11%) hence blankets (radial and axial) may have to be thicker to realize the full breeding advantages of the parfait design

[a] Both cores are rated at 1000 MWe and operated for the same number of full power days between refuelings. The parfait design has a 30 cm thick internal blanket, otherwise the core and fuel assembly dimensions are identical. Note that all results can be modified by changing the dimensions of the internal blanket.

[b] Percent steady state power (at 100% flow) at which incipient fuel centerline melting will occur.

design considered in this comparison permit its direct use as a replacement core for the conventional design, but, as will be pointed out later, do not permit the full advantages of the parfait configuration to be achieved. Similarly, even if no additional design changes were incorporated, one would undoubtedly try to trade-off some of the advantages quoted for other benefits - for example, driving the parfait core to a higher average burnup, should this prove practicable.

Note that the concept sketched in Fig. 1 involves an internal axial blanket in the central core enrichment zone, and therefore differs from modular or annular designs in which full-length internal radial blanket assemblies are employed, or heterogeneous concepts, which employ both axial and radial internal blanket zones. The parfait configuration foregoes the advantage of the higher uranium loading possible with the use of full length internal blanket assemblies, but avoids their inherent problem of assembly exit temperature mismatch (sodium striping). Equally as important, full-length internal blanket zones do not contribute to axial power flattening, which appears essential if one is to fully offset the attendant critical mass penalty. It is also not clear that large-diameter radial blanket fuel pins can successfully withstand end-of-burnup-cycle thermal conditions inside the core. Further, use of thin internal blanket intrusions (compared to a neutron mean-free-path) effectively re-homogenizes the core and thereby loses some of the neutronic advantages of heterogeneity.

The features of the present design have been carefully chosen, as noted above, and it is important to emphasize that many aspects related to both safety and breeding performance are quite configuration dependent. Hence other versions of the parfait design will exhibit a different complement of characteristics; and even more important, other related concepts such as the aforementioned annular or heterogeneous arrangements, may differ even more markedly.

II. SAFETY-RELATED CHARACTERISTICS

Safety-related characteristics of common interest, the sodium void and doppler reactivity coefficients, are affected by adoption of the parfait design. The positive reactivity associated with equal-volume voids at a given position (r,z) in the core is reduced by 25 to 50% in the parfait design. Because of the flatter power profile in the parfait design, sodium boiling, if it does occur, would be expected to be more coherent, however. Thus the reactivity effects of voiding caused by cover gas entrainment or fission product gas from random fuel pin failure would appear to be mitigated, while in assessing the consequences of boiling-induced voids more would have to be known about the ability of the parfait design to confine boiling to the zone of steep worth gradient at the upper end of the core or to the upper half of the core — in both of which respects it appears superior to conventional core designs. The effect of uniform sodium density reduction is also smaller for the parfait design, which reduces this component of the cold-to-hot reactivity swing by about 40% averaged over an operating cycle; the same reduction applies to a dilute uniform distribution of voids.

The sodium void reactivity of a conventional 1000 MWe core and a parfait design having a 40 cm thick internal blanket have been compared, with the results shown in Table II.

Table II illustrates the reduced sodium void reactivity worth characteristics of the parfait configuration. While the presence of control poison affects the absolute value of the void worth, the parfait configuration maintains a substantial relative advantage with or without control poison. The difference between the two designs decreases the burnup: as plutonium builds

up in its internal blanket, the parfait core tends to more closely resemble its conventional counterpart. Also note that voiding the internal blanket adds reactivity (although far less than voiding the equivalent zone in the conventional core) — opposite to what occurs if external blankets are voided.

TABLE II

Comparison of Sodium Void Reactivity Worth

Zones Voided	Condition[a]	Reactivity Increase, Dollars	
		Conventional Core	Parfait Core
Entire Core Plus Axial Blankets	BOC	1.22	0.65
	EOC	2.06	1.87
	BOC,P	2.21	1.30
Inner Core Zone 20 cm Above to 20 cm Below Midplane[b]	BOC	2.33	1.56
	EOC	2.49	2.03
	BOC,P	2.52	1.54

[a] BOC(EOC) = Beginning (End) of equilibrium cycle, P = with control poison in core

[b] i.e., the internal blanket region in the parfait design

Doppler reactivity coefficients are affected in an undesirable manner by the change in configuration between conventional and parfait designs. The isothermal doppler coefficient, 1/k dk/dT, increases by about 7% which implies a larger cold-to-hot doppler reactivity change (however the total reactivity change in going from the cold shutdown condition to the hot, full power condition for the conventional and parfait systems is, for all practical purposes, equal). The power doppler coefficient, 1/k dk/dP, decreases by about 8%, which reduces the inherent protection against an overpower excursion. The reduction in power coefficient in the parfait design is offset to some degree by a 7% increase in the allowable overpower margin before the onset of fuel melting.

Other safety-related characteristics of the parfait design may be inferred from Fig. 2 which provides a qualitative indication of the local reactivity worth of both fuel and control poison. Figure 2 shows the product of the total flux and adjoint flux at the centerline (R=0) and the inner/outer core interface (R=102.5 cm) for the parfait design, as a function of axial position. These curves may be contrasted with the cosine-squared shape of the same product in the reference core. Points worth noting in Fig. 2 are the steep decrease in worth near the hottest fuel just above the internal blanket, which would be beneficial in at least the early stages of core meltdown, and the steep increase in worth at the upper end of the core, which would enhance control rod reactivity insertion during the first several centimeters of stroke.

Additional safety aspects include:

1. the internal blanket forms a freeze-barrier to help guard against reassembly of a critical configuration in the event of extensive core meltdown,

2. careful specification of the radial and axial extent of the internal blanket can produce a core having a single fissile enrichment, which helps preclude compaction due to power density discontinuities during core disruptive accidents,

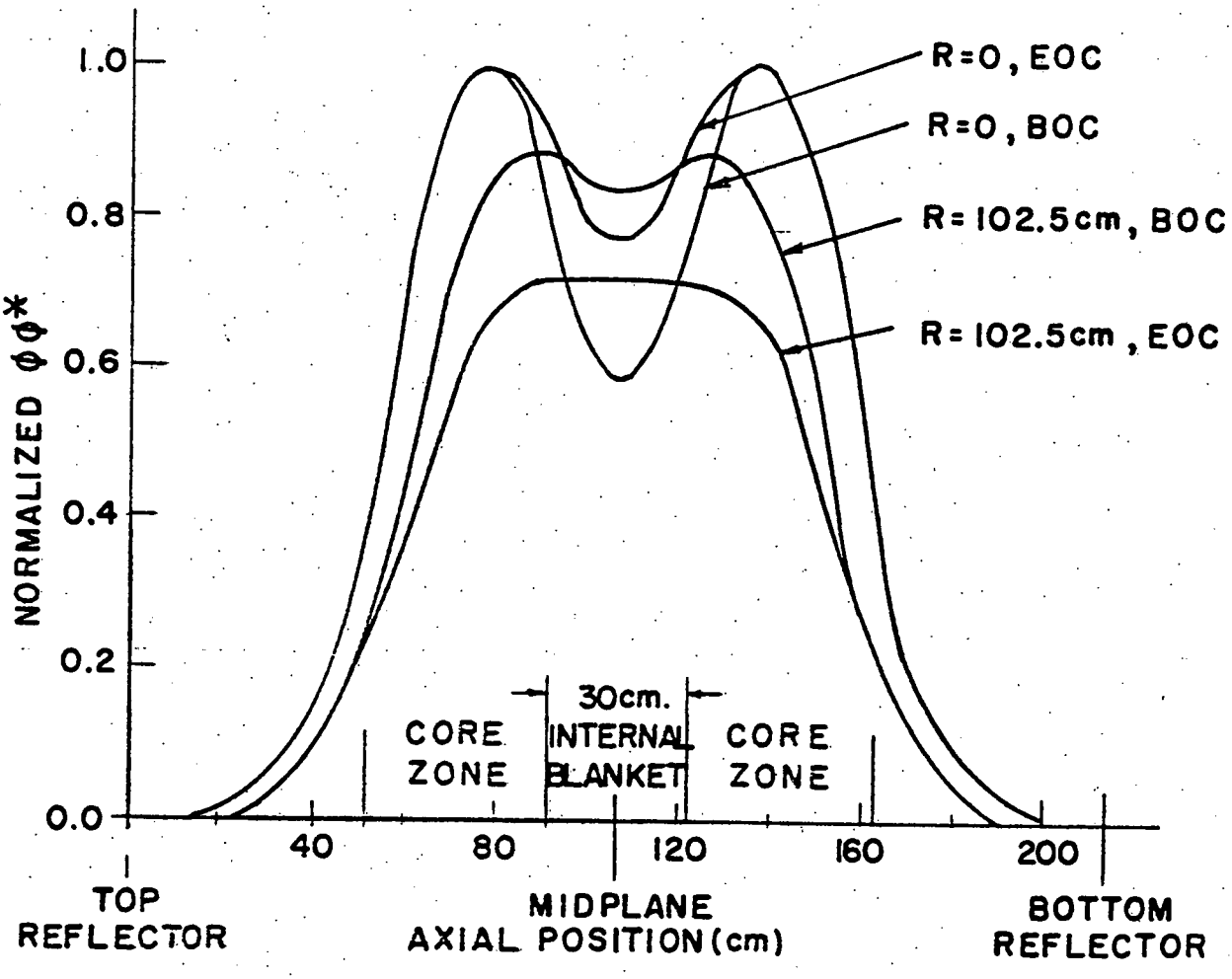

FIG. 2 AXIAL WORTH PROFILES FOR A PARFAIT CORE

3. fewer and/or lower worth control rods reduce the probability and consequences of control malfunction; deletion of control positions permits insertion of more fuel assemblies, which increases the internal breeding ratio, further reducing the reactivity swing during a burnup cycle.

All things considered, the two most significant safety-related changes are probably the large reduction in the sodium void reactivity and the small reduction in Doppler power coefficient — the first being favorable, the second being unfavorable. The full implications of each as regards the probability and consequences of abnormal operating conditions will require a more detailed analysis than has been performed in the present studies.

III. BREEDING PERFORMANCE

Breeding-related characteristics of internally-blanketed LMFBR cores are also of considerable current interest, and somewhat controversial as well (5, 6). At first glance Table I would appear to offer very little advantage in this area. However it should be noted that because of the constraints upon the comparison (imposed to insure that the parfait design could be installed as a replacement core) the full advantages of this concept are not exploited in the example shown.

The potential for improved breeding performance of the parfait configuration and of other internally-blanketed fast reactor cores is attributable to several factors: improved power flattening in the adjacent fissile zones; better neutron utilization due to the larger macroscopic cross section of core fissile material relative to cladding and fission products, higher fissile η due to spectrum hardening; and, if radial-blanket-type assemblies are used, higher uranium concentration (increasing uranium concentration by whatever the means can increase the fertile fission contribution as well as enhance the competition for neutrons vs. parasitic absorbers).

Table III summarizes the results of a series of analytical and empirical investigations undertaken to estimate the extent to which parfait or related core designs could improve the doubling time of fast breeder reactors. The largest single improvement could come through increases in volume fraction fuel permitted by the lower fluence and fluence/power/temperature gradients in the central core region of the parfait design.

One must be cautious in interpreting the results quoted in Table III. The prescriptions represent conservative upper-bound limits, and the total net effect of a design change is more than just the sum of the components listed: other changes (e.g., in enrichment or core shape or volume) are required to restore criticality; and we have not included doubling time penalties due to the increased critical mass which may result from such changes ($\Delta T/T = +\Delta M/M$). Likewise, part of the advantage resulting from the smaller reactivity swing accompanying burnup is not accounted for, and the full advantage of each effect may not be realized if excessively thin fissile and fertile zones are employed. Nevertheless generally beneficial consequences of increasing the fuel concentration and of power-flattening are confirmed.

Experience also underlines the necessity of exploiting all of the advantages permitted by the parfait configuration if an attractive final design is to be achieved — it is relatively easy to select a non-optimal configuration which, in fact, will show no advantage over a conventional design. For example, power flattening by fissile enrichment gradation in an LMFBR incurs an inherent critical mass penalty of on the order of 5% (7), with a comparable increase in doubling time. The use of internal blankets to flatten power may be thought of

TABLE III

Potential Reductions in Doubling Time Associated With the Use of Internal Blankets

	Change	Approximate Prescriptions*	Numerical Values* $(\frac{\Delta v}{v} = 10\%)$	Numerical Values* $(\frac{\Delta \varepsilon}{\varepsilon} = 20\%)$
1.	harder spectrum increases η	$\frac{\Delta T}{T} \leq \frac{-1}{g} \cdot \begin{cases} 0.046 \frac{\Delta \varepsilon}{\varepsilon} \\ 0.054 \frac{\Delta v}{v} \end{cases}$	-2.7%	-4.6%
2.	enhanced competition with parasitic absorbers	$\frac{\Delta T}{T} \leq -a \cdot \begin{cases} \frac{\Delta \varepsilon}{\varepsilon} \\ \frac{\Delta v}{v} \end{cases}$	-8%	-16%
3.	fertile fission factor changes	$\frac{\Delta T}{T} \leq -\delta \left[\frac{\eta}{g} \left(\frac{\nu - 1}{\nu} - a \right) - \frac{1}{1+\delta} \right] \cdot \begin{cases} -\frac{\Delta \varepsilon}{\varepsilon} \\ +\frac{\Delta v}{v} \end{cases}$	-10%	+20%
		Subtotal:	-20.7%	-0.6%
4.	power flattening (at same kw/ft peak power limit and pin diameter)	$\frac{\Delta T}{T} = -\left[\frac{(R/R')}{1 + (\frac{\Delta \varepsilon}{\varepsilon})} - 1 \right]$		-5%

*Derived from (except for η relations, which are empirical findings from multigroup calculations):

g = breeding gain $= \eta \left[\frac{1}{k} + (\frac{\nu - k}{k\nu}) \delta - a(1+\delta) \right] - 2$; here $k \equiv 1.0$ and $g \approx 0.2$

a = parasitic (coolant, clad, control and fission product poison, etc.) absorptions (in entire reactor: core, blanket, reflector) per fission neutron ≈ 0.16

η = mean neutron yield per fissile absorption ≈ 2.34

ν = mean neutron yield per heavy metal fission ≈ 2.95

δ = fertile fissions per fissile fission (in entire reactor: core, blanket) ≈ 0.20

R, R' = peak-to-average power ratios in conventional, parfait cores $\approx 1.45, 1.15$

$\frac{\Delta v}{v}$ = core-average fractional increase in fuel volume fraction = 0.10

$\frac{\Delta \varepsilon}{\varepsilon}$ = fractional increase in fissile concentration in core exclusive of internal blanket = 0.20

T = reactor fissile inventory, M, doubling time, $\propto \frac{\eta(1+\delta)M}{g}$

See Ref. (3) for additional details; empirical findings from multigroup calculations are also incorporated; prescriptions, especially for enrichment changes are quite conservative, i.e., $\leq$ is often $\ll$.

as a scheme for varying mean local enrichment, hence one also starts with a critical mass/doubling time penalty, which must be overcome by other trade-offs. Conversely one must guard against overinflating the attractiveness of the parfait design by comparing it to conventional cores which are not optimized to the same set of ground rules.

IV. IMPROVED CORE DESIGNS

As noted in the preceding section, the demonstrated and potential advantages of the parfait concept outlined in Tables II and III suggest several possible routes to improved system performance.

One might, on first thought, attempt to reduce the doubling time by driving the parfait core to higher burnups, thereby decreasing the ratio of total fuel cycle time to in-core residence time. However if the in-core time of 2 years could be extended by as much as 6 months, then, for a fixed 1 year out-of-core, the doubling time is reduced only 7% — a result which argues against this option. Furthermore, the fluence/power/temperature gradients at the outer core zone/radial blanket interface, which are no less severe than in conventional cores, might well not permit an extended operating cycle because of bowing limitations.

Thus a design having an increased fuel volume fraction in the center core zone (achieved, for example, by increasing the fuel pin diameter and decreasing that of the wire wrap) is proposed. Preliminary calculations indicate the following changes in core performance:

* Increasing the central zone fuel volume fraction from 30 to 35% increases the breeding gain by 17%, decreases the doubling time by 8% and decreases the reactivity swing over a burnup cycle by 9% compared to the uncompacted parfait core.

* The reduction in doubling time and reactivity swing are each about 90% of that which could be achieved by increasing the entire core's fuel fraction to 35%, were that possible.

* The positive reactivity effect of voiding the central zone's sodium is slightly less (~8%) than the corresponding value for the uncompacted parfait design.

Core designs in which the assembly duct walls were removed in the central core zone have also been investigated (2). The results indicated that cores of this type were feasible from a thermal-hydraulic standpoint, and that neutronic performance was improved as well. Such cores may also have interesting safety-related properties with respect to post-accident behavior.

It is interesting to note that design studies of LMFBR cores have been carried out in which the volume fraction of fuel in the inner and outer core zones differed, but in a manner opposite to the present case — the outer zone fuel concentration was increased to achieve power flattening (8).

Recent work at MIT has identified another advantage of the parfait concept: if thorium blankets are used, the U-233 production rate can be increased by about 35% over that from thorium-blanketed conventional core designs (3), also without appreciable penalty to the overall breeding ratio. Hence, if crossed-progeny LWR-LMFBR fueling should prove attractive, internally-blanketed LMFBR's may enhance the benefits achievable.

Our investigations have also confirmed the advantages of the parfait configuration for demonstration plant size LMFBR's, for carbide fueled reactors, and for GCFR's (1), (4).

V. CONCLUSION

These studies have indicated that modest but worthwhile improvements in both safety and breeding performance can be achieved by adoption of the moderately more complicated parfait blanket design for fast reactors. Based on this work, a design in which the volume fraction fuel in the inner core zone is increased would appear promising. While comparable advantages could be achieved in a conventional core if a similar increase in volume fraction were introduced, unlike the parfait design it does not have those other characteristics which permit this option.

ACKNOWLEDGEMENTS

This work was supported in part by the U.S. Energy Research and Development Administration.

REFERENCES

1. G.A. DUCAT, M.J. DRISCOLL and N.E. TODREAS, "Evaluation of the Parfait Blanket Concept for Fast Breeder Reactors," COO-2250-5, MITNE-157, January 1974.

2. R.A. PINNOCK, "Parfait Blanket Configurations for Fast Breeder Reactors," SM Thesis, MIT Nuclear Engineering Dept., June 1975.

3. D.C. ALDRICH, "Parfait Blanket Systems Employing Mixed Progeny Fuels," SM Thesis, MIT Nuclear Engineering Dept., June 1976.

4. M.W. GOLDSMITH, "Evaluation of a Gas-Cooled Fast Breeder Reactor for Ship Propulsion," Nuclear Engineers Thesis, MIT Nuclear Engineering Dept., Aug. 1972.

5. J.C. MOUGNIOT et al., "Breeding Gains of Sodium-Cooled Oxide Fueled Fast Reactors," Trans. Am. Nucl. Soc. 20, 348 (1975); full text translation available as ORNL-TR-2294.

6. Y.I. CHANG, "Review of the French Concept of Heterogeneous Core to Improve the Doubling Time," FRA-TM-77, August 18, 1975.

7. A. TAGISHI and M.J. DRISCOLL, "The Effect of Reactor Size on the Breeding Economics of LMFBR Blankets," COO-2250-13, MITNE-168, Feb. 1975.

8. G. VENDRYES and C.P. ZALESKI, "Etudes Preliminaires Conduisant à Un Concept de Reacteur à Neutrons Rapides de 1000 MWe," CEA-R-2254, (1964).

CHAPTER 5

TREATMENT OF UNIT CELL HETEROGENEITY

5.0 FOREWORD

The work summarized in this chapter will be reported in detail in the topical report: A.A. Salehi, M.J. Driscoll, and O.L. Deutsch, "Resonance Region Neutronics of Unit Cells in Fast and Thermal Reactors," COO-2250-26, MITNE-200, May 1977 (estimated).

In this work an improved equivalence theorem is developed in a form useful for determining heterogeneity-corrected self-shielding $f(\sigma_o)$ factors for fast reactor cross-sections. This work was supported in part by another ERDA-sponsored research project at MIT: i.e., that part dealing with light-water-reactor applications.

Self-shielding factor corrections due to heterogeneity (fuel lumping) are found to be small for typical LMFBR blanket (and core) fuel pins. Hence, it is unlikely that this phenomenon is responsible for any of the discrepancies between calculated and experimental results observed in blanket mockup experiments at MIT.

This chapter is comprised of three parts as follows: first a summary of the subject research will be given; next conclusions pertinent to the work will be drawn; and finally, suggestions for further work will be presented.

5.1 SUMMARY

5.1.1 Introduction

The purpose of this work is to explore and evaluate a new approach to the problem of unit cell homogenization. Two major needs motivated this work:

(a) The results of applying the conventional approach based on equivalence theory to the problem of cell homogenization are still not satisfactory. State of the art LWR computer methods, such as LEOPARD, presently rely upon normalization to an experimental base (L5).

(b) The common failure to consider the slowing down source in the fuel in fast reactors is a demonstrably incorrect oversimplification.

The basis for a new approach has been laid down by the prior investigations of Gregory (G1) and Kadiroglu (K1) at M.I.T. The essential feature is the use of an analytic approximation for the ratio of spatially-averaged moderator to fuel

fluxes in the expression for the equivalent homogenized cross-section. A major contribution of the present work is the development of a generalized correlation for this flux ratio ($R = \bar{\phi}_m/\bar{\phi}_f$), by recourse to various methods such as integral transport and collision probability theory. The derived relationship is valid over a broad range of fuel and moderator optical thicknesses. The final prescription for the flux ratio has been checked against, and normalized to, numerical calculations using the ANISN program (A1).

A linearized form of the flux ratio prescription is developed and used in the expression for the equivalent homogenized cross-section to yield a new equivalence relation that casts heterogeneous cross sections (for any physical process of any isotope) at a given constant background cross-section, σ_0, in terms of the corresponding homogeneous cross-sections evaluated at a modified background cross-section σ_0'. The new equivalence relation, which is applicable to both fast and thermal reactors, is the major achievement of this work.

5.1.2 Flux Ratio Calculations for Unit Cells

As noted in the introduction, the key to the approach analyzed in the present work is the use of simple analytic expressions for the ratio of coolant/moderator to fuel fluxes which can accurately describe the region-average fluxes in a cell. The proposed flux ratio model has the following form:

$$\frac{\bar{\phi}_m(E)}{\bar{\phi}_f(E)} = \frac{1 + F(\tau_{af},\tau_{am},\tau_{sf},\tau_{sm})\cdot\tau_{af}\cdot Q_m}{1 + F(\tau_{am},\tau_{af},\tau_{sm},\tau_{sf})\cdot\tau_{am}\cdot Q_f} \qquad (5.1)$$

where

$\tau_{xi}(E) = \Sigma_x(E)\ell_i$, the optical thickness for process x in region i

ℓ_i = mean Dirac penetration chord length through region i

$\Sigma_x = \sum_j \Sigma_x^j$ macroscopic cross section summed over all j isotopes in the region i (fuel, f, or moderator, m)

Q_m = fraction of neutron source originating in the moderator

Q_f = fraction of neutron source originating in the fuel

The next task is to find an explicit functional form for F in terms of the parameters shown in Eq. (5.1). It has been shown (G1), through the use of collision probability methods, that, in the limit of weak scattering and low absorption optical thicknesses for both the fuel and the moderator, F (for cylindrical unit cells) has the asymptotic value of 1/3. Similarly, it has been found (K1), through track length arguments, that in the limit of strong fuel absorption and weak moderator absorption (with weak scattering in both fuel and moderator) F takes the asymptotic value of 2/3. In the present work it has been shown that for nearly black fuel and moderator regions (still in the limit of weak scattering in

both fuel and moderator) F takes the asymptotic value of 1.0. Finally, we have also shown that for appreciable scattering in both fuel and moderator, the functional dependence of F on scattering optical thickness is of the form:

$$F \propto (1 + \omega'\tau_{sm})(1 + \omega'\tau_{sf}) \tag{5.2}$$

where ω' is a fitting parameter chosen to force agreement with numerical results.

Using the foregoing results as guidelines, an analytical expression for F has been developed to cover the intermediate ranges of optical thicknesses. Numerous functions could be used to smoothly join the various asymptotic limits; we have chosen one that is both simple in form and which agrees quite well with numerical results. This function has the following general form:

$$F(\tau_{af},\tau_{am},\tau_{sm},\tau_{sf}) = \frac{\frac{1}{3}\left(1+\frac{\omega\tau_{af}^{\,n}}{1+\tau_{af}^{\,n}}\right) + \omega\tau_{am}^{\,n'}}{1 + \omega\tau_{am}^{\,n'}} (1+\omega'\tau_{sm})(1+\omega'\tau_{sf}) \tag{5.3}$$

Noting the symmetry between the numerator and denominator of Eq. (5.1) (the necessity of symmetry can be shown quite rigorously by use of integral transport theory and/or the governing slowing down equations) the final form of the flux ratio model will thus be:

$$\frac{\bar{\phi}_m}{\bar{\phi}_f} = \frac{1+\dfrac{\frac{1}{3}\left(1+\dfrac{\omega\tau_{af}}{1+\omega\tau_{af}}\right)^{n}+\omega\tau_{am}^{\,n'}}{1+\omega\tau_{am}^{\,n'}}\cdot(1+\omega'\tau_{sf})(1+\omega'\tau_{sm})\cdot\tau_{af}\cdot Q_m}{1+\dfrac{\frac{1}{3}\left(1+\dfrac{\omega\tau_{am}}{1+\omega\tau_{am}}\right)^{n}+\omega\tau_{af}^{\,n'}}{1+\omega\tau_{af}^{\,n'}}\cdot(1+\omega'\tau_{sm})(1+\omega'\tau_{sf})\cdot\tau_{am}\cdot Q_f} \qquad (5.4)$$

where ω and ω' are fitting parameters

n and n' are positive powers to which τ_{af} and τ_{am} are raised, respectively.

So far no mention has been made of resonance cross sections, and the way in which the associated WR, IR, and NR approximations are to be incorporated into the flux ratio model. Here, we will only discuss, very briefly, the intermediate resonance approximation (IR) since it incorporates the wide resonance (WR) and narrow resonance (NR) limits. The basis for the IR approximation (B2, G3, G4, G5, H3, L4, S3, S4) is that it neither completely denies nor totally admits the role of scattering for removing neutrons: absorption plus a fraction of the scattering events remove neutrons from under a resonance. The IR approximation is implemented through the introduction of three new parameters λ, ν, $\bar{\mu}$. For a resonance absorber with no admixed moderator the removal cross section, $\sigma_r(E)$ becomes:

$$\sigma_r(E) \equiv \sigma_f(E) = \sigma_{af} + \lambda\sigma_{sf} \qquad (5.5)$$

where λ determines the fraction of scattering events contributing to removal.

Note that for $\lambda = 1$:

$$\sigma_f(E) = \sigma_{af}(E) + \sigma_{sf}(E) = \sigma_{tf}(E) \tag{5.6a}$$

which is the NR case; and for $\lambda = 0$:

$$\sigma_f(E) = \sigma_{af}(E) \tag{5.6b}$$

which is the WR case.

Similar arguments hold for moderator admixed with fuel and for moderator/coolant in the moderator/coolant region.

To implement the above ideas in conjunction with the flux ratio model, it is convenient to introduce the following parameters, which greatly simplify the subsequent notation:

$$\delta_f(E) = \tau_{af}(E) + \lambda\tau_{sf}(E) + \tau_{anf}(E) + \nu\tau_{snf}(E) \tag{5.7}$$

$$\delta_m(E) = \tau_{am}(E) + \bar{\mu}\tau_{sm} \tag{5.8}$$

$$\beta(E) = 1 + \omega'[(1-\lambda)\tau_{sf}(E) + (1-\nu)\tau_{snf}(E)] \tag{5.9}$$

$$\rho(E) = 1 + \omega'(1-\bar{\mu})\tau_{sm}(E) \tag{5.10}$$

$$\alpha_f(E) = \frac{\frac{1}{3}\left[1 + \frac{\omega\delta_f{}^n(E)}{1+\omega\delta_f{}^n(E)}\right] + \omega\delta_m{}^{n'}(E)}{1 + \omega\delta_m{}^{n'}(E)} \tag{5.11}$$

$$\alpha_m(E) = \frac{\frac{1}{3}\left[1 + \frac{\omega\delta_m{}^{n}(E)}{1+\omega\delta_m{}^{n}(E)}\right] + \omega\delta_f{}^{n'}(E)}{1 + \omega\delta_f{}^{n'}(E)} \tag{5.12}$$

where

τ_{anf} and τ_{snf} are the absorption and scattering optical thicknesses of the non-resonance material in the fuel.

The rest of the parameters are as previously defined.

Substituting Eqs. (5.7) - (5.12) in Eq. (5.4) there results:

$$\frac{\bar{\phi}_m(E)}{\bar{\phi}_f(E)} \equiv R(E) = \frac{1 + \alpha_f(E)\beta(E)\rho(E)Q_m(E)}{1 + \alpha_m(E)\beta(E)\rho(E)Q_f(E)} \tag{5.13}$$

which is the generalized form for the flux ratio taking into account the (IR) parameters. Note that Eq. (5.13) is a continuous function of energy; its discretization into energy groups by defining group-averaged parameters is straightforward:

$$\left|\frac{\bar{\phi}_m}{\bar{\phi}_f}\right|_g \equiv R_g = \frac{1 + \alpha_{fg}\beta_{gg}\rho_{gg}\delta_{fg}Q_{mg}}{1 + \alpha_{mg}\beta_{gg}\rho_{gg}\delta_{mg}Q_{fg}} \tag{5.14}$$

Cylindrical and spherical unit cells share similar functional forms for the flux ratio model: only the values of (n,n') and (ω,ω') are changed. The planar case, however, required inclusion of an extra term ($1+\omega'\ell n \frac{1}{\delta_m}$) multiplying β_{gg} in Eq. (5.14), introduced here without proof (see Ref.(Z1)).

Lastly, parameters (n,n') and (ω,ω') are found to have the following values for the three unit cell configurations:

(1) cylindrical:

$n = 1.0$; $n' = 0.5$

$\omega = 0.24$; $\omega' = 0.06$

(2) spherical:

$n = 0.5$; $n' = 0.5$

$\omega = 0.27$; $\omega' = 0.09$

(3) planar:

$n = 1.0$; $n' = 0.5$

$\omega = 0.15$; $\omega' = 0.03$

5.1.3 Numerical Verification of the Unit Cell Model

In what follows we will be discussing numerical results developed using the ANISN code, primarily employed in the S_8P_1 option , comparing them with our predicted results. The calculations are done for two-region unit cells with a white boundary condition used for the outer region of the cylindrical and spherical unit cells to minimize the effects of specular reflections (N1).

The dependence of the flux ratio on the magnitude of the scattering and removal cross-sections in cylindrical unit cells are shown in samples from an extensive series of numerical computations, summarized in Tables 5.1 and 5.2. As seen, the results of the analytical model are within a maximum discrepancy

Table 5.1

Numerical and Calculated Flux Ratios as a Function of Fuel Optical Absorption Thickness

τ_{af}	τ_{am}	τ_{sm}	τ_{sf}	ω	ω'	R calc.	R ANISN
0.01181	0.00006	0.12992	0.60355	0.24	0.06	1.004	1.005
0.42251	↓	↓	↓	↓	↓	1.161	1.176
0.84482						1.345	1.360
1.26713						1.545	1.551
1.68944						1.760	1.750
2.1117						1.985	1.954
2.53402						2.218	2.164
2.95619						2.459	2.380
3.37883						2.706	2.600
3.80095						2.958	2.825
4.22324						3.214	3.053
4.64556						3.474	3.286
5.06787						3.737	3.521
5.49017						4.003	3.760
5.91248						4.271	4.002
8.02775						5.641	5.247
8.87278						6.198	5.757
9.71781						6.758	6.271
10.56285						7.322	6.789
28.16759						19.367	17.825
45.71309						31.528	28.859
63.37708						43.805	39.969
218.29797						151.698	137.360
373.21802						259.641	234.779
528.14229						367.594	332.206
6.33771						4.543	4.248

$V_f/V_m = 0.30122$ $r_f = 0.3175$ $r_m = 0.6599$

Table 5.2

Numerical and Calculated Flux Ratios as a Function of Optical Scattering Thickness

τ_{af}	τ_{am}	τ_{sm}	τ_{sf}	ω	ω'	R calc.	R ANISN
1.00	1.8002	0.1000	0.1000	0.24	0.06	1.551	1.463
1.00	1.8002	0.5001	0.1000	↓	↓	1.564	1.473
1.00	1.8002	2.50028	0.100	↓	↓	1.630	1.527
1.00	1.8002	50.0057	0.100	↓	↓	3.191	2.855
1.00	1.8002	0.5001	0.800	↓	↓	1.588	1.523
1.00	1.8002	0.5001	5.000	↓	↓	1.729	1.818
1.00	1.8002	0.5001	50.000	↓	↓	3.244	3.711
1.00	1.8002	0.5001	99.9998	↓	↓	4.926	4.960

$r_f = 0.3175$ $r_m = 0.4490$ $V_f/V_m = 1$

Table 5.3

Numerical and Calculated Flux Ratios as a Function of Source Distribution

τ_{af}	τ_{am}	τ_{sm}	τ_{sf}	Q_m/Q_f	ω/ω'	R calc.	R ANISN
2.5	1.20709	1.20709	0.13970	1.0 0.0	0.24 0.06	2.545	2.390
				0.8 0.2		1.946	1.860
				0.6 0.4		1.484	1.445
				0.4 0.6		1.118	1.109
				0.2 0.8		0.820	0.832
				0.0 1.0		0.573	0.599

of 15%, and an average error of about 5%, of the ANISN results. As shown in Table 5.3 the flux ratio model correctly predicts the effects of source distribution; a property which is very important in fast reactor calculations.

As a final note, it is important to point out that the agreement between the predicted and the numerical results could be improved substantially, if desired, by a different choice of values for the fitting parameters (n,n') and (ω,ω') in the range of maximum interest for a specific application.

5.1.4 Homogeneous Self-Shielding Factors

The discussion which follows immediately is confined to homogeneous systems where the spatial and angular dependence of the flux are suppressed, and only the energy variable, E, is of concern. Homogeneous self-shielding is discussed first to introduce the basic concepts necessary for the later extension of the methodology to heterogeneous media.

The fundamental and physically meaningful assumption made in most reactor physics calculations is conservation of total reaction rate. In fact, it is through the utilization of the above assumption that we shall define the group-averaged homogeneous cross-section as:

$$\int_{V_{cell}}\int_{\Delta Eg}\Sigma_x^j(E)\phi(E)dVdE = \Sigma_{xg}^j\cdot\int_{V_{cell}}\int_{\Delta Eg}\phi(E)dVdE \qquad (5.15)$$

where the quantity on the left of Eq. (5.15) is the true reaction rate, "$\Sigma_{xg}{}^{j}$" is the macroscopic group-averaged cross section for the particular process "x" of isotope "j", and the double integral multiplying "$\Sigma_{xg}{}^{j}$" is the true total flux of neutrons in the energy range ΔE_g (ΔE_g is to be interpreted as a fine-width group containing only one resonance). The appropriate weighting flux $\phi(E)$ in Eq. (5.15) can be found by solving the slowing down equation for a uniform mixture of infinite extent:

$$[\sigma_0+\sigma_{tf}(E,T)]\phi(E,T,\sigma_0) = \int_E^{E/\alpha_m} \frac{\sigma_0}{(1-\alpha_m)}\,\phi(E')\frac{dE'}{E'} + \int_E^{E/\alpha_f} \frac{\sigma_{sf}(E',T)}{(1-\alpha_f)}\,\phi(E')\frac{dE'}{E'} \qquad (5.16)$$

where

$\sigma_0 = \frac{\Sigma_{tm}}{N_f}$; Σ_{tm} = constant moderator cross section ($\Sigma_{am} << \Sigma_{sm}$)

N_0 = number of resonance absorber nuclei per unit volume

σ_{af}, σ_{rf}, σ_{pf} = resonance absorption, resonance scattering, and potential scattering cross-section, respectively, of the resonance absorber

$\sigma_{sf}(E,T) = \sigma_{rf}(E,T) + \sigma_{pf}$

$\sigma_{tf}(E,T) = \sigma_{af}(E,T) + \sigma_{sf}(E,T)$

$\alpha_j = \left(\frac{A_j-1}{A_j+1}\right)^2$; A_j being the ratio of the mass of isotope j to the mass of the neutron.

Note that "moderator" in the above usage refers to all non-resonance-absorber nuclei present. Using the NR approximation for the moderator and the IR approximation for the absorber (G4), leads to:

$$\phi(E,T,\sigma_0) = \frac{\sigma_0 + \lambda\sigma_{pf}}{\sigma_{af}(E,T) + \lambda\sigma_{sf}(E,T) + \sigma_0} \frac{1}{E} \qquad (5.17)$$

where the source is normalized such that "$\phi = 1/E$" will be the off-resonance reference value for the flux per unit energy. Upon substituting Eq. (5.17) into Eq. (5.15), and specializing to the U-238 capture cross-section as an important example, one obtains:

$$\sigma_{cg}(T,\sigma_0) = \frac{\int_{\Delta Eg} \frac{\sigma_0 + \lambda\sigma_{pf}}{\sigma_{af}(E,T)+\lambda\sigma_{sf}(E,T)+\sigma_0} \sigma_c(E,T)\frac{dE}{E}}{\int_{\Delta Eg} \frac{\sigma_0 + \lambda\sigma_{pf}}{\sigma_{af}(E,T)+\lambda\sigma_{sf}(E,T)+\sigma_0} \frac{dE}{E}} \qquad (5.18)$$

Because σ_0 and σ_{pf} are essentially constant within ΔEg, they can be cancelled-out from the numerator and denominator of Eq. (5.18) to give:

$$\sigma_{cg}(T,\sigma_0) = \frac{\int_{\Delta Eg} \frac{\sigma_c(E,T)}{\sigma_{af}(E,T)+\lambda\sigma_s(E,T)+\sigma_0} \frac{dE}{E}}{\int_{\Delta Eg} \frac{1}{\sigma_{af}(E,T)+\lambda\sigma_s(E,T)+\sigma_0} \frac{dE}{E}} \qquad (5.19)$$

which is the effective capture cross-section at temperature T and constant background cross-section σ_0. If σ_0 in Eq. (5.19) approaches infinity, the following result will be obtained:

$$\sigma_{cg}^{\infty} = \frac{\int_{\Delta Eg} \sigma_c(E,T)\frac{dE}{E}}{\int_{\Delta Eg} \frac{dE}{E}} \qquad (5.20)$$

which is the definition of the infinite dilution cross-section.

For convenience one can represent the effective cross-section given by Eq. (5.19), which is a function of both T and σ_0, by an infinite dilution cross-section and a set of modifying functions called self-shielding factors; or to put it quantitatively:

$$\sigma_{cg}(T,\sigma_0) = f_{cg}(T,\sigma_0)\cdot\sigma_{cg}^{\infty} \qquad (5.21)$$

Thus the complications involved in the integration over resonance structure, as indicated by Eq. (5.19), are separated from the calculation of the effective multigroup constants for a specific material composition. Tables of f-factors are precomputed for the elastic, fission, capture, total, and transport cross sections and for arbitrary sets of T and σ_0 values (B3, K6). The f-factors for any given T and σ_0 can then be obtained by interpolating in these tables. The f-factor can then be multiplied by the proper infinite-dilution cross section to get the required effective cross section, $\sigma_{xg}(T,\sigma_0)$ as indicated by Eq. (5.21). The success of the above approach, however, relies heavily on the availability of accurate schemes for both

temperature and σ_0 interpolation of the self-shielding factor, $f_{xg}(T,\sigma_0)$. One expression used as a fitting function (K4) for the self-shielding factor as a function of σ_0, at a fixed temperature T, is:

$$f_{cg}(\sigma_0) = A \tanhB(\ell n\sigma_0 + C) + D \qquad (5.22)$$

where A, B, C, and D are constants determined by four values of f_{cg} at given σ_0 values. As for temperature interpolation at a fixed σ_0, a Lagrange-three-point interpolation scheme predicts, very accurately, the shielding factors for any current temperature, T.

Figures 5.1 and 5.2 (from Ref. (K4)) show the self-shielding factor for group 14 (86.5-111 Kev) of U-238 as a function of σ_0 and T, respectively. As seen, the results predicted by the aforementioned interpolation schemes (shown by the solid line) are in excellent agreement with the actual self-shielding represented by the dark circles. This concludes the discussion of homogeneous self-shielding, hopefully adequate to lay the groundwork for the introduction of heterogeneous self-shielding factors. For more complete expositions on the subject of homogeneous self-shielding the following references are recommended: B2, G1, K1, K4, K6, S6, S7.

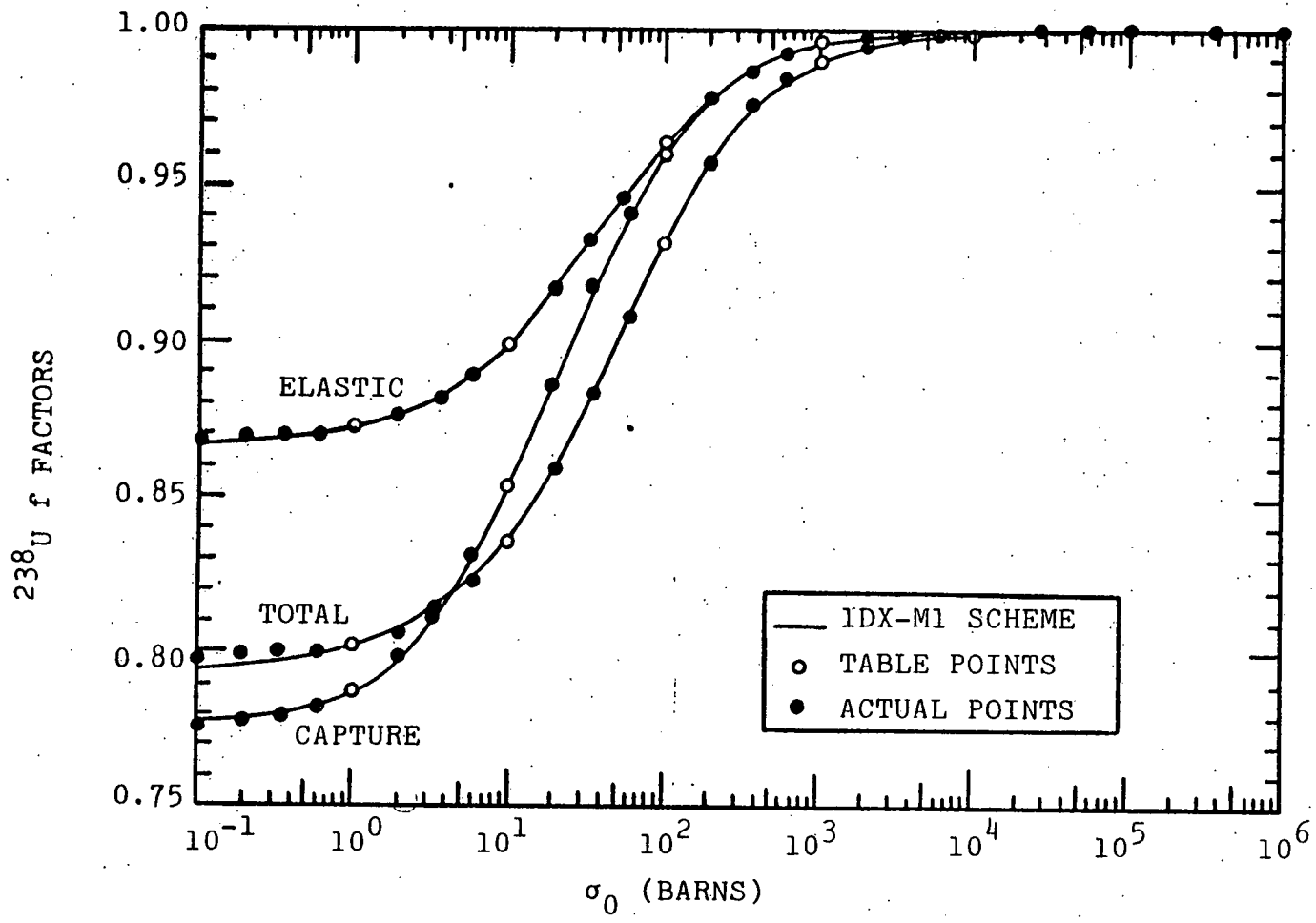

FIG. 5.1 A COMPARISON OF THE 1DX-M1 σ_0 INTERPOLATION WITH THE ACTUAL f FACTOR σ_0 BEHAVIOR (FOR GROUP 14 AND T=300°K)

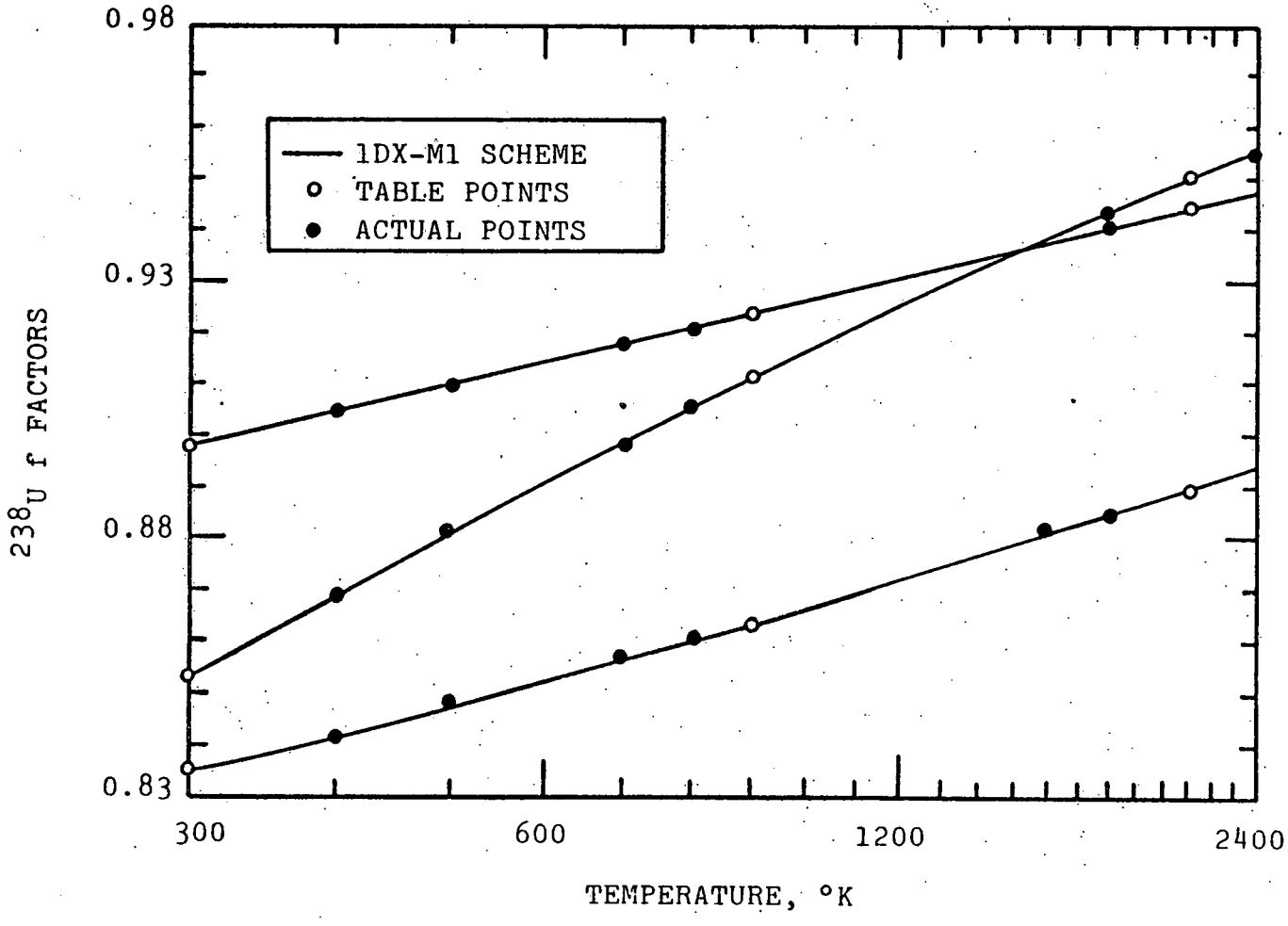

FIG. 5.2 A COMPARISON OF THE 1DX-M1 TEMPERATURE INTERPOLATION SCHEME WITH THE ACTUAL f FACTOR TEMPERATURE BEHAVIOR (FOR GROUP 14 AND σ_0 = 10 BARNS)

5.1.5 Heterogeneous Self-Shielding Factors

At this point almost all the groundwork necessary for generating "equivalent" group parameters, ($\overline{\nu\Sigma}_{fg}$, $\overline{\Sigma}_{cg}$, $\overline{\Sigma}_{gg'}$,.... etc.), which are constant over the entire volume occupied by any given cell in a reactor, has been developed. The group constants generated should, when used in a group-diffusion-theory calculation for the whole reactor, reproduce the same average reaction rates over a given cell as would be determined if an exact energy dependent transport calculation was performed for a heterogeneous reactor with all geometrical characteristics of the unit cells treated explicitly.

An appropriate starting point is with the definition of an equivalent homogenized capture cross-section specialized to a two-region unit cell:

$$\Sigma_{cg}^{j} = \frac{\int_{V_{cell}} dV \int_{\Delta Eg} dE\ \Sigma_c^j(\underline{r},E,T)\phi(\underline{r},E)}{\int_{V_{cell}} dV \int_{\Delta Eg} dE\ \phi(\underline{r},E)} \tag{5.23}$$

If the resonance absorber, j, is present only in the fuel region; then Eq. (5.23) can be expanded to yield the following form:

$$\Sigma_{cg} = \frac{\int_{\Delta Eg} \Sigma_{cf}(E,T)\overline{\phi}_f(E)dE}{\int_{\Delta Eg} [1+\frac{V_m}{V_f} R(E)]\overline{\phi}_f(E)dE} \tag{5.24}$$

where

$$\bar{\phi}_m(E) = \frac{1}{V_m} \int_{V_m} \phi(\underline{r},E)dV \; ; \qquad (5.25)$$

$$\bar{\phi}_f(E) = \frac{1}{V_f} \int_{V_f} \phi(\underline{r},E)dV \qquad (5.26)$$

To be able to solve Eq. (5.24) both R(E) and $\bar{\phi}_f(E)$ must be known. An expression for the flux ratio R(E) has already been derived in Section 5.1.2; as for the spatially averaged fuel flux $\bar{\phi}_f(E)$, one can write down the equivalent of Eq. (5.16) for each region of the assumed two-region unit cell, and solve the pair of relations to find:

$$\bar{\phi}_f(E) = \frac{V_m\Sigma_{sm} + V_f\Sigma_{snf} + V_f\lambda\Sigma_{pf}}{V_f[\Sigma_{af}(E)+\lambda\Sigma_{sf}(E)+\Sigma_{tnf}(E)]+V_m\Sigma_{tm}(E)R(E)} \frac{1}{E} \qquad (5.27)$$

Although expressions for R(E) and $\bar{\phi}_f(E)$ have been obtained, the problem is still intractable unless plausible simplifications are introduced into Eq. (5.13); the following are to be implemented:

(a) Linearization of the expression for R(E), by using group-averaged values for the values of τ appearing in α_f, α_m, β, ρ. Numerical studies confirm that this is an acceptable device. Thus the numerator of Eq. (5.13) becomes $[1+\bar{\gamma}_f\delta_f(E)]$, with $\bar{\gamma}_f=\alpha_f\beta\rho Q_m$ evaluated at group-averaged values for the τ involved. In like manner the denominator of Eq. (5.13) will

take the similar form $[1+\bar{\gamma}_m \delta_m(E)]$. As will shortly become clear, such linearization is apparently a sufficient and necessary condition for the existence of an equivalence theorem.

(b) $\Sigma_{tm}(E)$ and $\Sigma_{tnf}(E)$ are very weakly dependent on energy, especially within the range of energy covered by a typical group width. Hence we can treat $\delta_m(E)$ as constant over ΔEg. This last assumption in conjunction with the one made in part (a) immediately implies that the denominator of Eq. (5.13) can be taken as constant, and it shall henceforth be denoted by θ.

Based on assumptions (a) and (b), Eq. (5.13) can now be written in a more manageable form:

$$R(E,T) = \frac{1}{\theta}\left[1 + \bar{\gamma}_f \delta_f(E,T)\right] \tag{5.28}$$

where θ and $\bar{\gamma}_f$ are as previously defined.

Substituting Eqs. (5.27) and (5.28) into Eq. (5.24), the following is obtained:

$$\Sigma_{cg} = \frac{\displaystyle\int_{\Delta Eg} \frac{(V_m\Sigma_{sm}+V_f\Sigma_{snf}+V_f\lambda\Sigma_{pf})\cdot\Sigma_{cf}(E,T)}{V_f\Sigma_{af}(E,T)+V_f\lambda\Sigma_{sf}(E,T)+V_f\Sigma_{tnf}+V_m\Sigma_{tm}\frac{1}{\theta}[1+\bar{\gamma}_f\delta_f(E,T)]}\frac{dE}{E}}{\displaystyle\int_{\Delta Eg} \frac{(V_m\Sigma_{sm}+V_f\Sigma_{snf}+V_f\lambda\Sigma_{pf})\cdot\{1+\frac{V_m}{V_f}\frac{1}{\theta}[1+\bar{\gamma}_f\delta_f(E,T)]\}}{V_f\Sigma_{af}(E,T)+V_f\lambda\Sigma_{sf}(E,T)+V_f\Sigma_{tnf}+V_m\Sigma_{tm}\frac{1}{\theta}[1+\bar{\gamma}_f\delta_f(E,T)]}\frac{dE}{E}} \tag{5.29}$$

By performing some simple algebra on the above equation, it follows that:

$$\frac{V_f}{V_{cell}}\,\sigma_{cg} = \frac{\int_{\Delta Eg} \frac{\sigma_{cf}}{\sigma_{af} + \lambda\sigma_{sf} + \sigma_0'}\,\frac{dE}{E}}{\int_{\Delta Eg} \frac{1+\frac{V_m}{V_f}\left[\frac{1}{\theta}+\varepsilon'''\sigma_{cf}+\varepsilon'''\sigma_{ff}+\varepsilon'''\lambda\sigma_{sf}+\varepsilon'''\frac{\Sigma_{tnf}}{N_f}\right]}{\sigma_{af} + \lambda\sigma_{sf} + \sigma_0'}\,\frac{dE}{E}} \tag{5.30}$$

where

$$\sigma_0' = \frac{\bar{\Sigma}_{tnf}}{\bar{N}_f} + \frac{1}{\theta+\bar{\gamma}_f\delta_m}\,\frac{\bar{\Sigma}_{tm}}{\bar{N}_f} \tag{5.31}$$

with the bars denoting volume-weighted homogenization

$$\varepsilon''' = \frac{1}{\theta}\,\bar{\gamma}_f N_f\,\frac{V_m}{V_f}\,\ell_f$$

σ_{ff} = the resonance absorber fission cross-section

The rest of the parameters are as previously defined.

By inverting Eq. (5.30) and using the definition of the effective homogeneous cross-section, namely Eq. (5.19), one can show the following rigorous result:

$$\sigma_{cg}^{het}(T,\sigma_0) = \frac{\sigma_{cg}^{hom}(T,\sigma_0')}{\eta + \varepsilon''\sigma_{cg}^{hom}(T,\sigma_0')} \tag{5.32}$$

where

$$\eta = \frac{V_f}{V_{cell}} + \frac{1}{\theta}\frac{V_m}{V_{cell}} + \varepsilon''\sigma_{fg}^{hom}(T,\sigma_0') + \varepsilon''\sigma_{sg}^{hom}(T,\sigma_0') + \frac{\bar{\gamma}_f}{\theta}\frac{V_m}{V_{cell}}\tau_{tng}$$

$$\varepsilon'' = \frac{V_f}{V_{cell}}\varepsilon'''$$

σ_{cg}^{hom} = group-averaged homogeneous capture cross-section

σ_{fg}^{hom} = group-averaged homogeneous fission cross-section

σ_{sg}^{hom} = group-averaged homogeneous elastic scattering cross section

σ_{cg}^{het} = group-averaged "homogenized" capture cross-section

Σ_{tng} = total non-resonance cross-section in the fuel region for group g

It is important to note that Eq. (5.32) predicts the correct homogenized cross-section under any condition so long as the homogeneous part (i.e. $\sigma_{cg}^{hom}(T,\sigma_0')$) is treated correctly elsewhere in the literature.

Recalling Eq. (5.21) for the definition of the self-shielding factor, and applying it to Eq. (5.32), leads to the following important expression:

$$f_{cg}^{het}(T,\sigma_0) = \frac{1}{\eta + \varepsilon} f_{cg}^{hom}(T,\sigma_0') \qquad (5.33)$$

where $\varepsilon = \varepsilon' \; f^{hom}(T,\sigma_0')$.

Equation (5.33) and its accompanying prescriptions constitute a New Equivalence Relationship, whereby the corresponding f-factor for the heterogeneous cell is expressed in terms of the f-factor for a homogeneous cell evaluated at a modified value of the constant background cross-section - namely σ_0'.

Finally, it is worthwhile to present a brief review of what we will call the "conventional" methods used hitherto and compare their results with those of the present method - i.e. Eq. (5.33). Conventionally, one uses the second equivalence theorem to make the heterogeneity correction. The statement of the theorem is as follows (H1, L4): a heterogeneous system will have the same resonance integral as a homogeneous systems evaluated at:

$$\sigma_0' = \frac{\overline{\Sigma}_{tnf}}{\overline{N}_f} + \frac{1-c}{N_f \ell_f} \frac{a}{1+(a-1)c} = \frac{\overline{\Sigma}_{tnf}}{\overline{N}_f} + \frac{1}{1+\frac{1}{a}\tau_{tm}} \frac{\overline{\Sigma}_{tm}}{\overline{N}_f} \qquad (5.34)$$

where c is the Dancoff-Ginsberg factor given by:

$$1-c = \frac{\tau_{tm}}{1+\frac{1}{a}\tau_{tm}} \text{ , in Bell's approximation (B1)} \qquad (5.35)$$

The parameter "a" is known as the Levine correction factor (L2). It has been found that a value of $\frac{1}{a} \simeq 0.79$ yields accurate results over the entire range of practical lump sizes. Note that the σ_0' defined in Eq. (5.34) differs from that in Eq. (5.31).

Applying the theorem to Eq. (5.19) yields the following conventional result in terms of the f-factors:

$$f_{cg}^{het}(T,\sigma_0) = f^{hom}(T,\sigma_0') \tag{5.35}$$

Upon comparing Eqs. (5.33) and (5.36) we immediately note that the factor $\frac{1}{\eta + \varepsilon}$ has been set equal to 1.0 in the conventional method. This discrepancy raises questions as to the validity of the second equivalence theorem as applied to cross-sections but not to resonance integrals. The difficulty stems from the fact that the true integrated heterogeneous flux, as given by the denominator of Eq. (5.23), has in the conventional approach been replaced by a homogeneous flux evaluated at σ_0' in the denominator of Eq. (5.19), thus leading to the present disparity. The modified total background cross section, however, is smaller than σ_0' in Eq. (5.31), which helps cancel part of this discrepancy.

5.1.6 Numerical Verification of Self-Shielding Factors

In the present section homogeneous-to-heterogeneous corrections are calculated with the new equivalence theorem, and the results compared to equivalent output from the LEOPARD code (L5), a state-of-the-art LWR unit cell program. The base-case unit cell data used in both calculations is representative of current commercial PWR reactors (specifically, Maine Yankee). The EPRI version of LEOPARD was employed,

together with its ENDF/B IV derived cross-section library. For the self-shielding-factor method, cross-sections and f-factors as a function of σ_0 were taken from the LIB-IV fast reactor cross-section set developed by LASL (also derived from the ENDF/B IV library).

Figure 5.3 is a plot of homogeneous broad group capture cross-sections (σ_c^{hom}) for U-238 as a function of moderator optical thickness (τ_{tm}), with the fuel diameter kept constant. The broad group cross section is defined by a 1/E-weighted group collapse:

$$\sigma_c^{hom} = \sum_{GP26}^{GP49} \sigma_i \Delta u_i / \sum_{26}^{49} \Delta U_i \qquad (5.37)$$

where groups 26 through 49 span the energy range from 0.6826 ev to 5.53 Kev. As is evident from the figure the capture cross-sections obtained using self-shielding factors are in good agreement with the corresponding parameters generated using LEOPARD. Depending on one's point of view this either validates the f-factor formalism, LEOPARD, or both. Table 5.4 contains the tabulated results of Fig. 5.3, including percentage differences.

In Fig. 5.4 the analytic and the LEOPARD results for the ratio of heterogeneous-to-homogeneous self-shielding factors $[f^{het}(\sigma_0)/f^{hom}(\sigma_0)]$ as a function of moderator optical thickness (at constant fuel pin diameter) are shown. The agreement shown between the two results is tolerably good (particularly

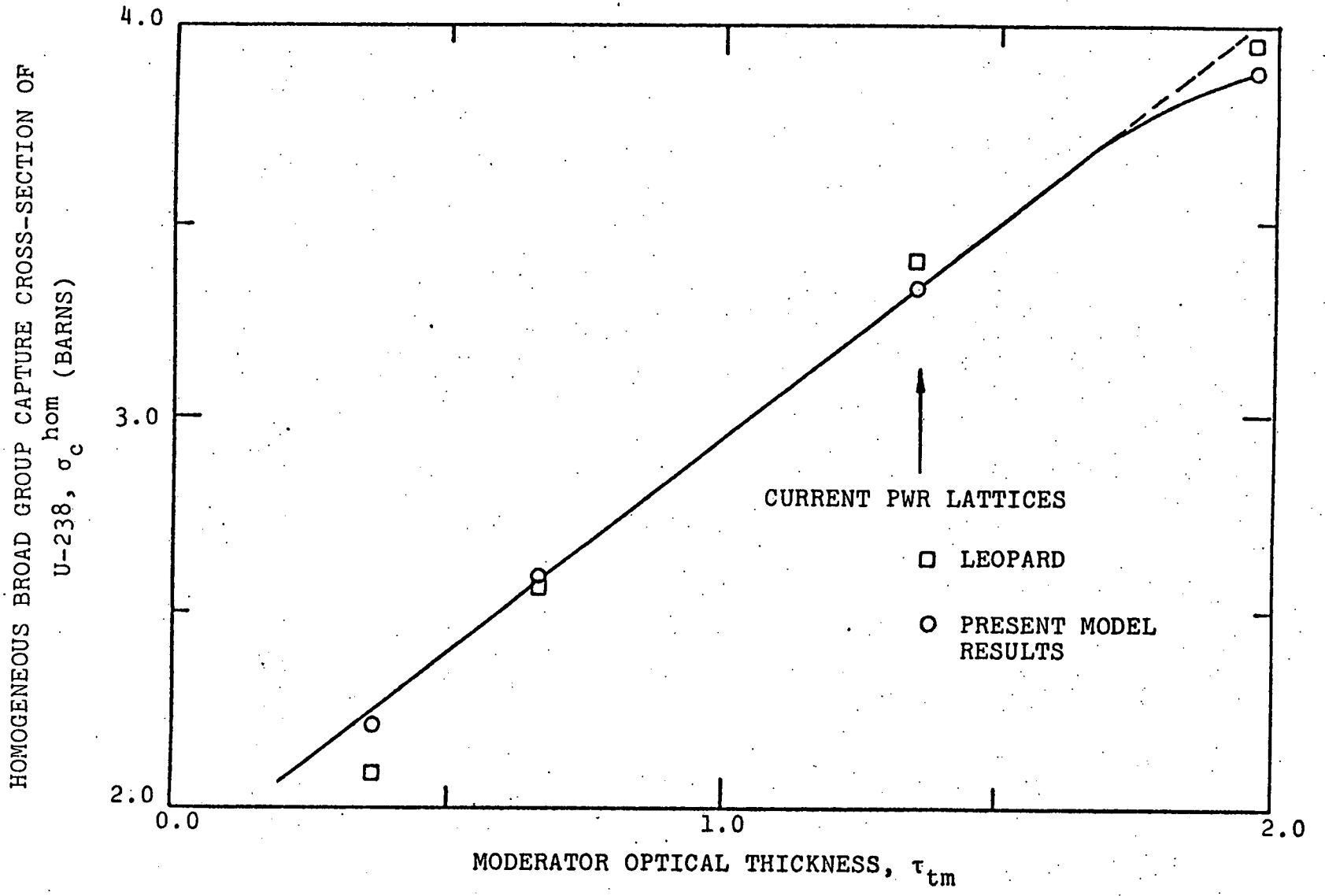

FIG. 5.3 HOMOGENEOUS BROAD GROUP CAPTURE CROSS-SECTION OF U-238 AS A FUNCTION OF MODERATOR OPTICAL THICKNESS

Table 5.4

Tabulated Results Applicable to Fig. 5.3

Moderator Optical Thickness	σ_c^{hom} (barns) analytical, using f-factor formalism	σ_c^{hom} (barns) LEOPARD	Δ% percent difference
0.361	2.218	2.088	+6.2
0.663	2.591	2.565	+1.0
1.354	3.336	3.410	-2.2
1.965	3.883	3.962	-2.0

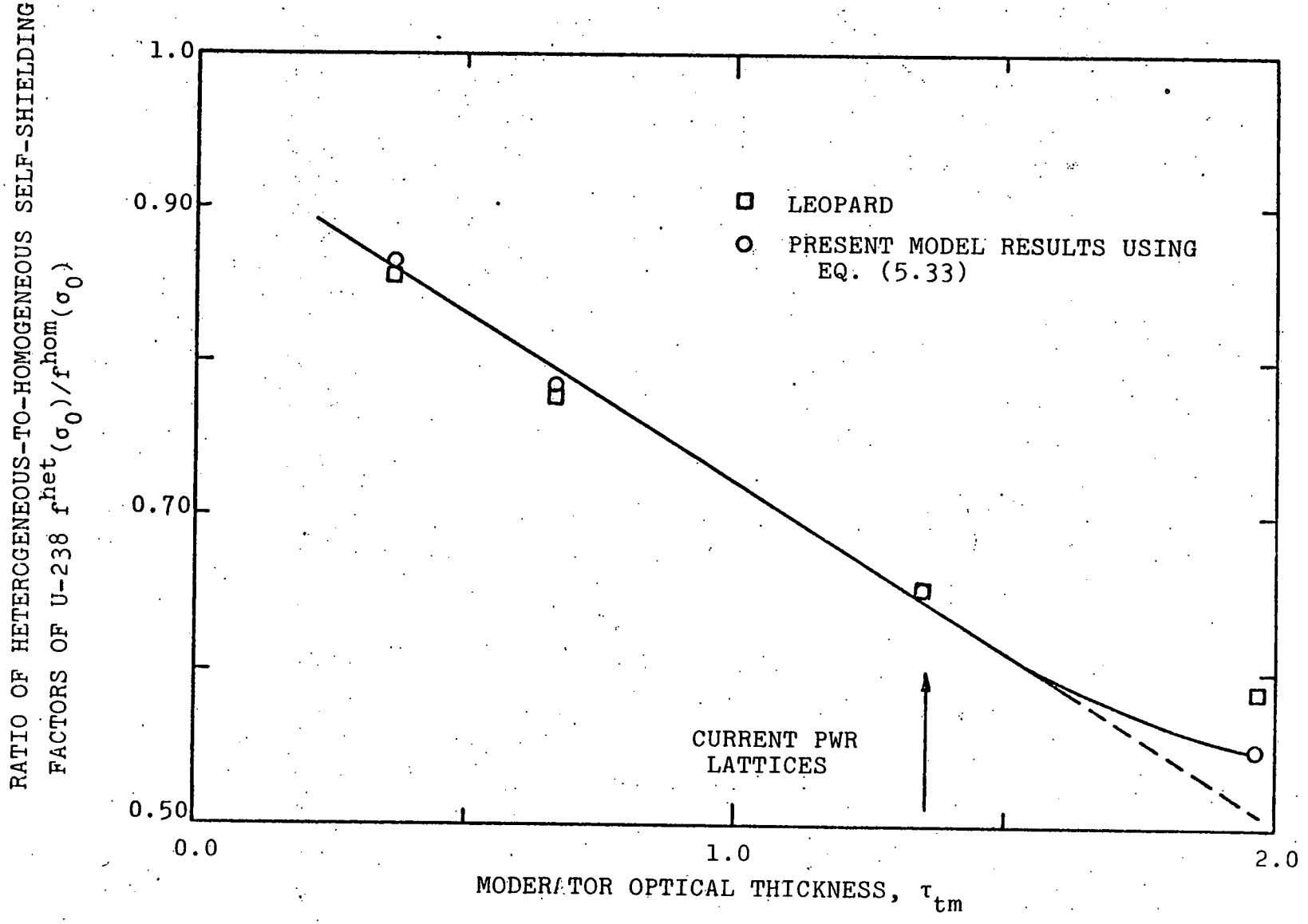

FIG. 5.4 RATIO OF THE BROAD GROUP HETEROGENEOUS-TO-HOMOGENEOUS CAPTURE SELF-SHIELDING FACTORS OF U-238 AS A FUNCTION OF MODERATOR OPTICAL THICKNESS

Table 5.5

Tabulated Results Applicable to Fig. 5.4

Moderator Optical Thickness	$\frac{f_c^{het}(\sigma_0)}{f_c^{hom}(\sigma_0)}$ present model (Eq. 5.33)	$\frac{f_c^{het}(\sigma_0)}{f_c^{hom}(\sigma_0)}$ LEOPARD	$\Delta\%$ percent difference
0.361	0.865	0.857	+0.9
0.663	0.784	0.782	+0.3
1.354	0.653	0.653	0.0
1.965	0.551	0.587	-6.5

for the point closest to current PWR designs); also note that the results fall very nearly on a straight line. This observation can be confirmed analytically by an appropriate simplification of Eq. (5.33). The data plotted in Fig. 5.4 are listed in Table 5.5, again with percentage differences shown: the agreement between the present model and LEOPARD is excellent for all but the thickest moderator case.

Table 5.6 contains the data for the U-238 broad group heterogeneous capture cross-sections evaluated at various moderator optical thicknesses and at a fixed fuel pin diameter. As seen from the table, the two central points agree within 2%, and the end points within 8%: these data are plotted in Fig. 5.5. The important point to note here is the approach of the curve to an asymptotic limit as the moderator thickness increases, the reason being that as the moderator optical thickness increases, the results approach the isolated lump limit.

Finally, Table 5.7 gives the calculated values for $[f^{het}(\sigma_0)/f^{hom}(\sigma_0)]$ for various groups of two typical fast reactor pin-cell assemblies (metal-fueled and oxide-fueled) that have been studied in the M.I.T. Blanket Test Facility (BTF). (The blanket is of particular interest here because the diameter of radial blanket fuel pins may be as much as twice that of the core fuel pins, and the ambient neutron spectrum is softer than that of the core - both of which circumstances accentuate the effects of heterogeneity). As seen from the

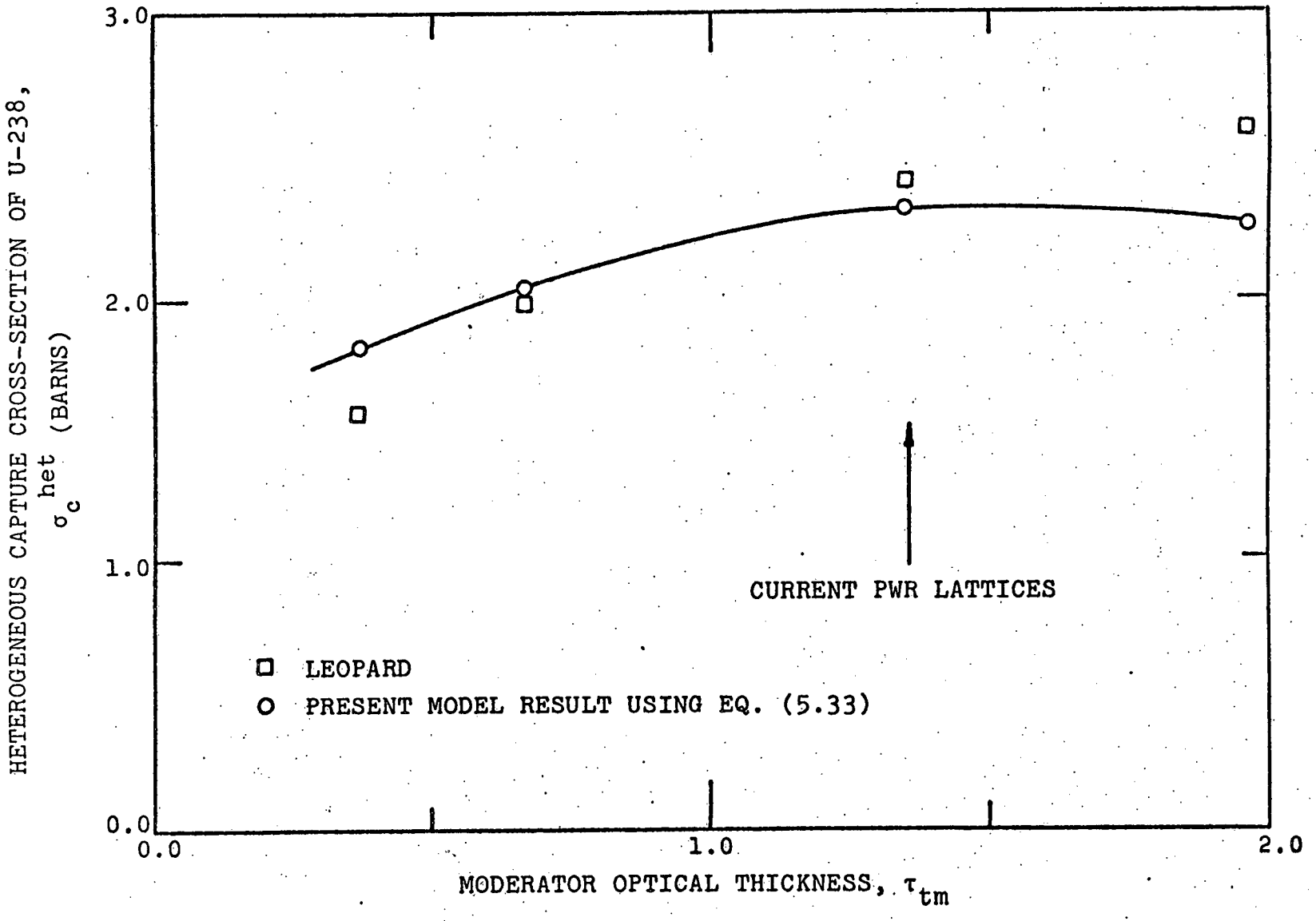

FIG. 5.5 HETEROGENEOUS BROAD GROUP CAPTURE CROSS-SECTION OF U-238 AS A FUNCTION OF MODERATOR OPTICAL THICKNESS

Table 5.6

Tabulated Results Applicable to Fig. 5.5

Moderator Optical Thickness	σ_c^{het} (barns) present model (Eq. 5.33)	σ_c^{het} (barns) LEOPARD	Δ% percent difference
0.361	1.919	1.790	+7.2
0.663	2.032	2.005	+1.3
1.354	2.180	2.228	-2.2
1.965	2.141	2.326	-8.6

Table 5.7

Group Values* for $f^{het}(\sigma_0)/f^{hom}(\sigma_0)$, $\sigma_c{}^{hom}$, and $\sigma_c{}^{het}$: Metal Fueled Blanket Mockup

G	$\frac{f^{het}(\sigma_0)}{f^{hom}(\sigma_0)}$ (present model) (Eq.5.33)	$\sigma_c{}^{hom}$(U-238) (barns)	$\sigma_c{}^{het}$(U-238) (barns)
26	0.972	0.821	0.798
29	0.951	1.102	1.048
32	0.964	1.274	1.228
35	0.963	1.006	0.968
38	0.971	1.377	1.337
40	0.975	2.120	2.067
43	0.958	4.923	4.718
45	0.941	14.118	13.284

* For the oxide fuel only group 45, which contains the largest (and hence most heavily shielded) U-238 resonance is reported:

45	0.989	12.887	12.742

magnitude of the results, the heterogeneity effects for both the metal-fueled and the oxide-fueled cells are very small indeed: less than the 10% uncertainty currently assigned to U-238 capture cross-section values in this energy range. Nevertheless the effect of internal moderation in the oxide fuel can be observed in the form of a self-shielding factor, f, which is much closer to 1.0.

In conclusion, although the present and the conventional equivalence relations differ by the factor $\frac{1}{\eta + \varepsilon}$, actual numerical results agree reasonably well. This is because, as previously noted, the σ_0' given by Eq. (5.34) is considerably lower than the σ_0' given by Eq. (5.31), because the Levine factor, 1/a, taken here as 1/a= 0.79 is considerably higher than the corresponding parameter $\bar{\nu}_f$ in the present model, which has an average value of 0.50 for the base-case PWR unit cell studied in this report (note that θ, appearing in Eq. (5.31), is approximately 1.0 for the case of thermal reactors, hence it is not responsible for the discrepancy). The lower σ_0' used in the conventional model results in a smaller value of f, which helps to partly offset the omission of a $(\eta+\varepsilon)$ term.

5.1.7 A Comparison Between the Conventional and the Present Dancoff Factor and Escape Probability Expressions

In this section expressions for the Dancoff factor and the fuel escape probability obtained by comparing the various

results of the present method with the corresponding conventional results will be reviewed. Before getting into the algebra, some simplifying assumptions are introduced, which are not to be taken as limiting approximations, however:

(a) Impose the NR approximation. Therefore, strictly speaking, all the results obtained in this section are for the NR case. Results for the WR and IR cases are obtainable by exactly the same methods.

(b) Consider only thermal reactors, where the slowing down source is in the moderator, hence $Q_f=0$ and $\theta=1$.

Using the above assumptions and comparing (as before) Eqs. (5.31) and (5.34) we get:

$$\frac{1}{1+\bar{\gamma}_f\tau_{tm}} \Leftrightarrow \frac{1}{1+\frac{1}{a}\tau_{tm}} \tag{5.38}$$

which says that $\bar{\gamma}_f$ corresponds to $\frac{1}{a}$, thus leading to an expression for the Dancoff correction factor: given by Eq. (5.35) with the only change being the replacement of $\frac{1}{a}$ by $\bar{\gamma}_f$.

$$1-C = \frac{\tau_{tm}}{1+\bar{\gamma}_f\tau_{tm}} \qquad \text{present method} \tag{5.39}$$

The next task is to find a corresponding expression for the escape probability, $P_f(E)$. It can be shown, using the slowing-down equations pertinent to a two-region unit cell that:

$$\frac{\bar{\phi}_m(E)}{\bar{\phi}_f(E)} = R(E) = \frac{1 + \left(\frac{\tau_{sf}(E)}{\tau_{tf}(E)} - 1\right)\frac{\tau_{tf}(E)}{\tau_{tm}(E)} P_f(E)}{1 + \left(\frac{\tau_{sf}(E)}{\tau_{tf}(E)} - 1\right)\left(1 - \frac{\tau_{tm}(E)}{\tau_{tf}(E)}\right) P_m(E)} \tag{5.40}$$

(I) in the asymptotic region $\tau_{sf}(E) \approx \tau_{pf} \approx \tau_{tf}(E)$, which when substituted in Eq. (5.40) results in $R(E) = 1$, as to be expected.

(II) in the resonance region where $\tau_{tf} >> \tau_{sf}$ (black fuel) one obtains:

$$R(E) = \frac{1}{P_f(E)} - \frac{\tau_{tf}(E)}{\tau_{tm}(E)} \tag{5.41}$$

Conventionally, the fully rational approximation for $P_f(E)$ is:

$$P_f(E) \doteq \frac{1}{1 + \frac{1+\frac{1}{a}\tau_{tm}}{\tau_{tm}} \tau_{tf}} \tag{5.42}$$

Substituting Eq. (5.42) into Eq. (5.41) gives:

$$R(E) = 1 + \frac{1}{a} \tau_{tf}(E) \tag{5.43}$$

which has exactly the same form as predicted by our results - namely:

$$R(E) = 1 + \bar{\gamma}_f \tau_{tf}(E) \tag{5.44}$$

Upon comparing Eqs. (5.43) and (5.44) we note, once again:

$$\frac{1}{a} \Leftrightarrow \bar{\gamma}_f \tag{5.45}$$

Using the above relation (Eq. (5.45)), and working backward, the following expression for $P_f(E)$ is obtained:

$$P_f(E) = \frac{1}{1 + \frac{1+\bar{\gamma}_f \tau_{tm}}{\tau_{tm}} \tau_{tf}(E)} \quad (5.46)$$

Equation (5.46) is the analog of Eq. (5.42). The above encouraging results encourage confidence in the present method.

Figure 5.6 shows a plot of the Dancoff correction obtained in Ref. (L3) using the MOCUP Monte Carlo program. The Monte Carlo program computation was performed on a two-region "square pin cell" of high fuel cross-section and with $V_m/V_f = 1$. As can be seen, the present analytical results are in as good agreement with the Monte Carlo computations as are the results of the analytical model proposed in Ref. (L3); with the exception that the present model is considerably simpler than the model proposed in the reference. Both models, however, are obtained assuming unit cell cylindricalization; as a result, they do not distinguish between square and hexagonal cells. Finally, the results of the two models are about 3% higher than the corresponding Monte Carlo computations.

One should not conclude from the above comparisons that the present work merely validates prior methodology: the results include previous work as limiting cases, but are more general.

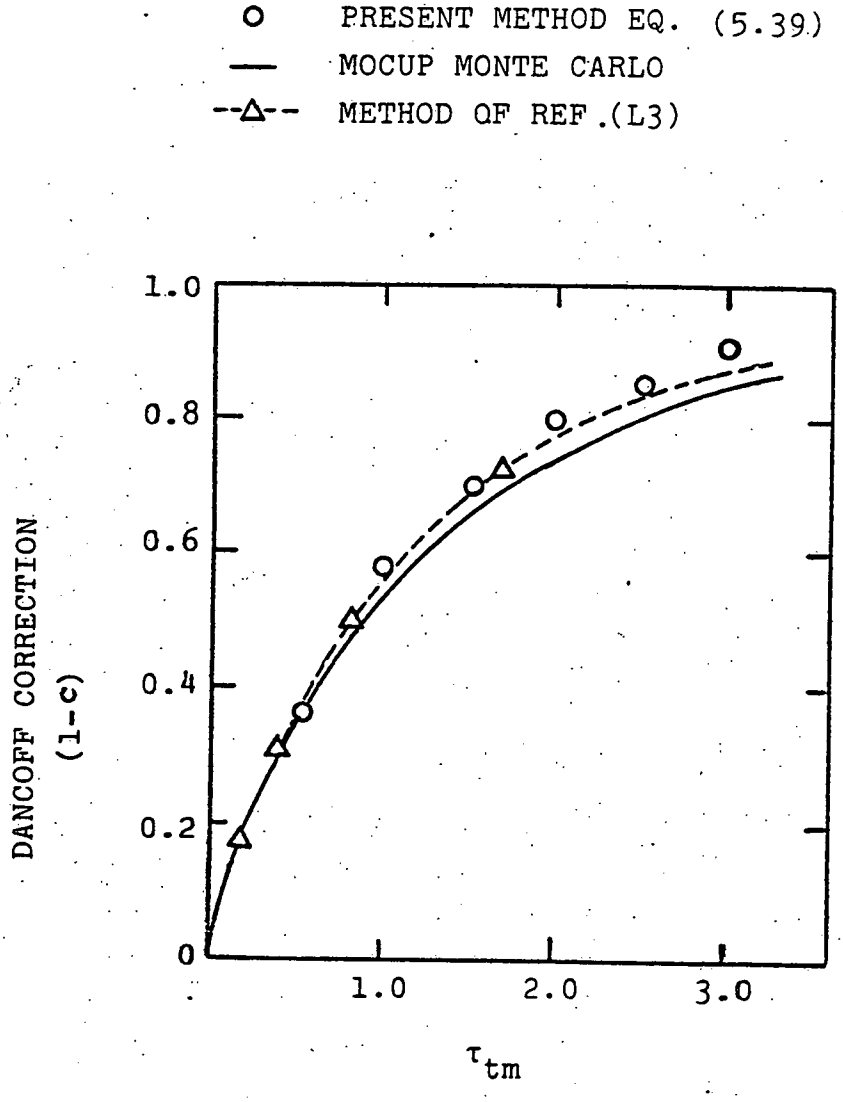

FIG. 5.6 VARIATION OF THE DANCOFF CORRECTION WITH MODERATOR OPTICAL THICKNESS FOR A SQUARE PIN CELL WITH $V_M/V_F=1$.

5.2 CONCLUSIONS

Based upon the work reported here the following conclusions are substantiated:

(1) A new and easily applied equivalence theorem, applicable to both fast and thermal reactors, has been developed.

(2) The present method handles cases not easily dealt with conventionally - e.g. when fuel moderation is not negligible compared to that of the coolant.

(3) The effects of heterogeneity in fast reactors are shown to be small: less than the uncertainty currently assigned to U-238 capture cross-section values.

5.3 RECOMMENDATIONS FOR FUTURE WORK

The following topics are envisioned as natural extensions of the present work:

(1) Treating mixtures containing more than one resonance absorber - i.e. accounting for the effects of resonance overlap (F4, S9).

(2) Dealing with cases in which cell leakage is permitted (perhaps by inclusion of a DB^2 term).

(3) Adapting the flux-ratio methodology to the thermal and fast energy region: for example as a flux group module in rapid versions of codes such as THERMOS (H5) or UNCOL and HEETR (W2).

(4) Utilizing the method to treat larger cells, such as (homogenized) core surrounding a control absorber or a reactivity sample in a critical facility.

In the above areas some additional theoretical developments are called for. However, it should be possible to adapt fast reactor processing codes to utilize the equivalence theorem proposed here without further ado, and to then use these codes for LWR calculations. This step is recommended as are further checks against LEOPARD, including eigenvalue and reaction rate comparisons, as well as comparisons with experimental benchmark data. All the above activities appear to be feasible extensions of what has been accomplished so far.

5.4 REFERENCES

A1 "ANISN - A One-Dimensional Discrete Ordinates Transport Code," RSIC Computer Code Collection, Oak Ridge National Laboratory, CCC-82.

B1 G.I. Bell, "A Simple Treatment for Effective Resonance Integrals in Dense Lattices," Nucl. Sci. Eng., 5, 138 (1959).

B2 G.L. Bell, S. Glasstone, Nuclear Reactor Theory, Van Nostrand Reinhold Co., New York (1970).

B3 I. Bondarenko, et al., Group Constants for Nuclear Reactor Calculations, Consultants Bureau Enterprises, Inc., New York (1964).

F4 F.L. Filmore, "Effective Group Absorption Cross-Section and Resonance Overlap," NAA-SR-11963, Atomics International (1966).

G1 M.V. Gregory, M.J. Driscoll, D.D. Lanning, "Heterogeneous Effects in Fast Breeder Reactors," COO-2250-1, MITNE-142 (1973).

G3 R. Goldstein, H. Brooks, "Intermediate Resonance Absorption in Nonhomogeneous System," Nucl. Sci. Eng., 20, 331 (1964).

G4 R. Goldstein, R. Cohen, "Theory of Resonance Absorptions of Neutrons," Nucl. Sci. Eng., 13, 132 (1962)

G5 A.J. Goodjohn and G.C. Pomraning, ed., "Intermediate Resonance Absorption," Reactor Physics in the Resonance and Thermal Region, Vol. II, 37, MIT Press (1966).

H1 A.F. Henry, Nuclear Reactor Analysis, MIT Press (1975).

H3 H. Haggblom, "Computation of Resonance-Screened Cross Section by the Dorix-Speng System," AE-334, Stockholm, Sweden (1968).

H5 H. Honeck, "THERMOS, a Thermalization Transport Theory Code for Reactor Lattice Calculations," BNL-5826 (1961).

K1 O.K. Kadiroglu, M.J. Driscoll, I. Kaplan, "Uranium Self-Shielding in Fast Reactor Blankets," COO-2250-17, MITNE-178 (1976).

K4 R.B. Kidman, et al., "The Shielding Factor Method of Generating Multigroup Cross-Sections for Fast Reactor Analysis," Nucl. Sci. Eng., 48, 189 (1972).

K6 R.B. Kidman, R.E. MacFarlane, "LIB-IV, A Library of Group Constants for Nuclear Reactor Calculations," LA-6260-MS, Los Alamos Scientific Laboratory (March 1976).

L2 M.M. Levine, "Resonance Integral Calculations for U^{238} Lattices," Nucl. Sci. Eng., 16, 271 (1963).

L3 D.C. Leslie, J.G. Hill, A. Jonsson, "Improvements to the Theory of Resonance Escape in Heterogeneous Fuel," Nucl. Sci. Eng., 22, 78 (1965).

L4 J.R. Lamarsh, Introduction to Nuclear Reactor Theory, Addison-Wesley, Reading (1966)

L5 "LEOPARD - A Spectrum Dependent Non-Spatial Depletion Code," Westinghouse Electric Corporation WCAP-3269-26 (1963).

N1 D.A. Newmarch, "Errors Due to the Cylindrical Cell Approximation in Lattice Calculations," AEEW-R34, Atomic Energy Establishment Winfrith (1960).

S3 B.R. Seghal and R. Goldstein, "Intermediate Resonance Absorption in Heterogeneous Media," Nucl. Sci. Eng., 25, 1974 (1966).

S4 P. Silvennoinen, Reactor Core Fuel Management, Pergamon Press, New York (1976).

S6 M. Segev, "The σ Ambiguity in the Method of Self-Shielding Factors," Trans. Am. Nucl. Soc., 18, 555 (1974).

S7 M. Segev, "A Theory of Resonance-Group Self-Shielding," Nucl. Sci. Eng., 56, 72 (1975).

S9 A. Santamarina, "Effects de Protection Mutuelle Dans les Interactions ^{238}U-^{235}U et ^{238}U-^{239}Pu," Annals of Nucl. Energy, 3, 1 (1976).

W2 G.L. Woodruff, et al., "A Study of the Spatial Distributions of Fast Neutrons in Lattices of Slightly Enriched Uranium Rods Moderated by Heavy Water," AT(30-1)2344, MITNE-67 (1965).

Z1 P.F. Zweifel, "Neutron Self-Shielding," Nucleonics, 1974, (1960).

CHAPTER 6

ADVANCED BLANKET DESIGNS

6.0 FOREWORD

The work summarized in this chapter will be reported in detail in the topical report:

J.I. Shin and M.J. Driscoll

"Evaluation of Advanced Fast Reactor Blanket Designs"

COO-2250-25, MITNE-199, March 1977 (est.)

In this work a self-consistent analysis is made of the neutronic and economic performance characteristics of the external blanket region in fast breeder reactors. As will be shown, there is very little prospect for improvement of the external breeding ratio of fast reactors. While this result is of some significance in itself, a number of other useful contributions are made in the area of methodology, especially as regards correlation and generalization of parametric studies.

The results are also of significance to MIT's, and other, experimental programs in as much as they suggest that there is not much incentive for extensive investigation of additional advanced external blanket configurations and compositions.

6.1 INTRODUCTION

The fast breeder reactor (FBR) is a technically feasible and economically attractive alternative for future energy production. A principal attraction of the FBR comes from its ability to breed more fissile fuel than it consumes, which leads to a low fuel cycle cost and to the effective utilization of uranium ore resources. Current fast reactor designs for practical large-scale power production promise breeding ratios in the range from 1.2 to 1.4. The blanket region contributes about one third of the total breeding ratio, and reduces the fuel cycle cost by about twenty five percent of total expenses. Achieving a high breeding ratio and a low fuel cycle cost, which are the strong points of the FBR, can not be accomplished without the contributions of the blanket regions.

Various modifications to improve blanket performance have been suggested by many previous investigators. However, a clearly defined strategy for improving blanket neutronics and economics has not yet been advanced. Frequently the alternatives selected as being most attractive in this manner are in conflict: softening the spectrum (UO_2 or UC_2 fueled blankets) vs. hardening the spectrum (UC or UN fueled blankets) or a moderated blanket vs. a fissile-seeded blanket, or thick blankets vs. thin blankets with high-albedo reflectors.

Thus the central objective of this work has been to provide a clearer explanation of the technical basis for improved breeding performance and enhanced economic contributions by the blanket region.

Another major objective has been evaluation of these advanced/new blanket concepts with respect to their neutronic and economic capability on a consistent analytical and technical basis.

In practice, all blanket concepts should be evaluated on the basis of a compromise among neutronics, economics and engineering considerations. Evaluation of the neutronic and economic characteristics of FBR blanket systems is emphasized in the present work, although engineering design constraints have been considered where appropriate. The emphasis is also on development of simple analytical models and equations, which are verified by state-of-the art computer calculations, and which are then applied to facilitate interpretation and correlation of blanket characteristics.

6.2 METHODS OF EVALUATION

To permit meaningful comparisons of FBR blanket concepts, the computational methods, the nuclear data used for the calculations, and the details of the economic and financial environment were all carefully considered.

6.2.1 Reference Reactor Configuration

The core size (power rating) is not an important variable for the purpose of this study as shown by Tagishi (T1); however, reference design features of an 1000 MWe LMFBR, selected as the standard system for previous MIT blanket studies, were again chosen as a reference reactor configuration. Figure 6.1 shows the pertinent physical dimensions and summarizes the important physical characteristics of the reference reactor system. The main features to note in this cylindrically symmetric layout are two approximately-equal-volume

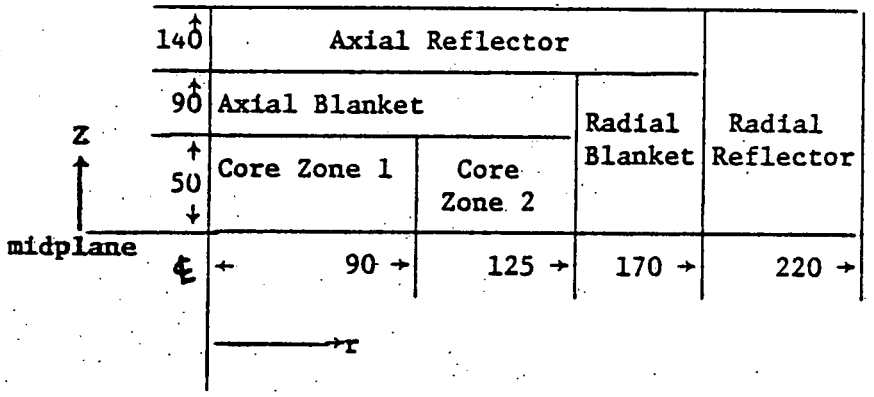

* All dimensions in cm

*Physical Characteristics of Reference Reactor

General:

Rated power, MWe/MWth = 1000/2560
Capacity factor, % = 82.2

Core and Axial Blanket:

Flat-to-Flat distance of a fuel assembly, cm = 15
Material Volume Fractions (Fuel/Na/Structure), % = 30/50/20
Pellet Smear Density, % T.D. = 85
Core Average Enrichment (Zone 1/Zone 2) at BOL, % = 15.2/20.8
Type of Fuel in the Core: $(Pu.U)O_2$

Radial Blanket:

Number of rows = 3
Type of fuel (reference): Depleted UO_2
Material volume fractions (Fuel/Na/Structure), % = 50/30/20
Pellet smear density, % T.D. = 96.5

Reflectors:

Type of material: stainless steel
Material Volume Fractions (Steel/Na), % = 80/20 (axial)
90/10 (radial)

Fig. 6.1 Elevation Schematic View of the Upper Right Quadrant of the Reference Reactor System

core enrichment zones (for radial power-flattening), a 40-cm thick axial blanket on the top and bottom of the core, and a three-row, 45 cm-thick radial blanket surrounded by a steel reflector.

6.2.2 Methods of Burnup and Neutronic Computations

Burnup analysis was performed with the two-dimensional diffusion theory code 2DB (L3). To determine the initial material compositions for various blanket design concepts, the same material volume fraction and fuel smear density (in % T.D.) were applied to all blanket fuel materials, because in the blanket region burnup and other environmental conditions are less severe than in the core regions. "Equilibrium" core and axial blanket compositions that remain fixed in time as the irradiation of the radial blanket progresses were adopted for this study.

In the interests of consistency, all computations were performed using the Russian (ABBN) 26-group cross-section set (B3) and 4-group cross-sections prepared by region-collapsing the original ABBN 26-group cross-section set using the one-dimensional transport theory code ANISN (E1). For simple neutronic calculations, a spherical reactor geometry whose blanket has the same characteristics as that of the radial blanket was also modeled.

6.2.3 Blanket Burnup Economics

6.2.3.1 Cost Analysis Model

Detailed fuel cycle cost analyses were performed utilizing the cash flow method (CFM) contained in the computer code BRECON, developed by Brewer (B4) and modified by Wood (W3).

The general CFM expression for the levelized cost of electricity (mills/KW-Hr) in a region or subregion under fixed fuel management is

$$e = \frac{1000}{E} M_{HM}(0) \left[\frac{C_{fiss}\, \varepsilon_o\, F^{MP}(T)}{T} \right.$$ material purchase cost component

$$+ \frac{C_{fab}\, F^{fab}(T)}{T}$$ fabrication cost component

$$+ \frac{C_{rep}\, F^{rep}(T)}{T}$$ reprocessing cost component

$$\left. - \frac{C_{fiss}\, \varepsilon(T)\, F^{MC}(T)}{T} \right]$$ material credit cost component (6.1)

where

e is the local levelized fuel component of the energy cost (mills/KW-Hr),

E is the electrical energy produced by the reactor in one year (KW-Hr/yr),

T is the local irradiation time (yr),

C_{fiss} is the fissile price ($/Kg Pu),

C_{fab} is the unit fabrication cost ($/Kg$M_{HM}$),

C_{rep} is the unit reprocessing cost ($/Kg$M_{HM}$),

ε_o is the initial enrichment,

$\varepsilon(T)$ is the discharge enrichment (Kg fissile discharged per Kg of heavy metal loaded),

$F^q(T)$ is the carrying charge factor for cost component q,

$M_{HM}(0)$ is the mass of heavy metal loaded.

The carrying charge factors, $F^q(T)$, are given by

$$F^q(T) = \frac{1}{1-\tau}\left[\frac{1}{(1-X)^{T_q}} - \tau\right] \quad \text{for capitalized costs or revenues}$$

$$= \frac{1}{(1+X)^{T_q}} \quad \text{for noncapitalized costs or revenues (expensed costs or taxed revenues)}$$

where (6.2)

$X = (1-\tau)r_b f_b + r_s f_s$ is the discount rate,

τ is the income tax rate,

f_b is the debt (bond) fraction,

f_s is the equity (stock) fraction,

r_b is the debt rate of return,

r_s is the equity rate of return,

T_q is the time between the cash flow transaction q and the irradiation midpoint.

An approximate form of Eq. (6.2), developed by Ketabi (K2), is

$$F^q(T) \simeq e^{\frac{XT_q}{1-\tau}} \quad \text{for capitalized costs or revenues}$$

$$\simeq e^{XT_q} \quad \text{for noncapitalized costs or revenues}$$

$$= F_q^{\Delta} e^{r_q T} \quad (6.3)$$

where

$F_q^{\Delta} = F_q(\Delta T_q)$, and

ΔT_q is the time between the cash flow transaction q and the beginning of irradiation (for fabrication) or the end of irradiation (for the reprocessing and material credits).

Considering the effects of non-linear fissile buildup histories and using the carrying charge factors expressed in Eq. (6.3), Equation (6.1) can be approximated as follows:

$$e = \frac{1000}{E} M_{HM}(0) \left[\frac{\bar{c}_1 e^{r_1 T} + \bar{c}_2 e^{-r_2 T} - \bar{c}_3 \varepsilon(T) e^{-r_3 T}}{T}\right] \qquad (6.4)$$

where

$\bar{c}_i = c_i \cdot F_i^{\Delta}$ is the modified cost component for operation i ($/Kg),

Subscript 1 refers to fabrication,

Subscript 2 refers to reprocessing,

Subscript 3 refers to material credit.

6.2.3.2 The Reference Economic and Financial Environment

Table 6.1 lists the reference economic and financial parameters used in this study. These conditions are within the range projected for the mature U.S. nuclear fuel cycle economy (Z1). (Note that 1965 dollars are employed to insure consistency with prior work at MIT by Brewer (B4)).

The reference unit fabrication and reprocessing costs shown in Table 6.1 were applied to all fuel materials uniformly because the unit fuel processing costs are not strongly influenced by the fuel pin diameter in the larger pin diamter range (>0.4 in.; a common fuel pin diameter in the radial blanket region is around 0.52 in.). In any case, this assumption provides a common basis for evaluation of the various blanket design concepts considered in this study.

Two cost accounting methods, A and B as originally defined by Brewer (B4), were considered for the blanket depletion - economic analysis. In method A, post irradiation transactions are not capitalized and in method B, post irradiation transactions are capitalized.

TABLE 6.1

REFERENCE ECONOMIC AND FINANCIAL ENVIRONMENT

Operation	Unit Fuel Processing Cost *, $/Kg M_{HM} (Radial Blanket Only)
Fabrication	69
Reprocessing	50

Isotope	Isotope Market Value* $/Kg$M_{HM}$
U-238	0
Pu-239	10,000
Pu-240	0
Pu-241	10,000
Pu-242	0

Financial Parameters	Value of Parameters (Private Utility)
Income Tax rate, τ	0.5
Capital Structure	
Bond (debt) fraction, f_b	0.5
Stock (equity) fraction, f_s	0.5
Rate of Return	
Bonds, r_b	0.07
Stocks, r_s	0.125
Discount Rate, $X = (1-\tau)f_b r_b + f_s r_s$	0.08
Cash Flow Timing	
ΔT_{fab}, yr	0.5
ΔT^{rep}, yr	0.5
ΔT_{mc}, yr	0.5

*1965 dollars, to conform to cases studied by Brewer (B4)

6.3 BREEDING CAPABILITY OF FBR BLANKETS

A high fissile gain in the fast breeder reactor (FBR) is extremely important if the utility industry is to become relatively independent of the need for mining of expensive low-grade uranium ores in the next 50 years or so, and to thereby assure lower average nuclear power plant fuel cycle costs.

The fast reactor has a relatively small, high-power-density core, and as a result has a very high net neutron leakage from the core region. Therefore, the radial and axial blankets make very important contributions to fissile breeding.

The purpose of this section is to evaluate the effects of various design parameters on the fissile production in FBR blankets and to review possible design modifications to enhance the breeding ratio. An evaluation of an analytical method for estimation of the external breeding ratio will be carried out followed by a detailed discussion of the various factors which affect external fissile breeding.

6.3.1 Breeding Potential of FBR Blankets

The fissile breeding in an FBR due to neutron capture in fertile materials in the core and blanket regions, is characterized by the breeding ratio, defined by

$$b = \frac{\text{Fissile production rate in core and blanket regions}}{\text{Fissile consumption rate in core and blanket regions}}$$

$$= \frac{\Sigma_{c,B} \, (C^{28} + C^{40})}{\Sigma_{c,B} \, (A^{49} + A^{41} + A^{25})} \qquad (6.5)$$

where

C is the total capture rate in the indicated species,

A is the reactor absorption integral,

c,B are core and blanket regions, respectively.

The breeding ratio can be split into two parts corresponding to the internal (core) contribution (b_i) and the external (blanket) contribution (bx):

$$b_i = \frac{\text{Fissile production rate in core}}{\text{Fissile consumption rate in core and blanket regions}}$$

$$= \frac{C_c^{28} + C_c^{40}}{\Sigma_{c,B}(A^{49} + A^{41} + A^{25})} \qquad (6.6)$$

$$bx = \frac{\text{Fissile production rate in blanket}}{\text{Fissile consumption rate in core and blanket regions}}$$

$$= \frac{C_B^{28}}{\Sigma_{c,B}(A^{49} + A^{41} + A^{25})} \qquad (6.7)$$

Considering the neutron balance in the region r, i.e.;

$$\nu F_r^{49} + \nu F_r^{28} + \nu F_r^{25} - F_r^{49} - F_r^{28} - F_r^{25} - C_r^{49} - C_r^{28} - C_r^{25} - A_r^{P,L} = L_r \qquad (6.8)$$

where

Pu-239, U-238 and U-235 were considered as the representative fissile and fertile species in the core and blanket, and

F is total fission rate in the indicated species

L_r is neutron leakage from the region r, and

P,L refers to parasitic absorption and neutron leakage losses,

The breeding ratio can then be rewritten as

$$b = \eta_c \left[1 + \frac{\bar{\nu}-1}{\bar{\nu}} \delta - a(1 + \delta) \right] - 1 \qquad (6.9)$$

where the power production contribution of U-235 was neglected and,

η_c is the fissile mean neutron yield per neutron absorbed in the fissile species in the core region ($\bar{\nu}F_c^{49}/A_c^{49}$),

$\bar{\nu}$ is the mean number of neutrons per fissile and fertile fission,

δ is the ratio of fertile to fissile fissions ($[F_c^{28} + F_B^{28}]/\bar{\nu}F_c^{49}$),

a is the parasitic absorptions and neutron leakage losses per fission neutron produced in the core and blanket regions

$$\left(\frac{A_c^{P,L} + A_c^{P.L}}{\bar{\nu}[F_c^{49} + F_c^{28} + F_B^{28}]}\right)$$

Equation (6.9) has the following interpretation:

a. fissile η_c is the dominant term and hence breeding performance can in principle be improved by creating a harder neutron spectrum in the core, which increases η_c of the fissile species: hence higher concentrations of heavy isotopes (metal and carbide fuel) in the core leads to a considerably higher breeding ratio,

b. the second term in brackets, $\frac{\bar{\nu}-1}{\bar{\nu}} \delta$, accounts for the "fast fission bonus" from fertile material,

c. the third term in brackets, $a(1+\delta)$, indicates that low parasitic absorption is essential for a high breeding ratio. The absorption cross-section of the fuel and non-fuel materials and the volume ratio of fuel to structural material are important factors here.

Generally speaking then, there are two basic approaches to improving the breeding ratio: one is to harden the neutron spectrum and the other is to decrease the relative amounts of parasitic absorption.

Inserting Eq. (6.8) into Eq. (6.7), the external breeding ratio can be rewritten as

$$bx = \frac{1}{\Sigma_{c,B}(A^{49} + A^{25} + A^{41})} \left[L_c + (\bar{\nu}-1)F_B - A_B^{P,L,C}\right] \qquad (6.10)$$

where

$$F_B = F_B^{25} + F_B^{28},$$

$$A_B^{P,L,C} = A_B^{P,L} + C_B^{25} \text{ and}$$

it is assumed that no plutonium is present in the blanket at BOL.

The fissile consumption rate in the whole reactor, $\Sigma_{c,B}(A^{49} + A^{41} + A^{25})$, is directly related to the reactor thermal power P, and can be considered as a fixed value. Therefore, Eq. (6.10) suggests several strategies for increasing the external breeding ratio, i.e.,

a) increase $\bar{\nu}$ by hardening the blanket neutron spectrum,

b) increase the fertile fission rate, F_B^{28}, by hardening the blanket neutron spectrum,

c) minimize parasitic absorptions

A high neutron leakage rate leads to a high external breeding ratio however it also reduces the internal breeding ratio and thus is not an appropriate means to improve the external breeding ratio.

Actually, δ, the ratio of fertile-to-fissile fissions, and $\bar{\nu}$ are nearly constant, unless one contemplates substituting thorium for uranium as the fertile species - an option not under consideration here. Therefore neutron wastage by parasitic absorption and leakage is the key factor.

6.3.2 Evaluation of Factors which Affect External Fissile Breeding

6.3.2.1 Neutron Leakage Rate from the Core Region (L_c)

Most neutrons absorbed in the blanket region come from the core region, and the blanket zone nearest the core has the highest breeding capability and dominates the neutronic characteristics of the entire blanket region.

The neutron leakage rate into the blanket is simply related to the blankets diffusion coefficient, D_B, and buckling, B_B^2, i.e.;

$$L_c \propto D_B B_B \propto \left[\frac{\Sigma_{a,B} - \nu\Sigma_{f,B}}{\Sigma_{tr,B}}\right]^{1/2} \cong \left[\frac{\bar{\sigma}^{28}_{a,B}}{\bar{\sigma}^{28}_{tr,B}}\right]^{1/2} \tag{6.11}$$

The variation of the cross-section ratio, $\left[\frac{\Sigma_{a,B}}{\Sigma_{tr,B}}\right]^{1/2}$, is so small in cases of practical interest that for all practical purposes the change in neutron leakage rate is insignificant as blanket composition is changed. The results of ANISN calculations show that blanket fuel density is not an important factor affecting the neutron leakage rate, and that while blanket thickness (e.g.1 vs 3 rows) and enrichment (Depleted U vs. Nat. U) are more sensitive parameters, their effects are also negligible ($< \pm$ 3%). Hence we can conclude that the neutron leakage rate from the core region into the blanket is affected only by core design parameters. We also reiterate that in all of the work reported here the core design and composition was held fixed.

6.3.2.2 Variation of $\bar{\nu}$-value by Spectrum Hardening

Since a higher net neutron production in the blanket region increases the external breeding ratio, achieving a high $\bar{\nu}$ value is one potentially favorable objective for the blanket designer. There is an empirical universal expression for $\bar{\nu}$-values (L2).

$$\bar{\nu}(E) = \bar{\nu}_o + aE \qquad (6.12)$$

where $\bar{\nu}_o$ and a are constant and E is the incident neutron energy in MeV. The constants are

for U-235, $\bar{\nu}_o = 2.43$, $a = 0.065$ $(0 \leq E \leq 1)$

$\bar{\nu}_o = 2.35$, $a = 0.150$ $(E > 1)$

for U-238 $\bar{\nu}_o = 2.30$, $a = 0.160$ (all E)

The average neutron energy in the blanket region is also affected by the core neutron spectrum, because most neutrons come from the core, and the magnitude of the neutron flux is sharply attenuated as the distance from the core/blanket interface is increased. Therefore, the possible range of variation of the average neutron energy in the blanket region, which can be achieved by varying blanket fuel composition or fuel materials is rather small, and the $\bar{\nu}$ value remains essentially constant. The incremental increase in the $\bar{\nu}$ value due to spectrum hardening (achieved by replacing UO_2 fuel by UC or U_2Ti fuel) is only 0.74%.

6.3.2.3 Neutron Fission Rate in the Blanket (F_B)

The number of neutrons consumed in the blanket region by absorption and out-leakage is equal to the sum of the neutron in-leakage from the core and the neutrons produced by fission in the blanket, a sum to which the external breeding ratio is linearly proportional. Without for a moment considering options such as addition of moderator or fissile material to the blanket, we can assume that the neutron leakage rate from the core is constant, hence increasing the neutron generation in the blanket is an important means to improve the external breeding ratio.

The total fission integral, F_B, in the blanket is the sum of the fission reactions of U-235 and U-238;

$$F_B = (N_B^{28}\,\bar{\sigma}_{f,B}^{28} + N_B^{25}\,\bar{\sigma}_{f,B}^{25})\bar{\phi}_B \cdot V_B \qquad (6.13)$$

Fission reactions in a fresh FBR blanket are predominently in U-238, and an increase in the population of high energy neutrons ($\geq$ 2.5 MeV) will increase the "effective" fission cross-section of U-238 because U-238 has a threshold near 1 MeV. Here we should note that a harder neutron spectrum does not improve the "effective" fission cross-section of U-238 without a concurrent increase in the number of high energy ($\geq$ 2.5 MeV) neutrons.

Since (a) most neutrons in the blanket come from the core and have an energy spectrum which is relatively independent of blanket composition, (b) the average energy and the most probable energy of prompt fission neutrons are 1.98 MeV and 0.85 MeV respectively and (c) inelastic scattering in Uranium itself dominates fast neutron downscattering, changing the neutron spectrum at high energies is difficult unless we can change core parameters. Hence increasing the effective U-238 fission cross-section in the blanket region is for all practical purposes impossible, and moreover multigroup calculations typically show that the space and spectrum averaged fission cross-section of the fertile species in the blanket is actually decreased by neutron spectrum hardening.

The average neutron flux, $\bar{\phi}_B$, shown in Eq. (6.13) should be, in a cylindrical blanket:

$$\bar{\phi}_B \simeq \frac{2\phi_o}{S_B}\left[\frac{a+t}{B_B} + \frac{1}{B_B^2}\right]\left[1 - e^{-B_B t}\right] \qquad (6.14)$$

where the flux distribution in the blanket was approximated as

$$\phi_B(r) \simeq \phi_o \, e^{-B_B(r-a)}, \text{ and}$$

a = the core radius,

ϕ_o = the neutron flux at the core/blanket interface,

$S_B = (a+t)^2 - a^2$

t = blanket thickness,

B_B^2 = the blanket geometrical buckling

A typical value of B_B for a 1000 MWe reactor having a 45 cm thick blanket is ~ 0.1 cm^{-1}. Therefore, for thick blankets $e^{-B_B t}$ is small, and since the outer blanket radius, a+t, is 150 cm for a large core we can neglect $e^{-B_B t}$ and $\frac{1}{B_B^2}$; and hence the average neutron flux in the blanket is approximately proportional to B_B^{-1}, i.e.:

$$\bar{\phi}_B \propto B_B^{-1} \propto [\Sigma_{tr,B}(\Sigma_{a,B} - \nu\Sigma_{f,B})]^{-1/2} \qquad (6.15)$$

From the above analysis one may conclude that a high fuel density and the relative absence of neutron moderation decreases both the average neutron flux and the average microscopic fission cross-section of U-238, hence the total fission rate in the blanket is not linearly proportional to fuel density. Combining Eqs. (6.13) and (6.15) and assuming constant microscopic cross-sections, one has, very crudely

$$F_B \propto [N_B^{28}]^{1/2} \qquad (6.16)$$

6.3.2.4 Neutron Loss by Parasitic Absorption and Neutron Leakage into the Reflector ($A_B^{P,L,C}$)

In addition to increasing the fuel density, an alternative approach to improvement of the external breeding ratio is to lower parasitic absorption and leakage losses. Parasitic neutron absorption consumes about 10% of the total available neutrons, and 4% of all neutrons are lost by neutron leakage into (and absorption in) the reflector regions external to the blankets.

The four main materials which absorb neutrons in a blanket are U-238, U-235, alloying constituents if metallic fuel is used (Ti, Mo etc.), and Iron in structural materials. Neutron absorptions by U-238 and U-235 are directly related to the blanket breeding function, hence to improve external breeding we should (a) reduce the volume fraction of structural material, (b) select structural materials which have low neutron absorption cross-sections, and (c) avoid metal-alloy fuel.

Ti in U_2T_i fuel absorbs $\sim$3% of the total available neutrons, while the oxygen and carbon in ceramic fuels consume almost no neutrons. Since low parasitic absorption is paramount, selection of the fuel material is an extremely important task, and oxide, carbide and pure metal fuels are by elimination almost the only favorable choices open to blanket designers.

Neutron loss by leakage into the reflector region, which amounts to roughly 4% of the total neutrons for a 45 cm thick blanket, is dependent upon blanket thickness, which is in turn determined by fuel cycle cost considerations.

The blanket diffusion coefficient, D_B, is a function of the blanket transport cross-section, $\Sigma_{tr,B}$, which remains nearly constant for composition changes of practical interest. Accordingly, we can not expect large reductions of neutron leakage losses.

In summary, a high heavy metal density and a low absorption cross-section for the non-fertile fuel constuents are important if one is to reduce the parasitic absorption in the blanket, and thereby to improve (however slightly the opportunity may be) the external breeding ratio.

6.3.3 Evaluation of Blanket Design Parameters for External Fissile Breeding

6.3.3.1 Fuel Density

High fertile density is perhaps the single most important parameter as far as achieving a high external breeding ratio is concerned. Although it reduces the average neutron flux in the blanket, a high fuel density reduces the relative amount of parasitic absorption and increases slightly the number of fission reactions, with the overall result that fertile breeding is improved.

The integral capture rate of U-238 is

$$C_B^{28} = k_1 \cdot k_2 \cdot (1 - e^{-k_3 N_{28,B}}) \qquad (6.17)$$

where

k_1 = a constant,

$$k_2 = \frac{\sigma_{c,B}^{28}}{[3(\sigma_{tr,B}^{28} + \frac{\epsilon_B}{1-\epsilon_B}\sigma_{tr,B}^{25})]^{1/2}} \cdot$$

$$\frac{1}{[(\sigma_{a,B}^{28} + \frac{\epsilon_B}{1-\epsilon_B}\sigma_{a,B}^{25}) - (\nu\sigma_{f,B}^{28} + \frac{\epsilon_B}{1-\epsilon_B}\nu\sigma_{f,B}^{25})]^{1/2}} \qquad (6.18)$$

$$k_3 = t/k_2 \cdot \sigma_{c,B}^{28} \tag{6.19}$$

t = blanket thickness

The external breeding ratio is proportional to the neutron capture rate in U-238, and the fractional change in the external breeding ratio, $\frac{\Delta bx}{bx}$, is :

$$\frac{\Delta bx}{bx} = \frac{\theta}{e^{\theta}-1} \left(\frac{\Delta N_{28,B}}{N_{28}}\right) \tag{6.20}$$

where

$$\theta = k_3 N_{28,B} \hat{=} [3\sigma_{tr,B}^{28} \cdot \sigma_{a,B}^{28}]^{1/2} \cdot N_{28,B} \cdot t \tag{6.21}$$

If there are no significant absorbing materials present except for U-238, Eq. (6.20) provides a useful approximation for evaluating changes in the external breeding ratio, and the agreement between Eq. (6.20) and multigroup results is rather good.

6.3.3.2 Blanket Thickness and Blanket Neutronic Efficiency (E_B)

Blanket neutron efficiency, E_B, defined here as the ratio of consumed neutrons to total available neutrons in the blanket, is a function of blanket thickness, t.

$$E_B = \frac{\bar{\phi}_B(t)}{\bar{\phi}_B(\infty)} = (1 - e^{-B_B t}) \tag{6.22}$$

thus, the neutronic blanket thickness, t, in contrast to the economic blanket thickness is given by

$$t = \frac{1}{B_B} \ln [1 - E_B] \tag{6.23}$$

We should note that there is little further improvement of blanket efficiency with increasing thickness, beyond a certain range.

The effect of blanket thickness on external fissile breeding is easily found from Eq. (6.17), namely:

$$\frac{\Delta bx}{bx} = \frac{\theta}{e^{\theta}-1} \left(\frac{\Delta t}{t}\right) \tag{6.24}$$

The relationship between blanket thickness, t, and the pertinent economic parameters is simply derived by the combination of Eqs. (6.14) and (6.46), i.e.:

$$k_4(1 - e^{-B_B t}) \geq 4\,\bar{\omega} r_4 \tag{6.25}$$

where

$$k_4 = \frac{2\bar{\sigma}^{28}_{c,B}\,\phi_o}{S_B}\left[\frac{a+t}{B_B} + \frac{1}{B_B^2}\right] \simeq \frac{2\bar{\sigma}^{28}_{c,B}\,\phi_o}{B_B t} \tag{6.26}$$

and $\bar{\omega}$ and r_4 are defined in Section 6.4.

Rearranging Eq. (6.26) for the blanket thickness, one obtains;

$$t \leq \frac{2(1 - 2\bar{\omega} r_4/\bar{\sigma}^{28}_{c,B}\,\phi_o)}{B_B} \tag{6.27}$$

which indicates, among other things, that the maximum Pu buildup rate, $\bar{\sigma}^{28}_{c,B}\,\phi_o$, should be larger than $2\bar{\omega} r_4$ for the existence of economic blankets of any thickness.

6.3.3.3 Blanket Enrichment

A main function of the FBR blanket is fissile breeding using neutrons leaking from the core, while power production in the blanket is a secondary and concomitant function. Therefore, blanket enrichment is not generally considered a particularly important factor to designers except as it complicates matching blanket power to flow over life. However, since blanket breeding capability depends on a high neutron availability, a superficially attractive design option capable of increasing neutron generation in the blanket is fissile seeding, that is, use of enriched fuel in the blanket. However we can expect that for a fixed core design a high fissile loading in the blanket region reduces core power, and also the neutron leakage rate into the blanket, and hence the external breeding ratio will suffer a compensatory loss.

Thus we will proceed at this point to assume that small variations of enrichment do not change the blanket characteristics significantly. In Eq. (6.18), transport, absorption and fission cross-section of U-235 are weighted relative to those of U-238 by the factor $\frac{\varepsilon_B}{1-\varepsilon_B}$ ($\sim$0.02). The ratio of the transport and absorption cross-sections of U-235 to those of U-238 is $\sim$1.33 and $\sim$12.83, respectively, hence the fission ($\frac{\bar{\sigma}^{25}_{f,B}}{\bar{\sigma}^{28}_{f,B}} \simeq \sim 220$) reaction of U-235 is relatively important when the enrichment is increased. However the most important reactions in the blanket with respect to fissile breeding are the neutron transport and absorption reactions, because most available neutrons leak in from the core regions, and fission-produced neutrons in the blankets are of considerably less consequence. Therefore, a small variation in enrichment does not affect the external breeding function appreciably.

6.3.4 Effect of Non-linear Fissile Buildup on External Fissile Breeding

In most of the preceding analysis the external breeding ratios were estimated using beginning-of-life (BOL) blanket parameters under the assumption of linear fissile buildup as a function of time. As discussed in more detail in Section 4.2, the non-linear dependence of the fissile buildup rate should be considered when accuracy is a paramount consideration.

Here we define the "exact" (time-averaged) external breeding ratio, $\bar{b}x$ as

$$\bar{b}x \equiv \frac{\text{(Fissile Inventory at EOL - Fissile Inventory at BOL) Blanket}}{\text{(Average Fissile Consumption Rate in Core and Blanket)}} \cdot \frac{1}{\text{(Total Irradiation Time)}} \tag{6.28}$$

Using results which were developed in the body of this report the "exact" external breeding ratio for an optimally-irradiated blanket can be expressed as

$$\bar{b}x = \frac{1}{\bar{M}_{a,\text{fissile}}} [M_{28}(0) \cdot \bar{\sigma}^{28}_{c,B} \cdot \bar{\phi}_B] \, e^{-\xi \frac{T_{op}}{T_c}_o}$$

$$= bx \cdot e^{-\xi \frac{T_{op}}{T_c}_o}$$

$$\simeq 0.766 \, bx \tag{6.29}$$

Equation (6.29) indicates that the external breeding ratio calculated using BOL parameters is overestimated by slightly over 20% due to the assumption of a linear fissile buildup time history.

However, Eq. (6.29) also indicates that the "exact" time-averaged external breeding ratio of various blankets having different optimum irradiation times are directly proportional to the external breeding ratio calculated using BOL blanket parameters. Since the constant of proportionality is the same for all cases (to a very good approximation), one can use BOL studies to correctly rank the breeding performance of various blanket design options.

6.3.5 Summary

The fissile breeding capability of FBR blankets has been reviewed, and the factors and design parameters which affect external fissile breeding have been evaluated in this section.

The main neutron source for the blanket region is neutron leakage from the core, which typically accounts for almost 90% of the total available neutrons in the blanket region; and non-fertile absorptions account for about 15% of the losses as shown in Table 6.2. Hence we can expect that without changing core parameters, improvement of the external breeding ratio by improving upon the 10% or so of blanket-fission-produced neutrons and the 15% or so of neutrons lost in the blanket will be relatively small.

The non-linear fissile-buildup-time-history was also considered in this section, and it was noted that the BOL external breeding ratio should be modified by a constant to obtain a valid quantitative estimate of the external breeding ratio averaged over life for blankets which are irradiated to their economically optimum exposure.

TABLE 6.2

SPECTRUM AND SPACE-WEIGHTED MACROSCOPIC ABSORPTION AND FISSION CROSS-SECTIONS FOR BLANKET MATERIALS

	UO_2	UC	U_2Ti
$\Sigma^{28}_{a,B}$	4.8619 E-03	5.9973 E-03	5.3057 E-03
$\Sigma^{25}_{a,B}$	1.2501 E-04	1.4619 E-04	1.2070 E-04
$\Sigma^{O}_{a,B}$	6.0733 E-06	-	-
$\Sigma^{C}_{a,B}$	-	2.1016 E-08	-
$\Sigma^{Ti}_{a,B}$	-	-	1.7775 E-04
$[\Sigma^{Fuel}_{a,B}]$	4.9935 E-03	6.1435 E-03	5.6042 E-03
$\Sigma^{Fe}_{a,B}$	3.0495 E-04	2.8451 E-04	2.5293 E-04
$\Sigma^{Cr}_{a,B}$	4.7955 E-05	4.3167 E-05	3.6393 E-05
$\Sigma^{Ni}_{a,B}$	4.3843 E-05	4.1630 E-05	3.5764 E-05
$\Sigma^{Na}_{a,B}$	2.6496 E-05	2.4450 E-05	1.9106 E-05
$[\Sigma^{Steel}_{a,B}]$	4.2324 E-04	3.9377 E-04	3.4420 E-04
$\nu\Sigma^{28}_{f,B}$	5.3903 E-04	7.1490 E-04	6.8269 E-04
$\nu\Sigma^{25}_{f,B}$	2.0697 E-04	2.4633 E-04	2.1136 E-04
$[\nu\Sigma_{f,B}]$	7.4601 E-04	9.5900 E-04	8.9405 E-04
$\frac{\Sigma^{28}_{a,B}}{\Sigma_{a,B}}$	0.8976	0.9174	0.8919
$\frac{\Sigma^{28}_{a,B}}{\Sigma^{steel}_{a,B}}$	11.4873	15.2305	15.4146
$\phi_B V_B$	5.21175 E+08	4.50135 E+08	4.91115 E+08
bx	0.35043	0.37500	0.36053

*All cross-sections are in cm^{-1}.

6.4 FUEL DEPLETION AND ECONOMIC ANALYSIS OF FBR BLANKETS

6.4.1 Generalized Fissile Material Buildup Histories for FBR Blankets

For simple neutronic/economic analyses, a linear fissile buildup approximation has been adopted in some previous work (K2),(T1). However, the linear buildup approximation can incur appreciable error for fuel depletion and economic calculations in the radial blanket region of a fast reactor (B6).

Several recent studies have been concerned with the development of accurate methods for fuel depletion calculations which rely upon conventional multigroup time step techniques (L4),(H3) or non-linear perturbation techniques (S2), (M1), which are currently performed using relatively expensive computer programs, and offer little insight upon which generalizations of the type of interest in this study can be based.

In view of the partial successes of prior work (B4), (B6) and the fact that practical engineering constraints, such as limitation of refueling to 6, 12 or 18 month intervals, relaxes the degree of accuracy required in estimation of optimum refueling dates, it was considered that a suitable simple model combining both the neutronic and the economic aspects of FBR performance could be synthesized.

The differential equation governing nuclide depletion can be rewritten on a mass basis for a given zone of the blanket (ignoring the mass difference per mole of U-238 and Pu-239):

$$\frac{dM_{49}}{dt} = M_{28}\,\bar{\sigma}_c^{28}\,\bar{\phi} - M_{49}\,\bar{\sigma}_a^{49}\,\bar{\phi} \tag{6.30}$$

and

$$\frac{dM_{28}}{dt} = -M_{28}\,\bar{\sigma}_a^{28}\,\bar{\phi} \tag{6.31}$$

Here, Pu-241 buildup was neglected and consideration was limited to Pu-239 and U-238 as the representative fissile and fertile species.

The solution for the fissile buildup history can be written in a particularly simple dimensionless form; after some rearrangement the following equation results:

$$M_{49}(t)/\hat{M}_{49} = \frac{t}{T_c} e^{-\xi_o \frac{t}{T_c}} \tag{6.32}$$

where

$T_c = (\bar{\sigma}_a^{49} \bar{\phi} - \bar{\sigma}_a^{28} \bar{\phi})^{-1}$ = the characteristic time constant,

$$\hat{M}_{49} = M_{28}(0) \quad \left(\frac{\bar{\sigma}_c^{28}}{\bar{\sigma}_a^{49} - \bar{\sigma}_a^{28}}\right)$$

$$\xi_o = 1/2 + [\hat{M}_{49}/M_{28}(0)](\bar{\sigma}_a^{28}/\bar{\sigma}_c^{28}).$$

The accuracy of Eq. (6.32) using only BOL parameters is obviously limited due to the variation of cross-sections and neutron flux as a function of time. However, empirical observations have shown that use of a corrected constant, ξ, instead of ξ_o can overcome this problem because the parameters, $\hat{M}_{49}$ and T_c, are exponential functions of time. Thus Eq. (6.32) can be rewritten as

$$M_{49}(t)/\hat{M}_{49} = \frac{t}{T_{c_o}} e^{-\xi \frac{t}{T_{c_o}}} \tag{6.33}$$

where subscript o refers, as usual, to the (constant) values calculated from BOL parameters.

Equation (6.33), together with the empirical finding that $\xi \cong 2/3$ for all blankets of interest, suggests that $M_{49}(t)/\hat{M}_{49}$ can be correlated against t/T_c^o. Figure 6.2 shows a selection of representative data points calculated using state-of-the-art physics depletion methods (2DB code and 4-group σ sets). The correlation is excellent and all points fall very nearly on the curve defined by Eq. (6.33).

We should also point out that Eq. (6.33) can be reformulated in terms of enrichment:

$$\varepsilon(t) = \frac{M_{49}(t)}{M_{28}(0)} = [\xi_o - 1/2] \frac{t}{T_c^o} e^{-\xi \frac{t}{T_c^o}} \tag{6.34}$$

Also, an entirely parallel and equally successful treatment can be applied to correlate higher isotope concentrations.

6.4.2 Optimum Economic Parameters for FBR Blankets

In this study the optimum blanket parameters of concern are the optimum and breakeven irradiation times, optimum enrichment and maximum blanket revenue per assembly, which are illustrated in Fig. 6.3.

6.4.2.1 Optimum Irradiation Time (T_{op})

From the general expression for the levelized fuel cycle cost shown in Eq. (6.4), the fuel cycle cost contribution by a given entity of blanket fuel can be expressed as

$$\frac{e}{M_{HM}} \propto \frac{\bar{c}_1 e^{r_1 T} + \bar{c}_2 e^{-r_2 T} - \bar{c}_3 \varepsilon(T)\, e^{-r_3 T}}{T} \tag{6.35}$$

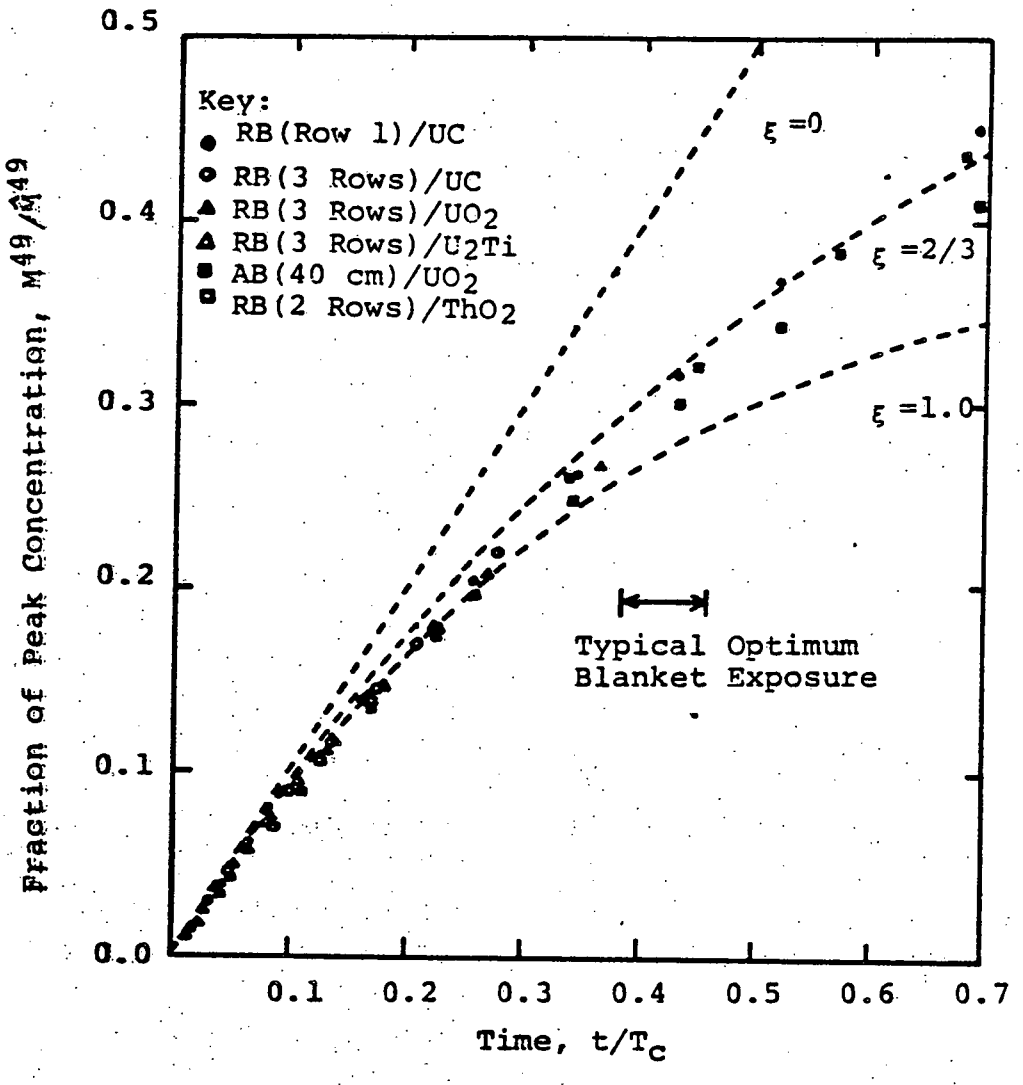

Fig. 6.2 DIMENSIONLESS CORRELATION OF FBR BLANKET BREEDING PERFORMANCE

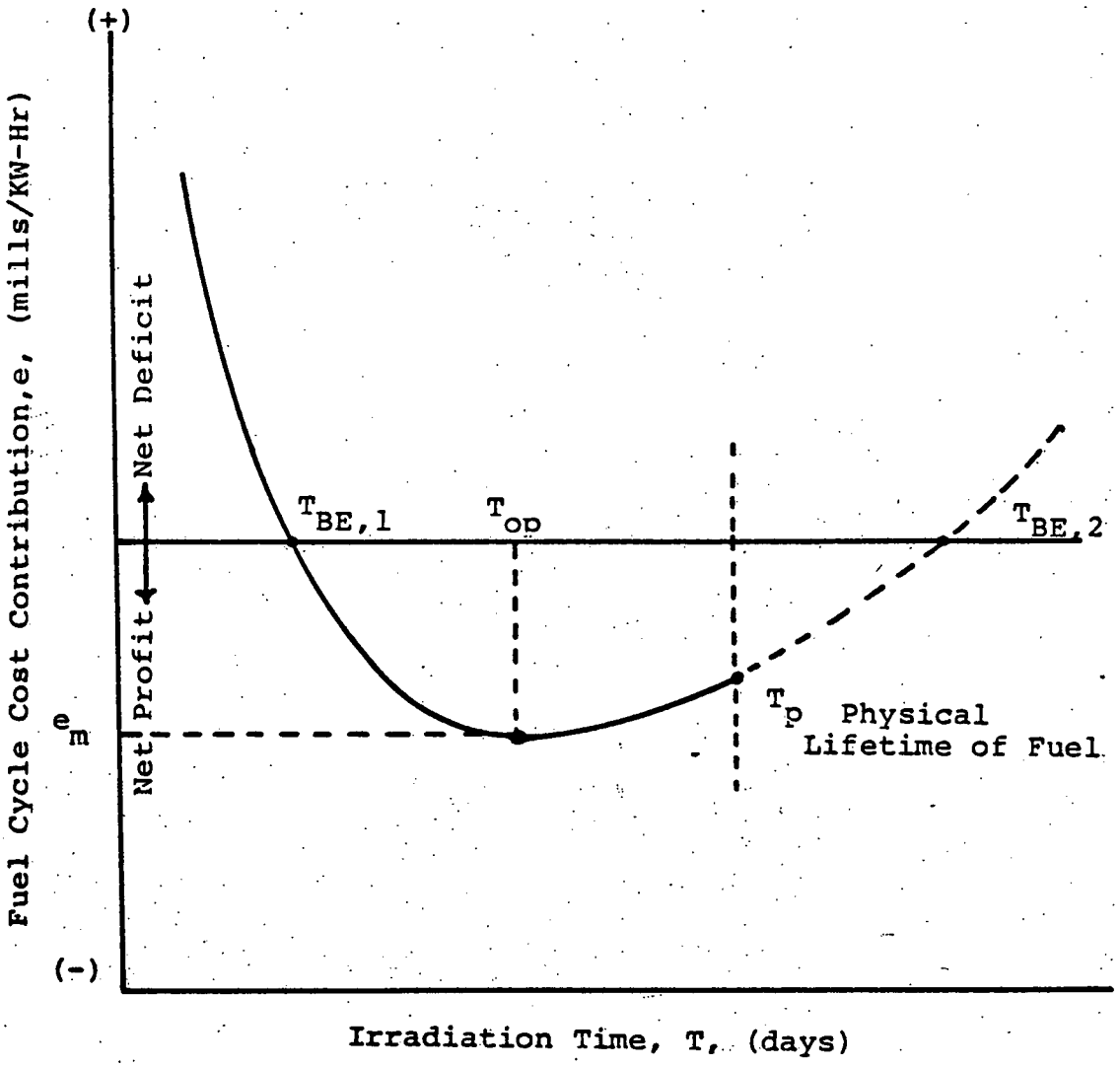

Fig. 6.3 TYPICAL VARIATION OF THE FUEL CYCLE COST CONTRIBUTION FOR A FAST REACTOR BLANKET

Using the simple correlation for the enrichment which was derived in the previous section, i.e.,

$$\varepsilon(T) = [\xi_o - 1/2] \frac{T}{T_c^o} e^{-\xi \frac{T}{T_c^o}} = S_o T e^{-\xi \frac{T}{T_c^o}} \tag{6.36}$$

(where S_o is the linear enrichment buildup rate determined by BOL conditions, equal to $\bar{\sigma}_c^{28} \bar{\phi}$.)

Eq. (6.35) can be rewritten as

$$\frac{e}{M_{HM}} \propto \frac{\bar{c}_1 e^{r_1 T} + \bar{c}_2 e^{-r_2 T} - \bar{c}_3 S_o T e^{-r_4 T}}{T} \tag{6.37}$$

where

$$r_4 = r_3 + \xi / T_c^o \tag{6.38}$$

To find the optimum irradiation time, the time derivative of the fuel cycle cost contribution is set equal to zero and the solution of this equation is approximated by the series expansion of the exponential function, dropping negligible terms. Thus one can obtain:

$$T_{op} = 1/r_4 \left[1 \pm \sqrt{1 - 2 \left\{ \frac{(\bar{c}_1 + \bar{c}_2) r_4}{\bar{c}_3 S_o} \right\}^{1/2}}\right] \tag{6.39}$$

Equation (6.39) can be futher simplified by algebraic rearrangements;

$$T_{op} = \left[\frac{\bar{\omega}}{S_o r_4}\right]^{1/2} F_1 \tag{6.40}$$

where

$$\bar{\omega} = \frac{\bar{c}_1 + \bar{c}_2}{\bar{c}_3} ,$$

$$F = (1 + 1/2\, x_1 + 1/2\, x_1^2 + 5/8\, x_1^3 + \ldots) \simeq \text{constant},$$

$$x_1 = \left[\frac{\bar{\omega} r_4}{S_o}\right]^{1/2}$$

The compensation factor, F_1, is nearly constant for all fuel materials loaded into the same blanket configuration, as shown in Table 4.3, if the economic parameter $\bar{\omega}$ is fixed (for radial blankets, F_1 assumes an average value of 1.45).

The optimum irradiation times calculated from the simple correlations are consistent with 2DB/BRECON results within $\pm 2\%$, as shown in Table 4.3.

6.4.2.2 Breakeven Irradiation Time

For the breakeven time, the fuel cycle cost contribution is set equal to zero,

$$e \propto \frac{\bar{c}_1 e^{r_1 T} + \bar{c}_2 e^{-r_2 T} - \bar{c}_3 S_o T\, e^{-r_4 T}}{T} = 0 \qquad (6.41)$$

Expanding the exponential functions through T^2 and neglecting the negligible terms, Eq. (6.41) becomes:

$$T_{BE}^2 - \frac{1}{r_4} T_{BE} + \frac{\bar{\omega}}{S_o r_4} = 0, \qquad (6.42)$$

which has the solutions:

$$T_{BE} = \frac{1}{2r_4}\left[1 \pm \sqrt{1 - \frac{4r_4\bar{\omega}}{S_o}}\right] \tag{6.43}$$

or

$$T_{BE} = \left[\frac{\bar{\omega}}{S_o}\right]F_2 \tag{6.44}$$

where

$$F_2 = (1 + x_2 + 2x_2^2 + \ldots) \cong \text{constant},$$

$$x_2 = \left[\frac{\bar{\omega}r}{S_o}\right] = x_1^2.$$

In equation (6.42), the discriminant should be positive for the existence of a breakeven time, which means that blanket fuel cycle cost contributions are negative and the blanket is economic. This requirement of a non-negative discriminant gives:

$$1 - 4\bar{\omega}r_4/S_{om} \geq 0 \tag{6.45}$$

or

$$S_{om} \geq 4\bar{\omega}r_4 \tag{6.46}$$

which indicates that the specific enrichment buildup rate (S_{om}) must not be less than a certain value ($4\bar{\omega}r_4$) if a given blanket region is to justify its existence on economic grounds.

6.4.2.3 Maximum Blanket Revenue

The maximum blanket revenue can be calculated by inserting the optimum irradiation time (T_{op}) and appropriate economic factors into the general cost equation.

If we select the approximate expression for the optimum irradiation time, $T_{op} = F_1[\frac{\bar{\omega}}{S_o r_4}]^{1/2}$, the maximum blanket revenue can thus be rewritten as

$$e_m = \frac{1000\, M_{HM}}{E}[(\bar{c}_1 + \bar{c}_2)\bar{c}_3 S_o r_4]^{1/2} F_3 \qquad (6.47)$$

where

$$F_3 = [\frac{F_1^2 + 1}{F_1} + \frac{(\bar{c}_1 r_2 - \bar{c}_1 r_2)}{\{(\bar{c}_1 + \bar{c}_2)\bar{c}_3 S_o r_r\}}^{1/2} - \frac{F_1^2}{2}(\frac{\bar{\omega} r_4}{S_o})^{1/2} - (\frac{S_o}{\bar{\omega} r_4})^{1/2}] \qquad (6.48)$$

Equation (6.47) indicates that

a. F_3 should be negative for positive blanket revenue,

b. F_3 and S_o are the dominant parameters determining the maximum blanket revenue, hence UO_2 fuel is more economical, as shown in Table 6.3.

Table 6.3 summarizes the maximum blanket revenue and the related parameters of oxide, carbide and metal-alloy fueled blankets. A hard neutron spectrum (UC or U_2Ti) leads to longer T_{op}, while a softer neutron spectrum (UO_2) forms a shorter T_{op} and large e_m due to the higher value of S_o.

6.4.2.4 Optimum Discharge Enrichment and Dimensionless Optimum Irradiation Time

The optimum discharge enrichment can be obtained by inserting the optimum irradiation time, T_{op}, into Eq. (6.36):

TABLE 6.3

OPTIMUM BLANKET PARAMETERS AND RELATED FACTORS FOR SIMPLE CORRELATIONS

	Accounting Method A†			Accounting Method B††		
	UO_2	UC	U_2Ti	UO_2	UC	U_2Ti
M_{HM}, Kg	17,299	23,233	24,759	5,180	6,957	7,414
So, $KgPu/KgM_{HM}yr$	0.005870	0.004663	0.004239	0.012030	0.010204	0.009101
r_4, yr^{-1}	0.081475	0.0707147	0.066265	0.16065	0.14495	0.13421
T_{op}, yr	7.49 7.72	9.02 9.21	9.78 9.73	3.77 3.63	4.31 4.17	4.75 4.70
T_{BE}, yr	2.83 3.09	3.56 4.38	3.92 4.58	1.42 1.44	1.67 1.55	1.87 1.96
F_3^*	-0.5064	-0.3881	-0.3443	-0.6420	-0.5744	-0.5366
e_{fab}, mills/KwHr	0.0767 0.0784	0.0921 0.0959	0.0937 0.0997	0.0371 0.0354	0.0451 0.0475	0.0447 0.0465
e_{rep}, mills/KwHr	0.0216 0.0231	0.0220 0.0244	0.0206 0.0242	0.0123 0.0117	0.0136 0.0157	0.0124 0.0142
$-e_{mat}$, mills/KwHr	0.1561 0.1548	0.1635 0.1626	0.1574 0.1597	0.0923 0.0824	0.1038 0.0990	0.0979 0.0912
$-e_m$, mills/KwHr	0.0578 0.0533	0.0494 0.0423	0.0431 0.0358	0.0429 0.0353	0.0451 0.0358	0.0408 0.0305

Key:

Eq. (6.39) or (6.43) or (6.47)
2DB/BRECON RESULT

† 3-row Radial Blanket
†† 1st-row in 3-row radial blanket
* $T_{op} = 1.45\ (\bar{\omega}/S_o r_4)^{1/2}$

$$\varepsilon_{op} = \frac{M^{49}(T_{op})}{M_{28}(0)} = S_o T_{op}\, e^{-\xi \frac{T_{op}}{T_c^\circ}} \tag{6.49}$$

or

$$\varepsilon_{op} \cong F_1 \left(\frac{S_o \bar{\omega}}{r_4}\right)^{1/2} e^{-\hat{\xi} \left(\frac{\bar{\omega}}{S_o r_4}\right)^{1/2}} \tag{6.50}$$

where

$$\hat{\xi} = \xi \cdot F_1 \cdot (\bar{\sigma}_a^{49}\, \bar{\phi} - \bar{\sigma}_a^{28}\, \bar{\phi})_{BOL}$$

The dimensionless optimum irradiation time can be defined as

$$\frac{T_{op}}{T_c^\circ} = F_1 \left(\frac{\bar{\omega}}{S_o r_4}\right)^{1/2} \cdot (\bar{\sigma}_a^{49}\, \bar{\phi} - \bar{\sigma}_a^{28}\, \bar{\phi})_{BOL}$$

The values of T_{op}/T_c° computed using Eq. (6.51) for various fuel materials and different blanket configurations are very nearly the same. Considering that the actual irradiation time is determined by the plant refueling schedule, which will permit fuel discharge only once or twice per year, we can therefore consider that T_{op}/T_c° of the various fuel materials are the same within practical limits.

This result is an important input for calculations estimating the time-varying characteristics of the blanket breeding ratio, as described in Section 6.3.4.

6.4.3 Sensitivity Analysis for Optimum Blanket Parameters

To trace the optimum blanket parameters impacted by the variation of the economic and financial environment, sensitivity functions were developed and evaluated.

Sensitivity coefficients have been defined as

$$\lambda_q^P(S) = \lim_{\substack{\Delta q \to 0 \\ q \to S}} \frac{\Delta P/P}{\Delta q/q} = \left[\frac{\partial P}{\partial q}\right]_{q=S} \cdot (q/P) \qquad (6.52)$$

where q is the independent parameter such as operating cost (Ci), income tax rate (τ) etc., which has reference value S and a small variation Δq; and P is the dependent optimum parameter such as the optimum irradiation time or breakeven time, etc.

By the algebraic rules of partial derivatives, we can express the differential, or variation, of optimum parameter P as follows:

$$\Delta P(\Delta S) = \sum_{i=1}^{n} \left[\lambda_q^P(S) \cdot \Delta q \cdot \frac{P}{q}\right]_i \qquad (6.53)$$

Table 6.4 summarizes the sensitivity coefficients for the optimum economic parameters.

As expected, the Pu market value ($\bar{c}_3$) and linear enrichment buildup rate (S_o) are the most important factors for all optimum economic parameters.

Note that the sensitivity coefficient for the non-linear factor, ξ/T_c°, has a rather high value compared to many of the other sensitivity coefficients, which illustrates that the non-linear characteristic of Pu buildup in FBR blankets is very important to determination of the optimum economic parameters (except for the breakeven time).

These results summarized in Table 6.3 also illustrate how oxide fuel, which has the highest value of S_o and a relatively large r_4, can produce the highest maximum blanket revenue compared to carbide and metal alloy fuels, because S_o is the most influential parameter, along with Pu market valve c_3. Therefore, to achieve the highest blanket revenue, a high fissile production rate - this does not necessarily mean high external

TABLE 6.4 SENSITIVITY COEFFICIENTS FOR OPTIMUM ECONOMIC PARAMETERS†

q	$T_{op} = F_1[\frac{\bar{\omega}}{S_o r_4}]^{1/2}$		$T_{BE} = F_2[\frac{\bar{\omega}}{S_o}]$		e_m	
u	$\lambda_q^{T_{op}}$	Reference Value *	$\lambda_q^{T_{BE}}$	Reference Value *	$\lambda_q^{e_m}$	Reference Value *
$\bar{\omega}$	0.5	0.5	1.0	1.0		-
c_1	$0.5/(1 + \bar{c}_2/\bar{c}_1)$	0.304	$(1 + \bar{c}_2/\bar{c}_1)^{1/2}$	0.609	$0.5(\frac{F_1^2+1}{F_1})[\frac{\bar{c}_1}{(\bar{c}_1+\bar{c}_2)F_3}] + \frac{\bar{c}_1(r_1 - \frac{F_1^2}{2}r_4)}{[(\bar{c}_1+\bar{c}_2)\bar{c}_3 S_o r_4]^{1/2}F_3}$	-1.251
c_2	$0.5/(1 + \bar{c}_1/\bar{c}_2)$	0.196	$(1 + \bar{c}_1/\bar{c}_2)^{1/2}$	0.391	$0.5(\frac{F_1^2+1}{F_1})[\frac{\bar{c}_2}{(\bar{c}_1+\bar{c}_2)F_3}] + \frac{\bar{c}_2(r_2 - \frac{F_1^2}{2}r_4)}{[(\bar{c}_1+\bar{c}_2)\bar{c}_3 S_o r_4]^{1/2}F_3}$	-0.320
c_3	-0.5	-0.5	-1.0	-1.0	$0.5(\frac{F_1^2+1}{F_1})(\frac{1}{F_3}) - \frac{\bar{c}_3 S_o}{[(\bar{c}_1+\bar{c}_2)\bar{c}_3 S_o r_4]^{1/2}F_3}$	2.576
ΔT_1	$\lambda_{c_1}^{T_{op}} \cdot (X\Delta T_1/1-\tau)$	0.024	$\lambda_{c_1}^{T_{BE}} \cdot (X\Delta T_1/1-\tau)$	0.048	$\lambda_{c_1}^{e_m} \cdot (X\Delta T_1/1-\tau)$	-0.1
ΔT_2	$\lambda_{c_2}^{T_{op}} \cdot (-X\Delta T_2)$	-0.008	$\lambda_{c_2}^{T_{BE}} \cdot (-X\Delta T_2)$	-0.016	$\lambda_{c_2}^{e_m} \cdot (-X\Delta T_2)$	0.013

continued on next page

ΔT_3	$0.5\ X\Delta T_3$	0.02	$X\Delta T_3$	0.040	$\lambda^{e_m}_{c_3} \cdot (-X\Delta T_3)$	-0.103
S_o	-0.5	-0.5	-1.0	-1.0	$0.5(\frac{F_1^2+1}{F_1}) \cdot \frac{1}{F_3} - \frac{\bar{c}_3 S_o}{[(\bar{c}_1+\bar{c}_2)\bar{c}_3 S_o r_4]^{1/2} F_3}$	2.576
r_4	-0.5	-0.5	-	-	$0.5(\frac{F_1^2+1}{F_1}) \cdot \frac{1}{F_3} - \frac{F_1^2(\bar{c}_1+\bar{c}_2) r_4}{2[(\bar{c}_1+\bar{c}_2)\bar{c}_3 S_o r_4]^{1/2} F_3}$	-1.238
X	$-0.25\ X/r_4$	-0.245	-	-	$\lambda^{e_m}_{r_4} \cdot (0.5\ X/r_4)$	-0.608
τ	0	0.0	-	-	0	0.0
ξ/T_c°	$-0.5\ \xi/T_c^\circ/r_4$	-0.255	-	-	$\lambda^{e_m}_{r_4}\ \xi/(T_c^\circ \cdot r_4)$	-0.63

†UO_2 Fueled 3-row Radial Blanket for Accounting Method A

*For the reference economic environment

breeding ratio - is a very important factor. Also note that this conclusion of oxide superiority is predicted on equal fuel fabrication costs per Kg of heavy metal for all fuels; if carbide fuel assemblies can be fabricated more cheaply then this may offset the economic disadvantages noted here.

6.4.4 The Effect of Fuel Management Options on Blanket Economics

The most commonly considered options for the fuel management of radial blanket assemblies are:

a. No Shuffling or Batch (NS); All fuel assemblies in the radial blanket are refueled at the same optimum time.

b. Zone or Region Scatter (RS): Each individual assembly is refueled at its own local optimum irradiation time.

c. In-Out Shuffling (IO): Fresh blanket assemblies are inserted into blanket positions at the core-blanket interface and later moved to outer positions.

d. Out-In Shuffling (OI); Fresh fuel assemblies are inserted at the blanket periphery and later moved to inner blanket positions.

There are several difficulties involved in comparing fuel management options under truly comparable conditions, and the following assumptions were used to permit a simple analysis in this study:

a. Each blanket "row" has an equal volume and number of fuel assemblies.

b. The average neutron flux and group-averaged cross-section are a function of position only and are not a function of fuel burnup.

c. All fuel assemblies have equal intervals of irradiation time, T_{op}/(no. of rows), in each row for the In-Out or Out-In Shuffling options.

6.4.4.1 The Impact of Fuel Management on Pu Production

The steady state fissile production rate of each fuel management option ($\bar{M}^{49}_{FM,0}$) which is defined as

$$\bar{M}^{49}_{FM,0} = \left(\frac{\text{Total Amount of Plutonium at the End of the Fuel Cycle}}{\text{Total Irradiation Time}}\right)_{\text{blanket}}$$

can be written in the general format:

$$\bar{M}^{49}_{FM,0} = 1/3\ M_{28}(0) \sum_i \left(S_{o,i}\ e^{-R_{FM,i}\ T_{op,0}}\right) \qquad (6.54)$$

where

subscript FM identifies the fuel management scheme

i refers to ith row of the blanket and

0 refers to the whole blanket.

The linear enrichment buildup rates of each row, $S_{o,i}$, were assumed constant for this study. Therefore, the differences caused by the different fuel management schemes are expressed in the exponential function, $e^{-R_{FM,i}T_{op,0}}$. Table 6.5 shows the steady state plutonium production rate, $\bar{M}^{49}_{FM,0}$, and associated parameter $R_{FM,i}$. The batch option produces about 15% less plutonium than the others and the Out-In scheme produces slightly more plutonium than do the other options.

Barthold (B1) reviewed fuel shuffling schemes in LMFBR blankets, and concluded that the plutonium production in the blanket is to a first order approximation the same for all shuffling schemes. Ketabi's

TABLE 6.5

COMPARISON OF STEADY-STATE Pu PRODUCTION RATES OF VARIOUS FUEL MANAGEMENT OPTIONS

Parameter \ Option	Batch (NS)	In-Out (IO)	Out-IN (OI)	Region Scatter (RS)
$R_{FM,1}$, yr^{-1}	0.07319	0.05191	0.02439	0.04201
$R_{FM,2}$, yr^{-1}	0.03221	0.01844	0.05529	0.03647
$R_{FM,3}$, yr^{-1}	0.01244	0.00415	0.06851	0.02774
$\sum_{i=1}^{3} (S_{o,i}\, e^{-R_{FM,i}\, T_{op,0}})$	0.01238	0.01410	0.01429	0.01392
$\bar{M}^{49}_{FM,0}$ KgPu/yr	71.3886	81.3091	82.4291	80.2506
$\bar{M}^{49}_{FM,0}/\bar{M}^{49}_{NS,0}$	1.0	1.139	1.155	1.124

† UO_2 Fueled 3-row Radial Blanket under Reference Economic/Neutronic Environment (for Accounting Method A)

work at MIT reached similar conclusions (K2). This difference in conclusions is caused in part, if not entirely, by the approximation in Bathold depletion equations of constant U-238 concentration. On the other hand, Lake et. al. (L1) found that the Out-In Shuffling option offers ≈0.005 higher breeding ratio over that of In-Out fuel shuffling options, a result which agrees with that of the present work.

6.4.4.2 Effects of Fuel Management Options on Blanket Optimum Parameters

To analyze the characteristics of various fuel management options simply, fixed neutron cross-sections and flux (in addition to a fixed economic/financial environment) were assumed.

Therefore, the only parameter which varies in response to a change of fuel management scheme is the non-linearity parameter, ξ/T_c°. For example, if ξ/T_c° is reduced by the switch from the batch to the Out-In Shuffling scheme, the r_4 (since $r_4 = r_3 + \xi/T_c^\circ$) will be smaller and will result in a longer optimum irradiation time and higher blanket revenue.

Using the definition of r_4 and a series combinations of equations, one can write

$$r_4 = r_3 + \xi/T_c^\circ \simeq r_3 + \frac{\sum_{i=1}^{3} S_{o,i} R_{FM,i}}{3 S_{\bullet,0}} \qquad (6.55)$$

Table 6.6 summarizes the effects on blanket parameters arising from the variation of r_4. Table 6.6 shows that the No-Shuffling option is the worst case for blanket economics and In-Out and Out-In Shuffling schemes are the best. The Region-scatter schemes are also advantageous compared to the No-Shuffling case; however the plutonium production rate and maximum blanket revenue achieved are less than those of the In-Out or Out-In shuffling schemes.

TABLE 6.6

EFFECTS OF FUEL MANAGEMENT OPTIONS ON BLANKET OPTIMUM PARAMETERS†

PARAMETER (EQ.)	EFFECTS OF SHUFFLING*
Optimum Irradiation Time $[T_{op} = F_1(\frac{\bar{\omega}}{S_o r_4})^{1/2}]$	• Optimum irradiation time is slightly increased (by ∿10%) because of smaller r_4 (0.097 vs. 0.078)
Breakeven Time $[T_{BE} = F_2(\frac{\bar{\omega}}{S_o})]$	• Breakeven time is not appreciably dependent on r_4. Therefore, it is not affected by the choice of fuel management option.
Maximum Blanket Revenue $[e_m \propto [(\bar{c}_1 + \bar{c}_2)\bar{c}_3 S_o r_4]^{1/2} F_3]$	• Lower r_4 and higher Pu production rate offers ∿30% higher (∿0.07 mills/KwHr vs. 0.05 mills/KwHr) blanket revenue.

*No-shuffling is reference case, using Accounting Method A;

†UO_2 fueled 3-row radial blanket.

6.5 EVALUATION OF FBR BLANKET DESIGN CONCEPTS

In practice, the design of FBR blankets involves a compromise between engineering considerations, safety problems, reactor physics and economics. Often, these requirements are in conflict. Low fuel cycle costs can be obtained at the expense of a low external breeding ratio, conversely the more complete neutron utilization required to achieve a high breeding ratio leads to thicker blankets, and the value of the additional fissile production may not cancel out the increased fabrication and reprocessing costs.

In this section, several advanced/new FBR blanket design concepts will be analyzed, emphasizing their neutronic and economic performance, although engineering desing constraints will be considered where appropriate.

Advanced blanket design concepts can be classified into the following four categories:

1. Design concepts emphasizing neutron spectrum variations -moderated blankets and spectrum-hardened blankets.
2. Design concepts emphasizing high neutron utilization -especially reflected blankets and blankets with high fuel volume fraction.
3. Design concepts emphasizing a high rate of internal neutron generation - fissile seeded blankets.
4. Design concepts emphasizing geometrical rearrangements, -parfait blankets, sandwiched blankets, and heterogeneous core concepts.

6.5.1 The Moderated Blanket

As described in the previous sections, a low relative density of fuel material (i.e. high diluent content), which leads to a soft neutron

spectrum in the blanket, is favorable from an economic aspect because of the high fissile breeding rate attainable; while, as regards breeding ratio, achieving a high fertile density (hence hard neutron spectrum) is a more important goal.

The ratio of the fertile density of carbide fuel to that of oxide fuel is 1.34 which is much larger than the ratio of the (space and spectrum-averaged) fertile microscopic cross-sections which is only about 1.09.

The purpose of adding moderator to the blankets is to create a softer neutron spectrum, which increases the fertile neutron capture cross-section and the blanket-averaged neutron flux: hopefully enough to offset the disadvantages of low fertile density.

The impacts of heterogeneous-seeding instead of homogeneous-seeding was also examined and both found to have similar effects on fissile breeding and blanket economics. Hence we need not make this distinction in our summarized discussions.

6.5.1.1 Neutronic Aspects of Moderated Blankets

The advantages of moderated blankets stem from high fertile capture cross-sections, high average neutron flux in the blanket region and lower neutron leakage into the reflector region. These factors are very favorable as regards achievement of a high external breeding ratio. However, two side effects counter the improvement; a) fertile inventory is decreased (some fuel must be displaced to make room for the moderator) and b) neutron absorption by the moderator increases the parasitic neutron absorption loss.

The net result is that the fraction of total neutrons absorbed by fertile species is actually the same or slightly smaller when the moderator

is added, as shown in Table 6.7. As described in Section 6.3, fertile density in the blanket region is the most sensitive parameter as regards breeding performance, and this result is to be expected regardless of the blanket thickness and fuel materials.

The internal (core) breeding ratio is not affected by moderator seeding in the blanket.

6.5.1.2 Economic Aspects of Moderated Blankets

A possibly attractive feature of moderated blankets may be their potential for the improvement of blanket revenue due to their high fissile buildup rate (S_o), achieved without significant loss of fissile breeding.

The sensitivity coefficient for S_o, $\lambda_{S_o}^{e_m} \equiv (\Delta e_m/e_m)/(\Delta S_o/S_o)$, is much larger than that of M_{HM} or ξ/T_c°, as shown in Fig. 6.4, which indicates that the same fractional variation of S_o would affect the maximum blanket revenue more than a comparable change in M_{HM} or ξ/T_c°. The sensitivity coefficient of M_{HM} for the maximum blanket revenue is always 1.0; therefore we may anticipate higher blanket revenue by adding moderator to increase S_o. However, it should be noted that it is easier to achieve large percentage changes in M_{HM} than in S_o, and in the high fissile breeding rate regions, the sensitivity coefficient for S_o sharply decreases, as shown in Fig. 6.4; hence, moderator-seeding loses its purported advantages.

Moderator seeding in the blanket is very effective when the fuel cycle cost contribution of the blanket is positive (the blanket revenue is negative) because of the lower fuel fabrication cost (due to the smaller heavy metal inventory or the number of fuel rods in the blankets) and the higher neutron capture rate of the remaining fertile material. Moderator seeding in the blanket is less effective when the

TABLE 6.7

NEUTRONIC CHARACTERISTICS OF REFERENCE (REF.) AND MODERATED (MOD.) RADIAL BLANKETS

			b	10^{-14} #/cm^2-sec	kg	10^{-19} #/zone-sec		
Fuel Mat.	Thickness (rows)	Unit	$\sigma_{c,B}^{-28}$	$\bar{\phi}_B$	$M_{28}(0)$	A_c^{49}	bi	bxr
UO_2	3	Ref.	0.4025	5.6269	17299	3.153	0.5888	0.2639
		Mod.	0.4677	5.8655	14416	3.154	0.5877	0.2650
	2	Ref.	0.4173	8.4077	10946	3.153	0.5880	0.2586
		Mod.	0.4876	8.9621	8063	3.155	0.5879	0.2511
UC_2	3	Ref.	0.4209	5.0691	18999	3.153	0.5889	0.2729
		Mod.	0.4709	5.3468	15833	3.155	0.5882	0.2697
	2	Ref.	0.4295	7.6320	12022	3.153	0.5887	0.2652
		Mod.	0.4854	8.2292	8856	3.157	0.5883	0.2568
UC	3	Ref.	0.3692	4.8720	23233	3.143	0.5899	0.2824
		Mod.	0.4216	5.0589	19361	3.145	0.5894	0.2805
	2	Ref.	0.3806	7.2872	14701	3.143	0.5898	0.2754
		Mod.	0.4386	7.7680	10827	3.146	0.5894	0.2688

All moderator material was seeded homogeneously in the 2nd row.

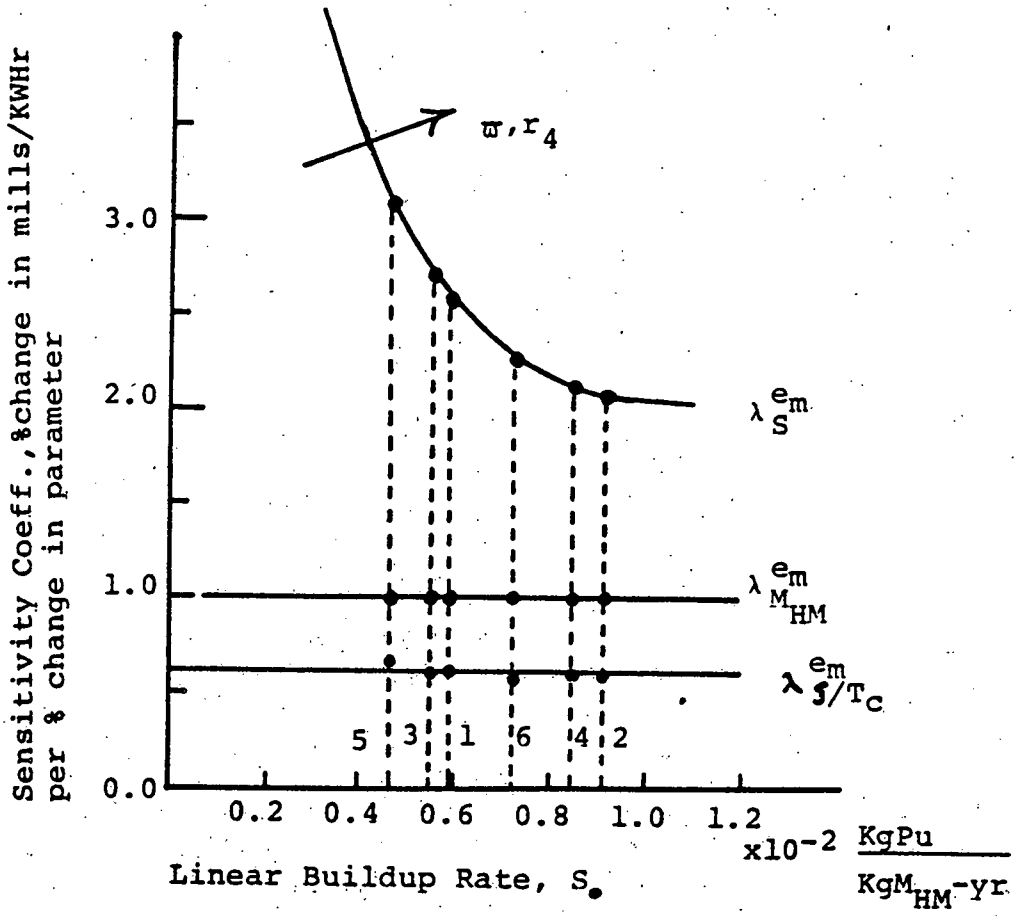

* 1: UO_2/3-row
2: UO_2/2-row
3: UC_2/3-row
4: UC_2/2-row
5: UC/3-row
6: UC/2-row

Fig. 6.4 SENSITIVITY COEFFICIENTS OF THE MAXIMUM BLANKET REVENUE AS A FUNCTION OF $S^*_\bullet$

fuel cycle cost contribution of the blanket is negative (positive blanket revenue) because a small heavy metal inventory leads to less fissile production and hence to a lower fissile material credit. The detrimental effect of moderator seeding in the blanket on the maximum blanket revenue is more pronounced for thin blankets, which have a high fissile buildup rate, because of the low effectiveness of improved S_o in this region. Table 6.8 compares the effects on maximum blanket revenue of moderator seeding.

In conclusion, the moderated blanket concept is only favorable for:

a. Thick blankets having a negative blanket revenue,

b. Thick blankets having a very low fissile buildup rate,

c. Thick blankets having a long optimum fuel irradiation time which is out of range of the metallurgically allowable fuel irradiation time, because the high fissile buildup rate always shortens the optimum irradiation time.

Under future economic conditions projected from todays perspective, only one or two-row (i.e. thin) blankets will be economically attractive. In this respect moderator seeding may be considered as an alternative to re-optimizing already-built systems committed to thick ($\geq$ 3 row) blankets.

6.5.2 Spectrum Hardened Blankets

As mentioned in the previous section, projected future economic conditions for fabrication and reprocessing costs and plutonium value (L3), (S4) indicate that thin blankets may be more economically attractive, hence, high fertile density is desirable to compensate for the disadvantages of thin blankets inherent to their low fertile inventory.

TABLE 6.8

EFFECTS OF MODERATOR SEEDING ON MAXIMUM BLANKET REVENUE

$\frac{\Delta q}{q}$ †	UO_2 Fuel (3-rows)		UC Fuel	
	Positive Blanket Revenue*	Negative Blanket Revenue**	Thick (3-row) Blanket	Thin (2-row) Blanket
$\frac{\Delta M_{HM}}{M_{HM}}$	-0.17	-0.17	-0.17	-0.26
$\frac{\Delta S_o}{S_o}$	0.19	0.21	0.19	0.23
$\frac{\Delta r_4}{r_4}$	0.025	0.22	0.16	0.24
$\frac{\Delta bxr}{bxr}$	-0.015	0.004	-0.007	-0.024
$\frac{\Delta e_m}{e_m}$	-0.976	0.058	0.122	-0.070
e_m^{***} (Ref.)	0.018853	-0.0578	-0.049	-0.071
e_m^{***} (Mod.)	0.000459	-0.0612	-0.055	-0.066

† $\frac{\Delta q}{q} = \frac{(q \text{ with moderator seeding}) - (q \text{ without moderator seeding})}{(q \text{ without moderator seeding})}$

* Refer to Appendix D for all parameters used.
** Refer to Chapter 2 for all parameters used.

With respect to the neutron spectrum, a soft spectrum is, in general, better both neutronically and economically: a hard neutron spectrum is only a by-product of the use of high-density fuel materials. Therefore, in this study "spectrum-hardened" blankets means only that the blankets in question used high-density fuel materials.

6.5.2.1 Neutronic Aspects of Spectrum-Hardened Blankets

As developed in section 6.3.3.1, the fractional change of external breeding ratio due to a variation of fertile density can be expressed as

$$\frac{\Delta bx}{bx} = \frac{\theta}{e^{\theta}-1} \left(\frac{\Delta N_{28,B}}{N_{28,B}}\right) \tag{6.20}$$

where

$$\theta \cong [3\bar{\sigma}^{28}_{a,B}\ \bar{\sigma}^{28}_{tr,B}]^{1/2} \cdot N_{28,B} \cdot t \tag{6.21}$$

Equation (6.20) indicates that the effect of fertile density on the external breeding ratio depends on the value of θ. If θ is small because the blanket is thin (small t), increasing fertile density will be a very effective way to improve the external breeding ratio. Here we should note that thick blankets, which have large θ values, are not improved by an increase of fertile density. Table 6.9 summarizes the variation of the sensitivity coefficient, $\lambda^{b_x}_{N_{28}} = \frac{\theta}{e^{\theta}-1}$, as a function of θ. If θ is larger than about 2.5 (which corresponds to that of a UC fueled blanket at 97% T.D.), the effect of high fertile density on the external breeding ratio will be negligible (hence metallic fuel does not improve the external breeding ratio significantly.)

TABLE 6.9

VARIATION OF $\lambda^{bx}_{N_{28},B}$ * AS A FUNCTION OF θ

θ	$\lambda^{bx}_{N_{28},B}$	Remarks
1.5	0.4308	UO_2 Fuel at ~70% T.D.
2.0	0.3130	UO_2 Fuel at ~97% T.D.
2.5	0.2236	UC Fuel at ~97% T.D.
3.0	0.1572	bx may not improve in this region, because of low $\lambda^{bx}_{N_{28},B}$ and high parasitic absorption
5.0	0.0339	

$$* \lambda^{bx}_{N_{28},B} \equiv \frac{\Delta bx/bx}{\Delta N_{28}/N_{28}} = \frac{\theta}{e^{\theta}-1}$$

Table 6.10 shows the variation of important neutronic parameters achieved by replacing UO_2 fuel by UC fuel, which can be generalized as:

a. lower fissile buildup rate (which erodes the advantage of high fertile density); and the net improvement of bx is relatively small,

b. increased blanket power contribution,

c. longer optimum fuel irradiation time,

d. no effect on core performance.

6.5.2.2 Economic Aspects of Spectrum Hardened Blankets

The most serious deficiency of the spectrum hardened blanket is its low fissile buildup rate, which leads to lower blanket revenue. However, for a thin(2-row) blanket, the effectiveness of the fissile buildup rate on the (positive) blanket revenue is reduced, as shown in Fig. 6.3, and the mertis of high fertile density overcome this handicap.

Another problem arising from the high fertile density is the longer optimum fuel irradiation time. For a thick blanket (3-row), the optimum (batch) irradiation time of a carbide blanket (3-row) is about 9 years, which is possibly beyond the allowable metallurgical irradiation time. Shortening the fuel irradiation time decreases the blanket revenue.

Numerical comparisons of the economic parameters and the maximum blanket revenue are summarized in Table 6.2.

6.5.3 Fissile-Seeded Blankets

Neutrons leaking from the core region dominate the total number of neutrons available for fissile breeding in the blankets, however this value remains very nearly constant even if the blanket fuel material is changed. An alternative method to improve the number of neutrons

TABLE 6.10

CHANGES IN NEUTRONIC PARAMETERS WHEN UO_2 FUEL IS CHANGED TO UC FUEL

Fractional changes of Parameters	2-row Blanket	3-row Blanket
Initial Heavy Metal Loading ($M_{28}(0)$)	1.343	1.343
$\bar{\sigma}^{-28}_{c,B}$	0.9120	0.9175
$\bar{\phi}_B$	0.8667	0.8658
Blanket Power Fraction (BOL)	1.106	1.118
Internal Breeding Ratio	1.003	1.002
Radial Blanket Breeding Ratio	1.0650	1.0625
Optimum Fuel Irradiation Time(T_{op})	1.25	1.25

available for fissile breeding is the generation of more fast fission neutrons in the blankets by means of fissile seeding.

6.5.3.1 Neutronic Aspects of Fissile-Seeded Blankets

From the neutron balance equation shown in Eq. (6.8), the breeding ratio in a fissile-seeded blanket can be expressed as

$$b = \eta_c^{49}\left(1 + \frac{\nu-1}{\nu}\delta_c^{28} - a_c\right)\left(\frac{A_c^{49}}{A_T^{49}}\right) + \eta_B^{49}\left(1 + \frac{\nu-1}{\nu}\delta_B^{28} - a_B\right)\left(\frac{A_B^{49}}{A_T^{49}}\right) - 1 \quad (6.56)$$

where

$$\eta_r^{49} = F_r^{49}/A_r^{49}, \text{ fissile neutron yield} \quad (6.57)$$

$$\delta_r^{28} = F_r^{28}/F_r^{49}, \text{ the fertile-to-fissile fission ratio} \quad (6.58)$$

$$a_r = (A_r^{P,L}/\nu F_r^{49}), \text{ parasitic losses per fissile fission neutron} \quad (6.59)$$

If plutonium exists only in the core region (as in a conventional core-blanket system at BOL), Eq. (6.56) reduces to Eq. (6.9), as shown in Section 6.3.1.

If we assume that system power is fixed and that the power is primarily determined by plutonium fissions (hence absorptions), $A_T^{49} \approx$ constant : $dA_c^{49} = -dA_b^{49}$.

Thus for $\frac{dg}{dA_b^{49}} \geq 0$, we have the criterion:

$$\eta_B^{49}\left(1 + \frac{\nu-1}{\nu}\delta_B^{28} - a_B\right) \geq \eta_c^{49}\left(1 + \frac{\nu-1}{\nu}\delta_c^{28} - a_c\right) \quad (6.60)$$

where g is the breeding gain defined by $g = b - 1$; hence $\Delta g = \Delta b$.

Equation (6.60) shows that it will be difficult to achieve this criterion for the following reasons;

a. $\eta_B^{49} \leq \eta_c^{49}$ (because the blanket spectrum is softer than the core spectrum),

b. $a_B > a_c$ (because of the smaller plutonium concentration in the blanket region than in the core),

c. δ_c^{28} decreases if Pu enrichment in the blanket becomes appreciable,

d. because of the $(\frac{A_B^{49}}{A_T^{49}})$ weighting, the advantage, if any, will be slight.

The differences in neutronic characteristics between homogeneous and heterogeneous seeding were also examined and found to be negligible.

Table 6.11 summarizes the parametric changes in fissile-seeded blankets.

6.5.3.2 Economic Aspects of Fissile-Seeded Blankets

Potentially favorable benefits of fissile-seeded blankets on blanket economics could come from a higher fissile buildup rate and a shorter fuel optimum irradiation time. Table 6.12 summarizes the key parameters and the maximum blanket revenue of fissile-seeded blankets. In this calculation, additional costs for the initial fissile loading were not considered. However, even so the economic improvement due to the slightly higher fissile buildup rate, S_o, is negligible because of a) the decreased total amount of fertile material loaded in the blankets, b) the decreased microscopic capture cross-section of U-238.

In conclusion, the total breeding gain can be increased by fissile-seeding only if η_B^{49} is larger than 2-g. (≥ 2.2) - but η_B^{49} is usually less than 2.0. Economic advantages are also

TABLE 6.11

PARAMETRIC CHANGES OF FISSILE-SEEDED BLANKETS

	UO_2	UC	U_2Ti
ϵ_B (RB2) w/o	0.050	0.42	0.35
η_c^{49}	2.3325	2.3352	2.3383
η_{RB}^{49}	1.9264	1.9969	2.1560
A_{RB}^{49}/A_T^{49}	0.0076	0.0053	0.0036
Fractional Change of:			
bi	0.9933	0.9955	0.9965
bxa	0.9929	0.9951	0.9960
bxr	1.0071	1.0104	1.0085
b	0.9963	0.9990	0.9993

† Pu-239 was seeded homogeneously in the second row of the radial blanket

TABLE 6.12

COMPARISON OF ECONOMIC PARAMETERS FOR REFERENCE AND FISSILE-SEEDED UO_2 BLANKETS

	Reference Blanket	Fissile-Seeded*
M_{HM}, kg	17, 299	17,124
$\bar{\sigma}^{28}_{c,B}$, b	0.40252	0.39391
$\bar{\phi}_B$, 10^{-14} #/cm^2-sec	5.6269	5.9032
S_o, KgPu/(KgM_{HM}, yr)	0.00587	0.006027
T^o_c, yr^{-1}	16.0738	15.9960
r_4	0.081475	0.081677
T_{op}, yr	7.40	7.23
T_{BE}, yr	2.83	2.73
e_{fab}, mills/KwHr	0.0767	0.0776
e_{rep}, mills/KwMr	0.0216	0.0225
$-e_{mat}$, mills/KwHr	0.1561	0.1608
$-e_m$, mills/KwHr	0.0578	0.0607

*Pu-239 was seeded in the second row of the radial blanket ($\varepsilon_B = 0.50$ %).

negligible because of the lower fertile volume fraction and decreased $\sigma_{c,B}^{-28}$.

These findings are compatible with the observation that breeding performance does not improve with irradiation - which may be regarded as a method for "self-seeding".

6.5.4 Parfait Blanket Concept for Fast Breeder Reactors

To achieve a uniformly high fuel burnup, core fuel subassemblies are generally arranged in two or three radial zones of roughly equal volume, each zone's subassemblies differing in fissile material enrichment, with the lowest fissile enrichment in the innermost core region. In general the fissile enrichment is uniform within each core zone - that is, zone loading is homogeneous. An alternative approach is to heterogeneously load the zone using a combination of fissile-loaded and fertile-only assemblies (or zones within an assembly). Many versions of these "heterogeneous" FBR core designs are now under intensive scrutiny by the international fast reactor community.

Parfait blanket concepts which adopt internal blankets limited in both radial and axial extent were developed and investigated in some detail previously at MIT (D3), (P2), (A1). Conventional and parfait core configurations are shown in Fig. 6.5.

6.5.4.1 Neutronic Aspects of Parfait Blanket Systems

From Eq. (6.9), the change in the breeding ratio due to the internal blanket will be

$$\Delta b = [1 + (1 - \frac{1}{\bar{\nu}} - a)\delta - a] \cdot \Delta\eta_c^{49} + \eta_c^{49}(1 - \frac{1}{\bar{\nu}} - a) \cdot \Delta\delta - (1 + \delta) \cdot \Delta a \qquad (6.61)$$

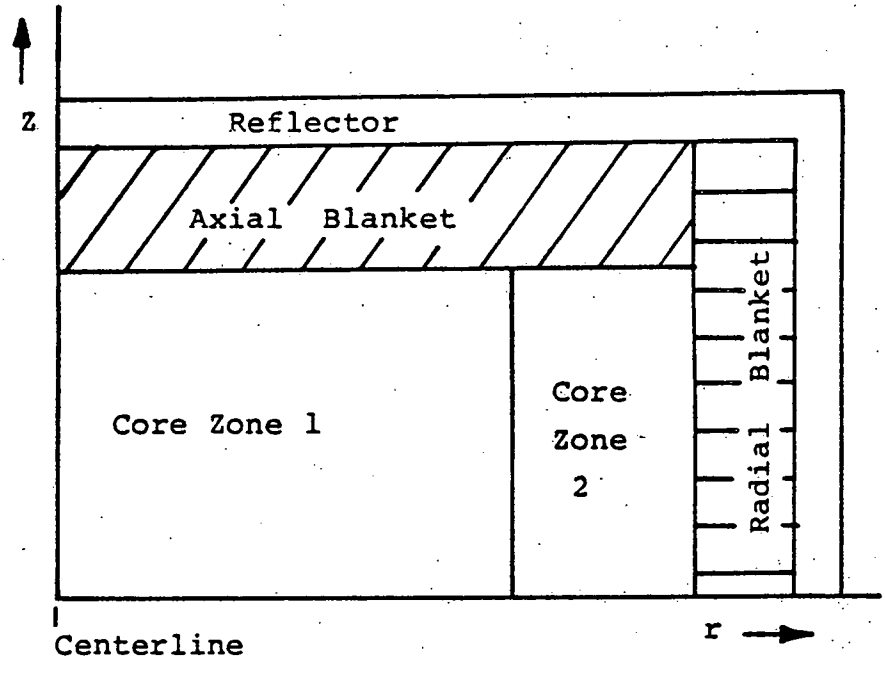

CONVENTIONAL DESIGN

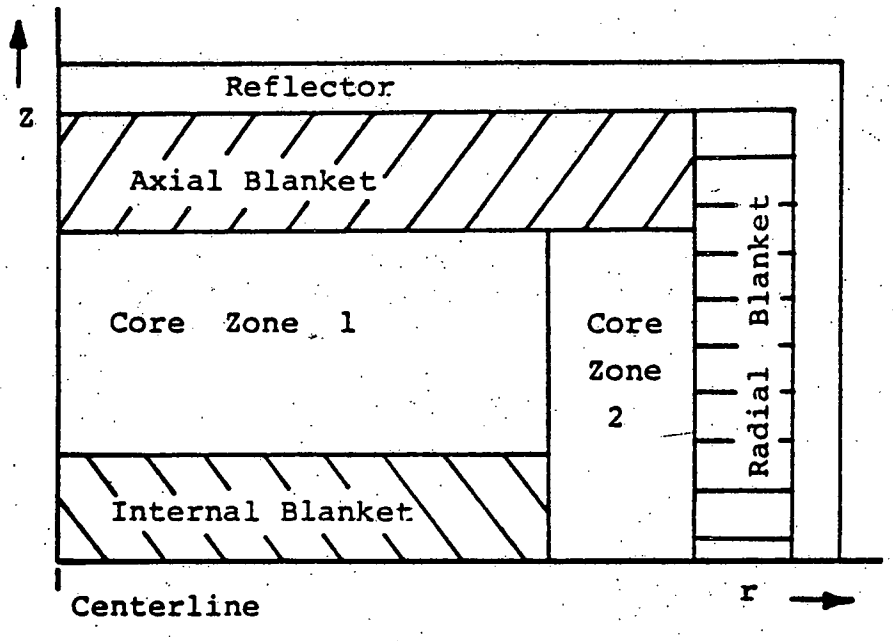

PARFAIT CONFIGURATION

Fig. 6.5 CONVENTIONAL AND PARFAIT CORE CONFIGURATIONS

where $\bar{\nu}$ was considered as a constant.

Equation (6.61) indicates that reduction of the parasitic absorption ($-\Delta a$) and core fissile consumption (hence $+\Delta\delta$) and increasing $\eta_c^{49}(+\Delta\eta_c^{49})$ are all important to increasing the breeding ratio.

Parfait blanket concepts can satisfy these requirements because

a. η_c^{49} is higher because of the harder core neutron spectrum created by higher core fissile-zone enrichment ($\Delta\eta_c/\eta_c \approx 0.04 \frac{\Delta\varepsilon_c}{\varepsilon_c}$; see Ref. (A1) for details),

b. a positive $\Delta\delta$ may be possible if $\Delta(\frac{F_B^{28}}{F_c^{49}}) >> 0.026\ \Delta(\frac{1-\varepsilon_c}{\varepsilon_c})$,

c. a negative Δa can be achieved by increasing the fuel volume fraction (permissible due to reduced control requirements and reduced fuel swelling and bowing).

The possible improvement in total breeding ratio is approximately 0.06, and more improvements can be anticipated by concurrent changes in core thermal-hydraulic design features. However it should be noted that use of a non-optimized internal blanket configuration can easily lead to a decreased breeding gain.

6.5.4.2 Economic Aspects of Parfait Blanket Systems

Assesment of the economic (fuel cycle cost) effects of parfait blanket systems can be most easily done by considering the influence of the internal blankets on the fuel depletion economics of the core and the external blankets.

A parfait blanket system can affect core fuel economics in three ways: a) by affecting the core fissile inventory required for criticality

and sustaining a specified burnup-reactivity life-time, and thereby affecting core inventory costs, b) by perturbing the magnitude and spectrum of the flux in the core, causing changes in depletion, and thus material credits, c) by reducing the core fertile inventory (hence internal breeding ratio), resulting in a smaller material credit.

These effects generally cause a net increase in the fuel cycle cost contribution in the core regions, but this can be compensated by the internal blanket revenue and increased external blanket revenues. In general, the differences in fuel cycle costs between the reference and parfait systems are negligible (e.g.1.1448 vs. 1.1499 mills/KwHr) as described in more detail in Ref. (D3).

6.5.5 Brief Review of the "Heterogeneous Core" and "Sandwich-Blanket" Concepts

Recently, fully heterogeneous core concepts which employ both axial and radial internal blanket zones have received considerable interest, both in the U.S. and abroad. The "parfait blanket" and "sandwiched-blanket" concepts are simpler versions of the fully heterogeneous concept. In the "sandwiched-blanket" concept the internal blanket is extended radially through both core regions (see Fig. 6.6.(a)),as described by Kobayashiet. al. (K4). Mougniot et. al. (M5) have suggested more complicated versions of the heterogeneous concept (see Fig. 6.6.(c)), which has aroused some controversy over the capabilities of this general class of core designs (C5). Chang (C6) has also studied a simple heterogeneous core concept constrained to fit within the CRBR configuration (see Fig. 6.6 (b)). All of these new concepts have very nearly the same design benefits and theoretical basis as already discussed for the "parfait

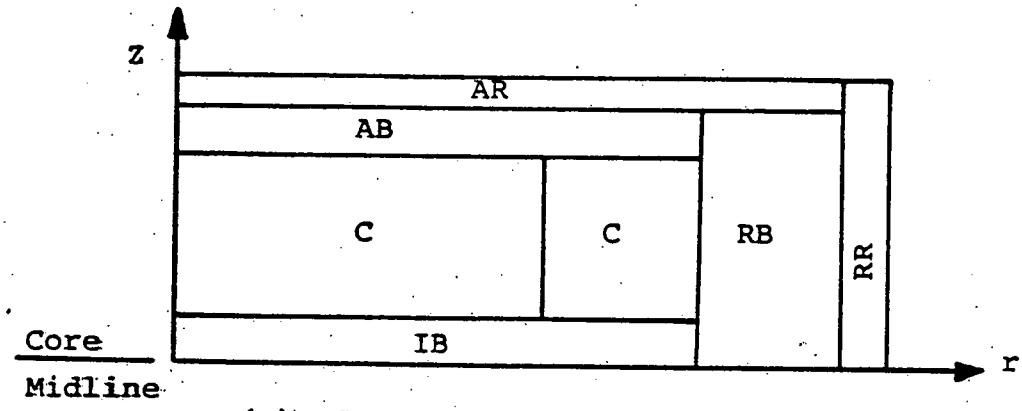

(a) SANDWICHED BLANKET

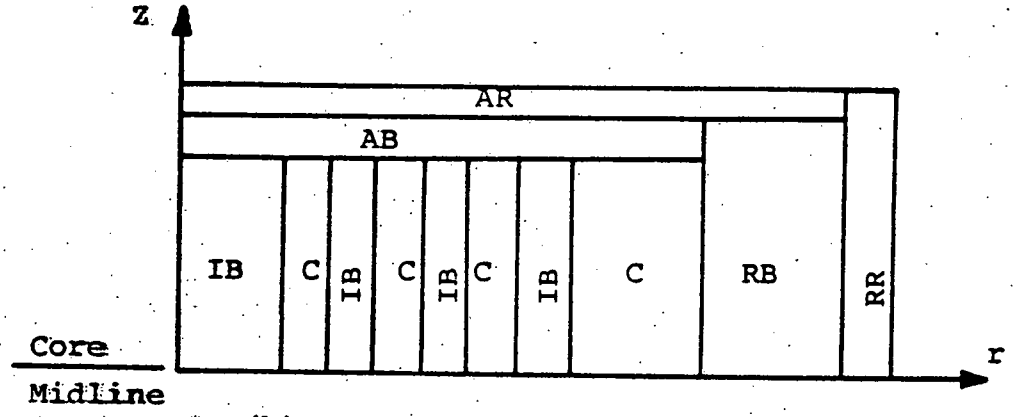

(b) HETEROGENEOUS CORE 1

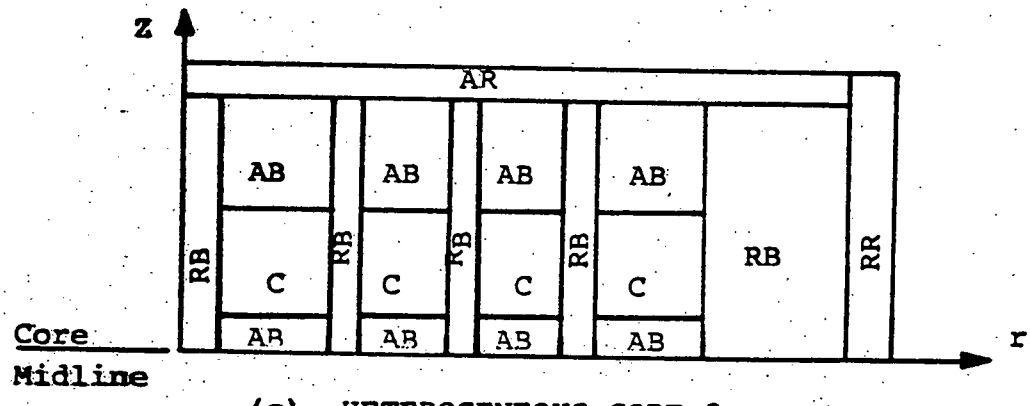

(c) HETEROGENEOUS CORE 2

* C: Core, AB: Axial Blanket, RB: Radial Blanket, IB: Internal Blanket, AR: Axial Reflector, RR: Radial Reflector

Fig. 6.6 CONFIGURATION OF "SANDWICHED-BLANKET" AND "HETEROGENEOUS CORE" DESIGNS

blanket" concept. Proponents claim: a) higher breeding ratio and shorter doubling times, b) better core power-flattening using a single fissile enrichment, c) better safety-related characteristics (e.g. reduced fuel swelling and bowing etc.).

However, with respect to fuel utilization and the fuel cycle cost of the entire reactor system, these design concepts will not offer substantial improvements unless they permit increasing the volumefraction of fuel loaded within the core envelope, since this is the only practical way to achieve significantly better breeding ratios and doubling times.

6.5.6 Summary

Analyses emphasizing the neutronic and economic performance of various blanket concepts have been presented.

Most of the evaluations have been devoted to blanket modifications which could be achieved without any perturbation of core performance. Few significant benefits were found under this constraint; in some cases a slightly higher breeding ratio could be realized at the expense of reduced blanket revenue (or vice versa).

Thin (2-row), spectrum-hardened (UC fueled) blanket concepts appear to be slightly preferable under future economic conditions, while moderated-blankets are only (at best) an alternative way to re-optimize already-built systems committed to thick ($\geq$ 3 row) blankets.

Fissile-seeded blankets have some characteristics similar to those of moderated blankets, however their potential is inferior to that of moderated blankets.

Heterogeneous core concepts having internal blanket(s) have been evaluated by several investigators. However the economic aspects of these advanced design concepts may not be particularly favorable, as

fuel cycle cost and average fuel utilization may well be nearly the same as those of equivalent homogeneous cores.

Throughout the present analysis, the most promising fuel materials have been found to be oxide and mono-carbide fuels. Carbide fuel has a better potential in the thermal-hydraulic and neutronic areas than does oxide fuel. Oxide fuel on the other hand creates the largest blanket revenue due to its high fissile buildup rate. However, if the unit fabrication cost for the carbide fuel ($/Kg M_{HM}) is less than about 90% of that for oxide fuels (based on the reference core configurations and economic environments used in this study), carbide fuel will be better than oxide fuel from an economic point of view as well.

6.6 RECAPITULATION OF MAJOR FINDINGS

In conclusion, the present work has established the following major points:

As regards fissile breeding capability:

1. External fissile breeding is primarily determined by neutron leakage from the core which makes improvement of the external breeding ratio a very difficult task without changes in core parameters; conversely, even extreme changes in external blanket design have very little effect on core performance.
2. Since the incident neutron spectrum and the total number of available neutrons in the blanket region are essentially determined by the core design, low parasitic absorption in the blanket is the single most important prerequisite for a higher external breeding ratio.

3. High blanket fuel density reduces the parasitic absorption and increases the fertile fission reaction in the blanket; although the average neutron flux is concurrently reduced, the net result is a slight improvement of the external breeding ratio.

4. It was shown that the external breeding ratio at the beginning of blanket life can be corrected by a constant to obtain a valid quantitative estimate of the external breeding ratio averaged over life for an optimally irradiated blanket. Henceone does not need to carry out burnup calculations to evaluate the effects of blanket design or composition changes.

As regards fuel depletion and economic analysis:

1. The fissile buildup history in the blanket can be expressed in a particularly simple dimensionless form, i.e.

$$\frac{M_{49}(t)}{\hat{M}_{49}} = \frac{t}{T_c^\circ} e^{-\xi \frac{t}{T_c^\circ}}$$

Thus all blankets (metal, oxide, carbide fuel, etc.) or subregions of a blanket (from pin to subassembly to whole blanket) can be correlated on a single functional plot.

2. The non-linear enrichment vs. time characteristics of plutonium buildup in FBR blankets is very important to determination of the optimum economic parameters (except for the breakeven time). Simple linearized models, while pedagogically attractive, are not adequate for fuel management in real reactors.

3. Oxide fuel, which has a higher fissile buildup rate, can produce a higher maximum blanket revenue than carbide or metal alloy fuels (note that this conclusion of oxide superiority is predicated on equal fuel fabrication costs per kg of heavy metal for all fuels). If carbide fuel assemblies can be fabricated on the order of 10% more cheaply then this may offset the foregoing disadvantage.
4. The batch fuel management option produces about 15% less plutonium than other commonly considered strateges, and an Out-In scheme produces slightly more plutonium than do the other shuffled options.

As regards FBR blanket design concepts:

1. Few significant benefits were found among those blanket modifications which could be achieved without any perturbation of core performance. In some cases a slightly higher breeding ratio could be realized at the expense of reduced blanket revenue or vice versa.
2. Thin (2-row), spectrum-hardened (UC fueled) blanket concepts appear to be slightly preferable under future economic conditions due to their excellent thermal and neutronic characteristics (hence higher external breeding ratios) and very minor economic deficiencies, while moderated-blankets are only at best an alternative way to re-optimize already-built systems committed to thick ($\geq$ 3 row) blankets.

Although particular emphasis has been placed on generalizing the results in the present work, there is no assurance that it encompasses

all possible design options for external blankets on FBR's. However, all cases examined could be fit into a self-consistent methodology, and all are consistent with the observation that very little improvement in external blanket breeding performance can be envisioned unless core design changes are allowed. On the other hand a wide latitude of design changes in the blanket could be accommodated without affecting core neutronics or breeding performance. The only option not yet resolved is the use of internal blankets to improve system performance, and it is recommended that an investigation of comparable scope to that of the present work be carried out on these "heterogeneous" or "parfait" core concepts.

6.7 RECOMMENDATIONS FOR FUTURE WORK

In fulfilling the goals of the present work several areas have been identified in which further analysis is required.

a. Blanket Design Concepts:

   1. More detailed analyses relating to the "heterogeneous core" concept should be carried out. The present work was confined almost exclusively to external blankets, which have virtually no effect on core performance.
   2. Further work on blanket shape optimization (S6) would appear worthwhile.

b. Evaluation Methods and Data:

   1. Parameters characterizing the economic and financial environments should be updated; reprocessing costs in particular, as they become better known. In order to be consistent with prior work at MIT, values used in this report are quoted 1965 dollars.

2. Throughout the evaluation of the various blanket design concepts, Brewer's accounting method A (in which material purchases and fabrication charges were capitalized and consequently depreciated for tax purposes; whereas reprocessing charges and material credit were treated as an expensed cost and taxable revenue, respectively.) was employed. Further work on Brewer's accounting method B will be necessary if method A can not be agreed on as a definitive convention.

3. Optimization of key blanket parameters (e.g. blanket thickness, enrichment, fertile density, etc.) should be performed in more detail for specific designs; carbide vs. oxide fueled blankets in particular, and using current best estimates of fabrication costs.

c. Evaluation of Blanket Performance:

1. This report has concentrated on the neutronic and economic aspects of the various blanket design concepts. Other aspects of blanket design - thermal - hydraulic aspects in particular (e.g. transient temperature behavior, blanket overcooling, etc.) should be reviewed.

6.8 REFERENCES

A1 Aldrich, D.C., "Parfait Blanket Systems Employing Mixed Progeny Fuels," S.M. Thesis, Nuclear Engineering Department, MIT (June, 1976).

B1 Barthold, W.I., "Fuel Shuffling in LFMBR Blankets," Argonne National Laboratory, FRA-TM-40 (August, 1972).

B3 Bondarenko, I.I., (Ed.), "Group Constants for Nuclear Reactor Calculations," Consultants Bureau, New York (1964).

B4 Brewer, S.T., E.A. Mason and M.J. Driscoll, "TheEconomics of Fuel Depletion in Fast Breeder Reactor Blankets," COO-3060-4, MITNE-123 (Nov. 1972).

B6 Bruyer, D., "Breeding-Economics of FBR Blankets having Non-linear Fissile Buildup Histories, S.M. Thesis, Nuclear Engineering Department, MIT (Aug. 1976).

C5 Chang, Y.I., "Review of the French Concept of Heterogeneous Core to Improve the Doubling Time," FRA-TM-77 (Aug. 1975).

C6 Chang, Y.I., W.P. Barthold and C.E. Till, "An Evaluation of the Cylindrical Parfait Core Concept," FRA-TM-88 (April, 1976).

D3 Ducat, G.A., M.J. Driscoll and N.E. Todreas, "Evaluation of the Parfait Blanket Concept for Fast Breeder Reactors," COO-2250-5, MITNE-157 (Jan. 1974).

E1 Engle, W.W., Jr., "A Users Manual for ANISN, a One-Dimensional Discrete Ordinates Transport Code with Anisotropic Scattering," K-1693 (March, 1967).

H3 Hirons, T.J. and R.D. O'dell, "Calculational Modeling Effects on Fast Breeder Fuel Cycle Analysis," LA-4187 (Sept. 1965).

K2 Ketabi, M., "The Breeding-Economic Performance of Fast Reactor Blankets," S.M. Thesis, Nuclear Engineering Dept., MIT (May 1975).

K4 Kobayashi, T., S. Kondo and Y. Togo, "Nuclear Characteristics of Sandwich-Blanket Type Core for Power Reactor," NSE, 10(11), 700-702 (Nov. 1973).

L1 Lake, J.A., et al., "Breeding Ratio and Doubling Time Characteristics of the Clinch River Breeder Reactor," Advanced Reactors; Physics, Design and Economics, Pergamon Press (Sept. 1974).

L2 Lamarsh, J.L., "Introduction to Nuclear Reactor Theory," Addison-Wesley Publishing Co., Inc. (1966).

L3 Little, W.W., Jr. and R.W. Hardie, "2DB User's Manual, Revision 1," BNWL-831, Rev. 1 (Aug. 1969).

L4 Little, W.W., Jr., R.W. Hardie, L.D. O'dell and R.B. Kidman, "Fuel Management Models and Analysis for the Fast Test Reactor," BNWL-SA-2758 (Dec. 1969).

M1 Masterson, R.E., "The Application of Perturbation Theory and Variational Principles to Fast Reactor Fuel Management," S.M. Thesis, Nuclear Engineering Dept., MIT (Sept. 1974).

M5 Mougniot, J.C., et al., "Breeding Gains of Sodium-Cooled Oxide Fueled Fast Reactors," Paper from European Nuclear Conference, April 1975, Paris ORNL-TR-2994 (1975).

P2 Pinnock, R.A., "Parfait Blanket Configurations for Fast Breeder Reactors," S.M. Thesis, Nuclear Engineering Dept., MIT (June 1975).

S2 Sierra, J.M. and M. Becker, "Sensitivity Analysis for the Fast Reactor Fuel Cycle," Trans. Am. Nucl. Soc., 23, 535 (1976).

S4 Simcha, G. and R. Salman, "Nuclear Fuel Logistics," Nuclear News, 47-53 (Feb. 1973).

S6 Spitzer, J., "Blanket Shape Optimization in Breeder Reactors," Ph.D. Thesis, the University of New Mexico (1971).

T1 Tagishi, A. and M.J. Driscoll, "The Effect of Reactor Size on the Breeding Economics of LMFBR Blankets," COO-2250-13, MITNE-168 (Feb. 1975).

W3 Wood, P.J., "Assessment of Thorium Blankets for Fast Breeder Reactors," COO-2250-2, MITNE-148 (July 1973).

Z1 DRDT, USAEC, "Reactor Fuel Cycle Cost for Nuclear Power Evaluation," WASH-1099 (Dec. 1971).

CHAPTER 7

SUMMARY, CONCLUSIONS, AND FUTURE WORK

7.1 Introduction

This is the seventh annual report of the LMFBR Blanket Physics Project at MIT. During the past year, work has been concerned primarily with the following:

1) Resumption of experimental work following the post-renovation startup of the MIT Reactor. During the report period efforts focused on measurements of the ratio of U-238 captures to U-235 fissions in a mock-up of a typical LMFBR blanket (Chapter 2), and supporting calculations.
2) Completion of development work on an RPL readout device for TLD detectors for use in gamma heating measurements (Chapter 3).
3) Continuation of conceptual analyses on the benefits of internal blankets (Chapter 4).
4) Development of an improved equivalence theorem for heterogeneous self-shielding calculations (Chapter 5).
5) Evaluation of a variety of potential means for improving the breeding performance of external LMFBR blankets (Chapter 6).

7.2 Discussion

The most important conclusions which may be drawn from the past year's work are as follows:

1) Calculations continue to over-predict the ratio of $\sigma_c^{28}/\sigma_f^{25}$ in the blanket. Parametric and sensitivity studies show that the most likely cause is a high value of the U-238 capture cross-section and/or a harder than actual driving spectrum computed for the BTF converter plate.
2) A useful RPL method for non-destructive readout of TLDs has been developed. Its applicability is limited by a background signal from unirradiated TLDs equivalent to approximately 100 rad.
3) The use of internal blankets in LMFBRs continues to look attractive. Full realization of their advantages requires that their inherently lower fluence and power/temperature/fluence gradients be traded off to achieve a higher volume fraction of heavy metal in the core.
4) Heterogeneous self-shielding effects in LMFBR cores and blankets, and in the MIT Blanket Mockup, have been shown to be very small, and an unlikely cause of any computational discrepancies in our work. The improved equivalence theorem appears capable of extension to LWR lattices and may thereby permit unification of LMFBR and LWR pin cell physics methods.
5) There appears to be very little prospect for significant improvement of the breeding performance of external (radial, axial) LMFBR blankets. Conversely this implies considerable engineering flexibility to

meet blanket thermal, hydraulic and materials constraints without significant degradation in neutronic efficiency.

7.3 Future Work

During the coming contract year, October 1, 1976 through September 30, 1977, work is planned in the following areas:

1) Experimental investigation of fast neutron penetration in the reflector region of Blanket Mockup No. 5B.
2) Participation in interlaboratory comparisons as part of the Large Core Code Evaluation Working Group (LCCEWG) and Large Heterogeneous Reference Fuel Design Study (LHRFDS) efforts.
3) Conceptual, parametric and sensitivity studies needed to design Blanket Mockup No. 6 and to prepare a work proposal for submission to ERDA.
4) Increased emphasis on preparation of benchmark computational problems centered around the MIT Blanket Mockups. As part of this effort, the cross-section libraries used at MIT will be updated to use the LASL LIB-IV 50 group set as a reference source library.
5) Continue analysis of data from earlier blanket mockups using up-dated cross section sets and numerical methods to rationalize some of the more persistent discrepancies between calculation and experiment.

Appendix A

BIBLIOGRAPHY OF BLANKET PHYSICS PROJECT PUBLICATIONS

In this appendix are tabulated all publications associated with work performed in the MIT Blanket Physics Project. Sc.D. and Nuclear Engineer's theses are listed first, followed by S.M. and B.S. theses and then by other publications.

A.1 Doctoral and Engineer's Theses

(Also see section 3 for corresponding topical reports.)

Forbes, I.A.

Design, Construction and Evaluation of a Facility for the Simulation of Fast Reactor Blankets, Feb. 1970

Sheaffer, M.K.

A One-Group Method for Fast Reactor Calculations, Aug. 1970.

Tzanos, C.P.

Optimization of Material Distributions in Fast Breeder Reactors, Aug. 1971.

Kang, C.S.

Use of Gamma Spectroscopy for Neutronic Analysis of LMFBR Blankets, Nov. 1971.

Leung, T.C.

Neutronics of an LMFBR Blanket Mockup, Jan. 1972

Ortiz, N.R.

Instrumental Methods for Neutron Spectroscopy in the MIT Blanket Test Facility, May 1972.

A.1 Doctoral and Engineer's Theses (continued)

Brewer, S.T.

The Economics of Fuel Depletion in Fast Breeder Reactor Blankets, Oct. 1972

Gregory, M.V.

Heterogeneous Effects in Fast Breeded Reactors, Dec. 1972.

Wood, P.J.

Assessment of Thorium Blankets for Fast Breeder Reactors, July 1973.

Ducat, G.A.

The Parfait Blanket Concept for Fast Breeder Reactors, Jan. 1974.

Brown, G.J.

Evaluation of High-Performance LMFBR Blanket Configurations, May 1974.

Scheinert, P.A.

Gamma Heating Measurements in Fast Breeder Reactor Blankets, (Engineer's Thesis), Aug. 1974.

Tagishi, A.

The Effect of Reactor Size on the Breeding Economics of LMFBR Blankets, Feb. 1975

Kalra, M. S.

Gamma Heating in Fast Reactors, Feb. 1976.

Kadiroglu, O. K.

Uranium Self-Shielding in Fast Reactor Blankets, March 1976.

A.2 S.M. and B.S. Theses

Ho, S.L.

Measurement of Fast and Epithermal Neutron Spectra Using Foil Activation Techniques

S.M. Thesis, MIT Nucl. Eng. Dept., Jan. 1970

Mertens, P.G.

An Evaluation of a Subcritical Null-Reactivity Method for Fast Reactor Applications

S.M. Thesis, MIT Nucl. Eng. Dept., May 1970

Westlake, W.J.

Heterogeneous Effects in LMFBR Blanket Fuel Elements

S.M. Thesis, MIT Nucl. Eng. Dept., June 1970

Shupe, D.A.

The Feasibility of Inferring the Incident Neutron Spectrum from Prompt Capture Gamma-Ray Spectra

S.M. Thesis, MIT Physics Dept., Aug. 1970

Pant, A.

Feasibility Study of a Converter Assembly for Fusion Blanket Experiments

S.M. Thesis, MIT Nucl. Eng. Dept., Jan. 1971

Passman, N.A.

An Improved Foil Activation Method for Determination of Fast Neutron Spectra

S.M. Thesis, MIT Nucl. Eng. Dept., Jan.1971

Forsberg, C.W.

Determination of Neutron Spectra by Prompt Gamma-Ray Spectrometry

M.S. Thesis, MIT Nucl. Eng. Dept., June 1971

Brown, G.J.

A Study of High-Albedo Reflectors for LMFBRs

S.M. Thesis, MIT Nucl. Eng. Dept., March 1972

Thompson, A.M.

Activation Profiles in Reactor Fuel Elements

B.S. Thesis, MIT Physics Dept., June 1972

Lal, D.

Determination of the Neutron Spectrum in the MITR Transistor Irradiation Facility

B.S. Thesis, MIT Chem. Eng. Dept., June 1972

Ho, S.Y-N.

Selection of Foil Materials for LMFBR Neutron Spectrometry

S.M. Thesis, MIT Nucl. Eng. Dept., May 1973

Choong, T.P.

Fast Neutron Spectrometry in an LMFBR Blanket Reflector

S.M. Thesis, MIT Nucl. Eng. Dept., Aug. 1973

Kennerley, R.J.

Proton-Recoil Neutron Spectrometry in a Fast Reactor Blanket

S.M. Thesis, MIT Nucl. Eng. Dept., Aug. 1973

Chan, J.K.

A Foil Method for Neutron Spectrometry in Fast Reactors

S.M. Thesis, MIT Nucl. Eng. Dept. , Jan. 1974

Yeung, M.K.

A Stacked-Foil Method for Epithermal Neutron Spectrometry

S.M. Thesis, MIT Nucl. Eng. Dept., Dec. 1974

Masterson, R.E.

The Application of Perturbation Theory and Variational Principles to Fast Reactor Fuel Management

S.M. Thesis, MIT Nucl. Eng. Dept., Sept. 1974

A.2 Continued

Pinnock, R. A.

Parfait Blanket Configurations for Fast Breeder Reactors, S.M. Thesis, MIT Nucl. Eng. Dept., June 1975.

Chambers, C. A.

Design of a Graphite Reflector Assembly for an LMFBR S.M. Thesis, MIT Nucl. Eng. Dept., Aug. 1975.

Ketabi, M.

The Breeding-Economic Performance of Fast Reactor Blankets, S.M. Thesis, MIT Nucl. Eng. Dept., May 1975.

Bruyer, D. A.

Breeding-Economics of FBR Blankets Having Non-Linear Fissile Buildup Histories, S.M. Thesis, MIT Nucl. Eng. Dept., Aug. 1975.

Morneau, R. A.

Improved Radiophotoluminescence Technique for Gamma Heating Dosimetry, S.M. Thesis, MIT Nucl. Eng. Dept., Sept. 1975.

Wu, S. S.

Experimental Verification of Breeding Performance in Fast Reactor Blankets, Nuclear Engrs. Thesis, MIT Nucl. Eng. Dept., June 1976.

Aldrich, D. C.

Parfait Blanket Systems Employing Mixed Progeny Fuels, S.M. Thesis, MIT Nucl. Eng. Dept., June 1976.

A.3 Other Publications

I.A. Forbes, M.J. Driscoll, T.J. Thompson, I. Kaplan and D. D. Lanning

Design, Construction and Evaluation of a Facility for the Simulation of Fast Reactor Blankets

MIT-4105-2, MITNE-110, Feb. 1970

M.K. Sheaffer, M.J. Driscoll, and I Kaplan

A One-Group Method for Fast Reactor Calculations

MIT-4105-1, MITNE-108, Sept. 1970

I.A. Forbes, M.J. Driscoll, D.D. Lanning, I. Kaplan and N.C. Rasmussen

LMFBR Blanket Physics Project Progress Report No.1

MIT-4105-3, MITNE-116, June 30, 1970

I.A. Forbes, M.J. Driscoll, T.J. Thompson, I. Kaplan and D. D. Lanning

Design, Construction and Evaluation of an LMFBR Blanket Test Facility

Trans. Am. Nucl. Soc., Vol.13, No.1, June 1970

S.T. Brewer, M.J. Driscoll and E.A. Mason

FBR Blanket Depletion Studies - Effect of Number of Energy Groups

Trans. Am. Nucl. Soc., Vol. 13, No. 2, Nov. 1970

M.K. Sheaffer, M.J. Driscoll and I. Kaplan

A Simple One-Group Method for Fast Reactor Calculations

Trans. Am. Nucl. Soc., Vol. 14, No. 1, June 1971

T.C. Leung, M.J. Driscoll, I. Kaplan and D.D.Lanning

Measurements of Material Activation and Neutron Spectra in an LMFBR Blanket Mockup

Trans. Am. Nucl. Soc., Vol. 14, No. 1, June 1971

A.3 Other Publications (continued)

S.T. Brewer, E.A. Mason and M.J. Driscoll

On the Economic Potential of FBR Blankets

Trans. Am. Nucl. Soc., Vol. 14, No. 1, June 1971

I.A. Forbes, M.J. Driscoll, N.C. Rasmussen, D.D. Lanning and I. Kaplan

LMFBR Blanket Physics Project Progress Report No. 2

COO-3060-5, MITNE-131, June 1971

C.P. Tzanos, E.P. Gyftopoulos and M.J. Driscoll

Optimization of Material Distributions in Fast Breeder Reactions

MIT-4105-6, MITNE-128, August 1971

T.C. Leung and M.J. Driscoll

A Simple Foil Method for LMFBR Spectrum Determination

Trans. Am. Nucl. Soc., Vol. 14, No. 2, Oct. 1971

C.S. Kang, N.C. Rasmussen and M.J. Driscoll

Use of Gamma Spectroscopy for Neutronic Analysis of LMFBR Blankets

COO-3060-2, MITNE-130, Nov. 1971

T.C. Leung, M.J. Driscoll, I. Kaplan and D.D. Lanning

Neutronics of an LMFBR Blanket Mockup

COO-3060-1, MITNE-127, Jan. 1972

N.R. Ortiz, I.C. Rickard, M.J. Driscoll and N.C. Rasmussen

Instrumental Methods for Neutron Spectroscopy in the MIT Blanket Test Facility

COO-3060-3, MITNE-129, May 1972

V.C. Rogers, I.A. Forbes and M.J. Driscoll

Heterogeneity Effects in the MIT-BTF Blanket No. 2

Trans. Am. Nucl. Soc., Vol. 15, No.1, June 1972

A.3 Other Publications (continued)

S.T. Brewer, E.A. Mason and M.J. Driscoll

The Economics of Fuel Depletion in Fast Breeder Reactor Blankets

COO-3060-4, MITNE-123, Nov. 1972

M.K. Sheaffer, M.J. Driscoll and I. Kaplan

A One-Group Method for Fast Reactor Calculations

Nucl. Sci. Eng., Vol. 48, p. 459 (1972)

C.P. Tzanos, E.P. Gyftopoulos and M.J. Driscoll

Optimization of Material Distributions in Fast Reactor Cores

Nucl. Sci. Eng., Vol. 52, p. 84 (1973)

M.J. Driscoll, D.D. Lanning and I.Kaplan

LMFBR Blanket Physics Project Progress Report No. 3

COO-3060-6, MITNE-143, June 1972

M.V. Gregory, M.J. Driscoll and D.D. Lanning

Heterogeneous Effects in Fast Breeder Reactors

COO-2250-1, MITNE-142, Jan. 1973

P.J. Wood and M.J. Driscoll

Assessment of Thorium Blankets for Fast Breeder Reactors

COO-2250-2, MITNE-148, July 1973

G.A. Ducat, M.J. Driscoll and N.E. Todreas

The Parfait Blanket Concept for Fast Breeder Reactors

Trans. Am. Nucl. Soc., Vol. 16, No. 1, June 1973

G.A. Ducat, M.J. Driscoll and N.E. Todreas

The Parfait Blanket Concept for Fast Breeder Reactors

COO-2250-5, MITNE-157, Jan. 1974

A.3 Other Publications (continued)

G.J. Brown and M.J. Driscoll

Evaluation of High-Performance LMFBR Blanket Configurations

COO-2250-4, MITNE-150, May 1974

P.A. Scheinert and M.J. Driscoll

Gamma Heating Measurements in Fast Breeder Reactor Blankets

COO-2250-10, MITNE-164, Aug. 1974

P.J. Wood and M.J. Driscoll

Economic Characterization of Breeder Reactor Blanket Performance

Trans. Am. Nucl. Soc., Vol. 17, Nov. 1973

P.J. Wood and M.J. Driscoll

The Economics of Thorium Blankets for Fast Breeder Reactors

Trans. Am. Nucl. Soc., Vol. 17, Nov. 1973

M.V. Gregory, M.J. Driscoll, D.D. Lanning

Heterogeneous Effects on Reactivity of Fast Breeder Reactors

Trans. Am. Nucl. Soc., Vol. 17, Nov. 1973

M.J. Driscoll, et al.

LMFBR Blanket Physics Project, Progress Report No. 4.

COO-2250-3 , MITNE-149, June 30, 1973

M.J. Driscoll, et al.

LMFBR Blanket Physics Project Progress Report No. 5

COO-2250-14, MITNE-170, June 30, 1974

A.3 Other Publications (continued)

A. Tagishi and M.J. Driscoll

The Effect of Reactor Size on the Breeding Economics of LMFBR Blankets

COO-2250-13, MITNE-168, Feb. 1975

M.S. Kalra and M.J. Driscoll

Gamma Heating in LMFBR Media

COO-2250-18, MITNE-179, Feb. 1976

A. Tagishi and M.J. Driscoll

The Effect of Core Size on Fast Reactor Blanket Performance

TANSAO Vol. 21, June 1975

M. J. Driscoll, ed.

LMFBR Blanket Physics Project Progress Report No. 6,

COO-2250-21, MITNE-185, June 30, 1975

O. K. Kadiroglu and M. J. Driscoll

Uranium Self-Shielding in Fast Reactor Blankets

COO-2250-17, MITNE-178, March 1976

M. Ketabi and M. J. Driscoll

The Breeding Economics of Fast Reactor Blankets

Trans. Am. Nucl. Soc., Vol. 22, Nov. 1975

J. I. Shin and M. J. Driscoll

Generalized Fissile Buildup Histories for FBR Blankets

Trans. Am. Nucl. Soc., Vol. 23, June 1976

G. J. Brown and M. J. Driscoll

Evaluation of LMFBR Blanket Configurations

Trans. Am. Nucl. Soc., Vol. 23, June 1976

A.3 Other Publications (continued)

M. J. Driscoll, G. A. Ducat, R. A. Pinnock and D. C. Aldrich

Safety and Breeding-Related Aspects of Fast Reactor Cores Having Internal Blankets

To be published in the Proceedings of the International Meeting on Fast Reactor Safety and Related Physics, Oct. 1976